Addis Ababa University

Addis Ababa Institute of Technology

African Railway Center of Excellence

Passenger Ride Comfort Analysis of a Rail Vehicle Running with Polygonized Wheel Using Dynamic Simulations

(A case study of Addis Ababa Light Rail Transit)

By

Mazuri Erasto Lutema

ID: GSR/0224/14

Advisor: Dr. Haileleoul Sahle HABTE (PhD)

A Thesis Submitted to the School of Graduate Studies of Addis Ababa University in Partial Fulfillment of the Requirements for the Degree of Masters of Science in Railway Engineering (Rolling Stock)

July 2023

Addis Ababa

Ethiopia

APPROVAL

The undersigned has examined the thesis entitled "**Passenger ride comfort analysis of a rail vehicle running with polygonized wheel using dynamic simulations"** presented by Mazuri Erasto Lutema of registration number GSR/0224/14, in partial Fulfillment of the Requirements for the Degree of Master of Science in Railway Engineering (Rolling Stock).

Submitted by:

Mazuri Erasto Lutema Student	_____ Signature	_____ Date

Approved by:

Haileleoul Sahle HABTE (PhD) Advisor	_____ Signature	_____ Date
Mr. Biniyam Ayalew Internal Examiner	_____ Signature	_____ Date
Mulugeta Habtemariam (PhD) External Examiner	_____ Signature	_____ Date
Mr. Zewdie Moges A/Director of ARCE	_____ Signature	_____ Date

DECLARATION

I, Mazuri Erasto Lutema, do declare that this thesis titled “Passenger ride comfort analysis of a rail vehicle running with polygonized wheel using dynamic simulations” is my original work except for that which has been referenced. It has never before been submitted for a degree or other type of academic recognition.

Signature…… Date…….

Mazuri Erasto Lutema

Email: mazurilutema@yahoo.com

ACKNOWLEDGEMENT

I thank the all-powerful, most merciful, and gracious God first and foremost for his blessings on me throughout my studies and in finishing this thesis.

Special thanks go to my advisor, Dr. Haileleoul Sahle Habte, for the material support and advice that enabled me to complete this study. I am grateful to Mr. Awel Mohammedseid for his vast knowledge, inspiration, unwavering help, patience, and friendship throughout my studies.

I would also like to thank the lecturers of the African Railway Center of Excellence, Addis Ababa Institute of Technology, and Addis Ababa University for their devotion and dedication during the period of course work; they helped me to expand my knowledge and skills in the railway engineering field. My sincere gratitude goes to Associate Professor Wondwossen Bogale for his fantastic lectures and notes concerning a research methodology course.

In particular, I want to thank the management team at the National Institute of Transport (NIT) in Tanzania, under the rector, Eng. Professor Zakaria Mganilwa, for granting me permission to take advantage of this opportunity to study a master's degree at Addis Ababa University in Ethiopia under a World Bank scholarship.

Another source of gratitude and appreciation goes to my family for their moral support, which they always give me. Your encouragement for me cannot be measured. My parents, wife, and children, these credits go to you since you have always been my light and unique motivation, which gave me reason to stand.

Finally, I would like to thank my friends and classmates for their support during the course work period and this thesis.

ABSTRACT

The railway transportation system is currently undergoing a significant expansion. As a result, train lines are upgraded, and the technical condition of the rail vehicles that use them is also taken into consideration. However, under certain circumstances, wheels on rail vehicles may sustain damage while in use. Then, depending on the kind and degree of flaws, the profile of the wheels is no longer circular but rather changes. The passenger's ride comfort is diminished when a rail vehicle with a damaged wheel is in operation. The research considered one type of railway wheel damage, which is wheel polygonization, and focused on analyzing the ride comfort for passengers based on results obtained from multibody dynamic analyses. Simulations and calculations were done in numerical and dynamic multibody software. The findings demonstrate that the wheel polygonization of 0.3 mm has a greater impact on ride comfort compared to the other amplitudes (0.1mm and 0.2mm). This implies that with an increase in polygonization amplitude, the ride index will also increase. However, running an overloaded carrying capacity vehicle has minimal comfort compared to an empty and rated carrying capacity vehicle when the wheel has a polygonization defect. Moreover, it found that with increasing vehicle speed, the ride index also increases, which means that at high speeds, the ride comfort will be diminished. Furthermore, it found that the orders of wheel polygonization have an effect on ride comfort. With the increasing order of polygonization, the ride index also increases. According to the findings, this study has a significant impact on the maintenance planning for wheels and rails as well as operation management.

Keywords: *Rail vehicle, Ride comfort, Flexible wheelsets, Wheel polygonization, Finite element analysis, Multibody dynamic simulations*

TABLE OF CONTENTS

LIST OF FIGURES

LIST OF TABLES

ACRONYMS AND ABBREVIATION

AALRT	Addis Ababa Light Rail Transit
FEM	Finite Element Method
OOR	Out of Roundness
UIC	International Union of Railways
CAD	Computer Aided Design
ISO	International Organization for Standardization
PSD	Power Spectral Density
TIMP	Track Irregularity Probabilistic Model
MBDS	Multibody Dynamic System
FEMBS	Finite Element Multibody System
DOF	Degree of Freedom
APDL	Ansys Parametric Design Language
SUB	Substructure Analysis files
FBI	Flexible Body Input file
NIT	National Institute of Transport
FEA	Finite Element Analysis
TM	Torsional Mode
MB	Bending Mode
UM	Umbrella Mode
ANSYS	Analysis System

CHAPTER ONE

1.0 INTRODUCTION

1.1 Background

The railway industry is a significant component of the national economy. More people are opting to take trains to travel due to their convenience, safety, speed, and environmental protection [1]. So, it must offer a high comfort level for passengers and crew. However, the comfort that passengers experience is usually perceived differently from one individual to another. A low vibration level is one of the important factors of a good ride comfort. The vibrations are mainly caused by track irregularities, from which they are transmitted via the bogies and the car body to the passengers [2]. The bogies' excitation causes the carbody to bend and twist since it is not stiff. In some circumstances, the structural flexibility of the car body accounts for half of the vibrations that are felt, with the remaining vibrations coming from rigid body motions. The problem of vehicle vibration is significant in the design and development of competitive cars given the present trend toward lighter vehicles and faster speeds. Additionally, the desire for high comfort standards necessitates a greater comprehension of the vibration interaction between passengers and vehicles [3].

The passenger experience is directly related to the level of the vehicle comfort index. Consequently, the comfort of railway cars has drawn public attention. The comfort of the trip depends on many different adverse effects to which passengers are exposed. These effects mostly include vibrations caused by moving vehicles, as well as noise, air humidity, illumination, temperature, and ventilation. Running imperfections in the track and wheel untrueness can also result in negative vibrations [4]. One of the most common types of wheel damage is polygonization [5]. This particular form of wheel defect manifests itself when the wheel locks and slides along the rail due to faulty brakes or excessive braking power in comparison to the practical friction in the wheel/rail contact.

Numerous techniques for evaluating ride comfort have been developed over the years, each with varying degrees of application depending on the type of traffic-urban, suburban, long distance, etc. These methods are included standards, such as BS 6841 [6] and UIC 513 [7]. All of the methods involve evaluating the level of vibrations from a comfort standpoint based on acceleration in

different directions, through specific weighting filters that trigger the influence of the differentiated sensitivity of human subjects to vibrations, depending on direction and frequency. The majority of European railway administrations have adopted the comfort index calculation approach employed in many other railway operations. The reason is that it represents a high level and an instrument of skill that takes into account a number of specific issues of the railway vehicles vibration behavior, important as they influence the comfort state, but neglected by other methods. However, one of the main presumptions of a rail vehicle's success and popularity with passengers and transportation providers is the trip comfort. Due of this, a lot of focus is placed on the rail car analysis prior to operation [8], [9]. For analysis computer simulations and detailed analysis of measured experimental values are widely used.

Most of researchers who investigated the effect of wheel damage on ride comfort they study how the wheel flat, wheel polygonization and OOR affect the ride comfort by considering vehicle speed and track irregularity only. They didn’t investigate how does variable load (empty vehicle, normal loaded vehicle and overloaded vehicle) affect the ride comfort of rail vehicles moving with wheel polygonization. This study addressed the role played by vehicle speed, flexible wheelset, vehicle carrying loads, and wheel polygonization in ride comfort. Due to the high experiment cost and significant impact on regular operation, it is difficult to conduct this kind of fundamental research through experiments, therefore simulation emerges as the best option. However, the reasonability and robustness of the prediction program must be ensured.

1.2 Statement of the Problem

Wheel polygonization is a widespread phenomenon that has been observed in a variety of rolling stock for many years, including locomotives, metro trains, and light rail vehicles. By periodically stimulation in the wheel-rail interface, it introduces damaging vibration to the vehicle track system [10], [11]. One of the failure mechanisms in the railway industry that results in wheel polygonization is wheel wear, which causes wheel flats. Uneven wear in the circumferential direction of the wheel is caused by large variations in the normal force, tangential force, area of the contact patch, and creepages between one circumferential revolution and the next. The majority of this uneven portion is found after the wheel flat's trailing edge. Furthermore, the tire flat is very difficult to remove by regular wheel-rail wear, resulting in a localized area of the wheel tread being subjected to reciprocating impact for an extended period of time. Therefore, as the mileage rises,

the uneven wear will transform into polygonal wear. The wheel flat will exacerbate the polygon phenomenon if it already exists. Moreover, the effects may include noise, diminished comfort, component degradation, and track deterioration [12], [13]. Therefore, this research will have a significant impact on the maintenance planning for wheels and rails as well as operation management, helping to ensure the comfort and safety of passenger and railway rolling stock by either shortening the time needed for wheel maintenance or altering vehicle speed when a wheel develops polygonization defects.

1.3 Objectives

1.3.1 Main objective

The general objective of this study is to analyze the passenger ride comfort of a rail vehicle running with polygonized wheels by using dynamic simulations.

1.3.2 Specific objectives

i. To investigate the influence of wheel polygonization amplitude on passenger ride comfort.
ii. To investigate the influence of vehicle carrying loads on ride comfort when a rail vehicle moves with polygonal wheels.
iii. To examine how vehicle speeds affect ride comfort when the rail wheel experiences a polygonization defect.
iv. To determine the effect of polygonization orders on passenger ride comfort.

1.4 Research Questions

i. How does the wheel polygonization amplitude affect the ride comfort?
ii. How does variable load affect the ride comfort of rail vehicles moving with wheel polygonization?
iii. How does the vehicle speed affect the passenger's ride comfort when the wheel is polygonised?
iv. How does passengers ride comfort affected by polygonization orders?

1.5 Significance of the Research

The damaged wheel triggers the amplification of the vibration behavior at the car's body level, with a negative impact on the rolling comfort. These conditions are the most common problems in rail vehicles, including the AALRT. This research determined the effect of wheel polygonization

on passenger ride comfort. Thus, it has a significant impact on the maintenance planning for wheels as well as operation management, helping to ensure the comfort and safety of passenger and railway rolling stock by either shortening the time needed for wheel maintenance or altering vehicle speed when a wheel develops polygonization defects. However, this study will also be valuable to scientific researcher's in future advanced and exploratory research on the impacts of wheel polygonization on light rail vehicle dynamics, including passenger ride comfort.

1.6 Scope of the study

A rail vehicle operating with wheel polygonization was taken into account in the study. To perform a numerical simulation, a flexible wheel set was modeled in CAD and loaded into FEM. The carbody got just master and superposition nodes from the FEM, which were represented by SIMPACK for dynamic simulation. However, the investigation was only done to assess how flexible wheel sets, vehicle carrying loads, vehicle speed, and wheel polygonization affect passenger ride comfort. Due to the high cost of experiments and their significant impact on regular operations, it is difficult to conduct this kind of fundamental research through experiments; therefore, simulation emerges as the best option.

1.7 Work organization

This work is organized in five parts. Chapter one is the introduction part which contains the background of the study, statement of the problem, objectives, significance of the study and scope of the study. Chapter two discusses the literature review from previous work done in the similar topic and it incorporates the use of published articles and journals. Chapter three shows the appropriate selection of materials and methods that used to accomplish the objective of the study. The fourth chapter contains the research findings, which are discussed in detail utilizing figures, tables, and graphs. The last chapter contains the conclusion of the study, recommendations, and future work suggestions.

CHAPTER TWO

2.0 LITERATURE REVIEW

2.1 Introduction

Passenger satisfaction is concerned with more than just safety and travel time. Furthermore, ride comfort is not just assessed based on the passenger's mental and physiological aspects. However, there is a widespread belief that the lack of unfavourable characteristics is the essence of comfort. The discomfort of the journey is provided by a number of various negative impacts, nevertheless, to which the passengers are subjected. These effects mostly include vehicle vibrations, noise, air humidity, illumination, temperature, and ventilation. Negative vibrations can occur during operation as a result of track abnormalities as well as wheel damage (wheel polygonization) [14]. Wheel polygonization is one of the most common wheel inaccuracies. Wheel flats aggravate this particular kind of wheel issues. Wheel flat happens when the brakes fail or when there is too much braking force compared to the amount of friction that can be achieved between the wheel and the rail. One of the key presumptions of a rail vehicle's success and popularity with both passengers and transit operators is the ride comfort [15]. For this reason, extensive analysis of measured experimental data and analysis computer simulations are frequently used.

2.2 Passenger ride comfort

Ride comfort is one of the main evaluations for the vibration level of the passenger. Thus, ride comfort evaluation is critical in order to sustain and monitor the railway company's services. However, there are no universally appropriate criteria for evaluating travel comfort because railways, vehicle condition, tracks, and operations vary per country. Therefore, the evaluation for ride comfort has to be developed independently [1], [16]. Due to local considerations, it is very challenging to develop a method for evaluating ride comfort that can be used universally, but it is still worthwhile to look into the relationships between different ride comfort indices and compare the findings [17],[18].

The evaluation of ride comfort is critical for understanding and assessing the quality and experience of a passenger on a train travel. Passenger comfort is determined by a combination of physical and psychological variables. As a result, characteristics such as vibration, temperature, acoustic noise, humidity, scent, visual stimulation, and design layout can all impact ride comfort. Vibration is regarded as the most important factor influencing user comfort; once created by train

motion, passengers are subject to it throughout the journey due to contact with the seat, backrest, and floor [19]–[22].

Oboknb and Clarke employed a questionnaire to find out how comfortable the traveler felt [23]. They acknowledged that there can be a lot of problems when interpreting the data. A delicate questionnaire and data interpretation can still be utilized to obtain useful information. A survey was undertaken by Shinkansen to determine the effects of physical characteristics on passenger comfort, including vibration, acoustics, humidity, illumination, air freshness, air pressure, seat size, etc. According to the study, air freshness, seat size, vibration, acoustics, and interior design all have a 70% link with passenger comfort [24].

In certain regions, including ISO 2631, Sperling's technique, and UIC 513, the use of vibration to estimate passenger comfort is well established. An R.M.S.-based method is provided by ISO 2631 to assess people's whole-body vibration in a variety of settings, such as a building or a vehicle that hasn't been adjusted for train passengers. Sperling's approach is better suited for comparing different vehicles. The purpose of UIC 513 is to direct the measurement of train passenger comfort using train vibration [24]–[26].

Other research examined using additional factors, such as ventilation and lighting, in addition to vibration to evaluate the comfort of train passengers. In addition to strictly mechanical metrics, biological parameters such as heart rate variation were used to determine the passenger's comfort. In order to measure the passenger comfort on a high-speed train, additional physical characteristics (air pressure, noise, humidity, illumination and temperature,) and physiological aspects (body pressure distribution, Electroencephalography, and Electromyography) were taken into consideration [27]–[29]. The use of physiological parameters to reflect human status is backed up by a lot of studies. However, because additional sensors are required and it is suspicious to invade people' privacy to collect the physical feature, using these traits to gauge passengers' satisfaction is impractical and expensive. Also, there isn't a physiological factor evaluation criterion that can be used everywhere.

2.2.1 Factors affecting ride comfort

The following are some factors that affect the comfort of passengers in railway transport:

(a) Vibration

Every means of transportation has vibration. Additionally, it has a significant impact on passenger comfort. Vertical and lateral vibrations are the two main categories of vibration. People are greater lateral vibration sensitivity. The recommended lateral vibration to vertical vibration ratios are 0.7 and 0.3, respectively[30].

(b) Area per capita in a passenger coach

Passenger coach area per capita is a factor that directly impacts passenger travel comfort during the rail transport process, and a large space per capita for passengers signifies good passenger travel comfort. The specific standards for each method of transportation are explicitly established in the design specifications[30], [31].

(c) Pressure changes

During train operation, the air pressure in the passenger coach will fluctuate, and severe pressure changes can make passengers uncomfortable or even harm their bodies, such rupturing an eardrum[30], [31].

(d) Noise

In the passenger coach, noise levels are typically higher at high speeds. Passengers' health could be negatively impacted by noise pollution, which can cause hearing loss, headaches, and neurasthenia. The link between speed and noise in a train's operation is linear; for every 10 km/h increase in speed, the noise level rises by 1-2 dB. Each type of transportation method has a maximum noise level cap. If the train is running at 80 km/h, the passenger coach noise level shall be kept at no more than 68 dB. The International Union of Railways (UIC) mandates that passenger train noise levels not rise above 65 dB [30], [31].

(e) Passenger travelling time

According to ergonomics study [18], [30]–[32], passengers will become uncomfortable if the trip lasts longer than 6 hours. Train delays can happen, which can be uncomfortable for travelers.

(f) Temperature

In recent years, air conditioning systems have been installed in most passenger coaches. There is a significant temperature difference between the passenger coach and the outside environment, according to reports from passengers. Poor ventilation and air conditioning can cause passengers' aches and pains, including dizziness, sneezing, weariness, memory loss, and muscle and joint pain. The IS07730 temperature setting standard, which mandates a 21–24 °C range for human thermal comfort, is extensively used in European nations. Additionally, the ASHRAE55-92 standard adopted in the USA mandates a temperature range for thermal comfort of 20 to 23.6 °C. However, the set thresholds for human skin's perception of heat and cold are 20–25 °C[18], [30].

2.3 Methods for analyzing ride comfort

Peter outlines three methods for assessing ride comfort that are based on vibration data collected from an in-service railway vehicle running on a rail track.

- Vibrational level equivalent (L_{aeq})
- Ride comfort index (Wz)
- EN 12299 (according to ISO 2631)

2.3.1 Equivalent level of vibration

Vertical and lateral acceleration signals are filtered in the frequency region, and vibration levels are calculated for 1-second intervals using the following expression [33]:

$$L_a = 20\log_{10}\left(\frac{a}{a_0}\right) \tag{2.1}$$

Where L_a is the level of acceleration in dB, a is the effective value of acceleration (m/s^2), and a_0 is the reference acceleration of 10^{-6} m/s^2. The equivalent level is calculated for some railway track section based on time segments, taking into account the energy level by the following expression;

$$L_{aeq} = 10\log_{10}\left[\frac{1}{N}\left(10^{\frac{L_{a1}}{10}}+10^{\frac{L_{a2}}{10}}+10^{\frac{L_{a3}}{10}}+\ldots+10^{\frac{L_{aN}}{10}}\right)\right] \tag{2.2}$$

Where L_{aeq} is the equivalent level of vibrations for segment along the line expressed in dB, N is the number of second intervals that is taken into account, L_{a1} to L_{aN} is the second level of vibrations at any point on the track.

The indices I_c and I_q are calculated by ranking the observed segments of the line on a scale of 0 to 1, based on the entire network rating (0 being the network section with the least vibrations and 1 being the network section with the highest vibrations), taking into account the average L_{aeq} from all the measured signals responsible for ride quality or ride comfort.

2.3.2 Ride Index (Wz)

Sperling's Wz ride index method [6], [14], [20], [22], [34]–[36] is used to assess the ride quality and comfort of railway vehicles. When evaluating ride quality, the vehicle itself is taken into account. Ride comfort implies that the vehicle should be evaluated based on the impact mechanical vibrations have on the occupants. Because it is determined as a function of the level of vehicle vibrations, the ride index Wz provides information on dynamic behavior of the vehicle, which enables identification of solutions for improving dynamic performance of the vehicle in terms of ride quality and ride comfort. Table 2.1 shows the ride comfort evaluation scale.

Table 2.1: Comfort index evaluation scale [5]

$W_z < 1.5$	Very comfortable
$1.5 \leq W_z < 2.5$	Comfortable
$2.5 \leq W_z < 3.5$	Medium
$3.5 \leq W_z < 4.4$	Uncomfortable
$W_z > 4.5$	Very uncomfortable

This vibration analysis technique necessitates the processing of data at acceleration rates of up to 30 Hz. The method's value is in its simplicity and ability to constantly monitor Wz index along the track, thereby pointing out track irregularities. The ride index Wz is weighted based on the frequency range using the formulas below.

$$Wz = \sqrt[10]{a^3 \times B^3} \quad \text{(Minorća hoda)} \tag{2.3}$$

$$Wz = \sqrt[6.67]{a^3 \times B^3} \quad \text{(udobnost vožnje)} \tag{2.4}$$

Where B represents a weighted factor and is calculated for ride quality, according to the following expression:

$$B(f) = 1.14 \times \sqrt{\frac{[\,(1-0.056f^2)^2 + 0.645f^2 + (3.55f^2)\,]}{[(1-0.252f^2)^2 + (1.547-0.000444f^3)^2](1+3.55f^2)}} \tag{2.5}$$

The ride comfort weighted factor B is calculated according to expression below:

$$B(f) = k \times \sqrt{\frac{1.911f^2+(0.25f^2)^2}{(1-0.277f^2)^2 + (1.563f-0.0368f^3)^2}} \quad (2.6)$$

Where k = 0.588 for vertical vibrations (B_s), and k = 0.737 for lateral vibrations (B_w).

2.3.3 Ride comfort assessment according to EN 12299

The European Committee for Standardization CEN/ TC256/WG7 is preoccupied with passenger ride comfort. The European pre-standard ENV 12299 was released in 1999. The standard for measuring and evaluating ride comfort was revised and ultimately adopted as a European standard in 2009 [33]. Two methods are suggested as a foundation for determining ride comfort:

- Indirect measurement: measuring the motion environment using various motion quantities such as acceleration or roll velocity.
- Direct measurement: Measuring actual passenger responses, such as by having passengers fill out a questionnaire.

EN 12299 defines five different comfort evaluation technique methods:

- Continuous comfort C_{CX}, C_{CY} and C_{CZ},
- Mean comfort standard method N_{MV},
- Mean comfort complete methods N_{VA} and N_{VD}
- Comfort on discrete events P_{DE}
- Comfort on curved transitions P_{CT}

Each technique specifies the vehicle condition, accelerometer position, test speed, test sections, pertinent time intervals, and so on. Acceleration signals are filtered through band-pass or low-pass filters and weighted against Wc and Wd curves for lateral and longitudinal motion (curves are the same as in ISO 2631-1 [33]), while the low-pass filter Wp (used in PCT and PDE methods) and the weighting curve W b for vertical direction are specially designed for railway applications. Post-processing is also specified for each method. It entails sliding window computations, RMS calculations, averaging, statistical analysis, and so on.

2.3 Car body vibration

Vibration is the major factor that contributes to ride comfort. Vibration is either localized vibration or vibration that affects the whole body [37], [38]. Localised vibration happens when a person holds a vibrating object that only affects the arm and hand. Whole body vibration is a result of vibration that would affect the whole body of the exposed person, which is usually transmitted through seats, backrests, and throughout the floor while standing or lying down [16]. Rail car body movements are conveyed to the human body via contact points based on passenger position as shown in Figure 2.1 [5]. Standing position that has floor-feet and seated position that includes headrest-neck, armrest-arms, seat-hip, backrest-back, floor-feet.

Figure 2.1: Interfaces points [5]

Carlbom et al. in 2019 conducted a thorough analysis of the train vehicle's carbody structural dynamics. A Swedish commuter bus is used as a case study for the simulations and observations. The research looks at the structural flexibility of the carbody and how it affects ride quality. Up to 20 Hertz of vibrations are taken into account. The structural flexibility of the carbody has the greatest impact in this frequency band. In some instances, the comfort weighted rms values of the vertical vibrations are nearly half explained by the structural flexibility of the carbody [39], [40].

2.4 Wheelset structural flexibility

A standard wheelset comprises of two conical wheels securely coupled to a wheelset axle, axle-boxes mounted via roller bearings on the two axle ends, and braking discs mounted either on the

axle or on the wheel. In the instance of a powered wheelset axle, a gear wheel is attached to the wheelset and a gear-box is attached to the wheelset axle via a roller bearing

The wheelset of a railway vehicle is an important component. It aids in the delivery of longitudinal forces via the main suspension, supports the car while rolling, and regulates the transfer of longitudinal forces during braking and, in the case of a powered wheelset, traction. According to Peng et al. 2019, the wheelset is by far the most significant component in terms of running behavior and elastic deformation in the frequency range of 50-500 Hz. Natural frequencies and structural elasticity are characteristics of wheelsets, as well as other mechanical systems. The wheelset deforms due to its dead weight when subjected to external pressures. The majority of the dynamic contribution to the wheel-rail forces was supplied by irregularities in the wheels and tracks [41]. Figure 2.2 shows an example of wheelset flexibility modes.

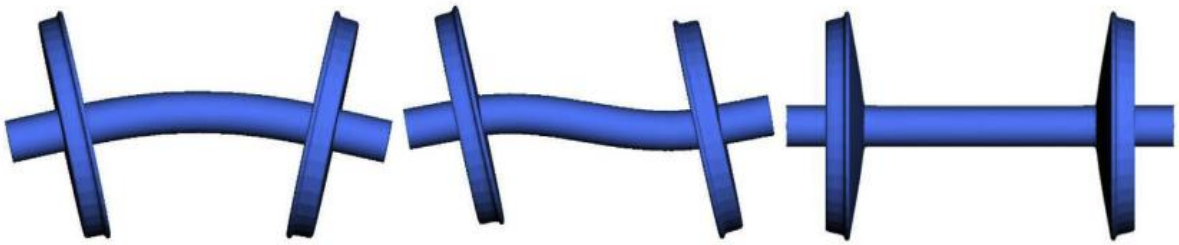

(a) The 1st bending mode (71Hz) (b) The 2nd bending mode (136HZ) (c) The umbrella mode (288Hz)

Figure 2.2: Flexible mode shapes of the wheelset[41]

2.4.1 Flexible wheelset model

Most scholars agree that wheelset flexibility should be measured in the mid- and high-frequency ranges (50-500 HZ and 500-20k HZ, respectively), because it can influence vehicle-track dynamic behavior [41]–[43].

The flexible wheelset model was meshed in the current research using a 3D solid element with eight nodes. The commercial program ANSYS was used to calculate the natural frequencies and eigenmodes. The wheelset's modes were extracted in a frequency range of up to 500 Hz. The total amount of nodes and elements was 433206 and 101268 [44], [45]. Figure 2.3(a) depicts the flexible wheelset's mode shapes, which can be classified into three types based on their deformation features: torsional mode (TM), bending mode (BM), and umbrella mode (UM). Furthermore, the black wire frame symbolizes an undeformed configuration.

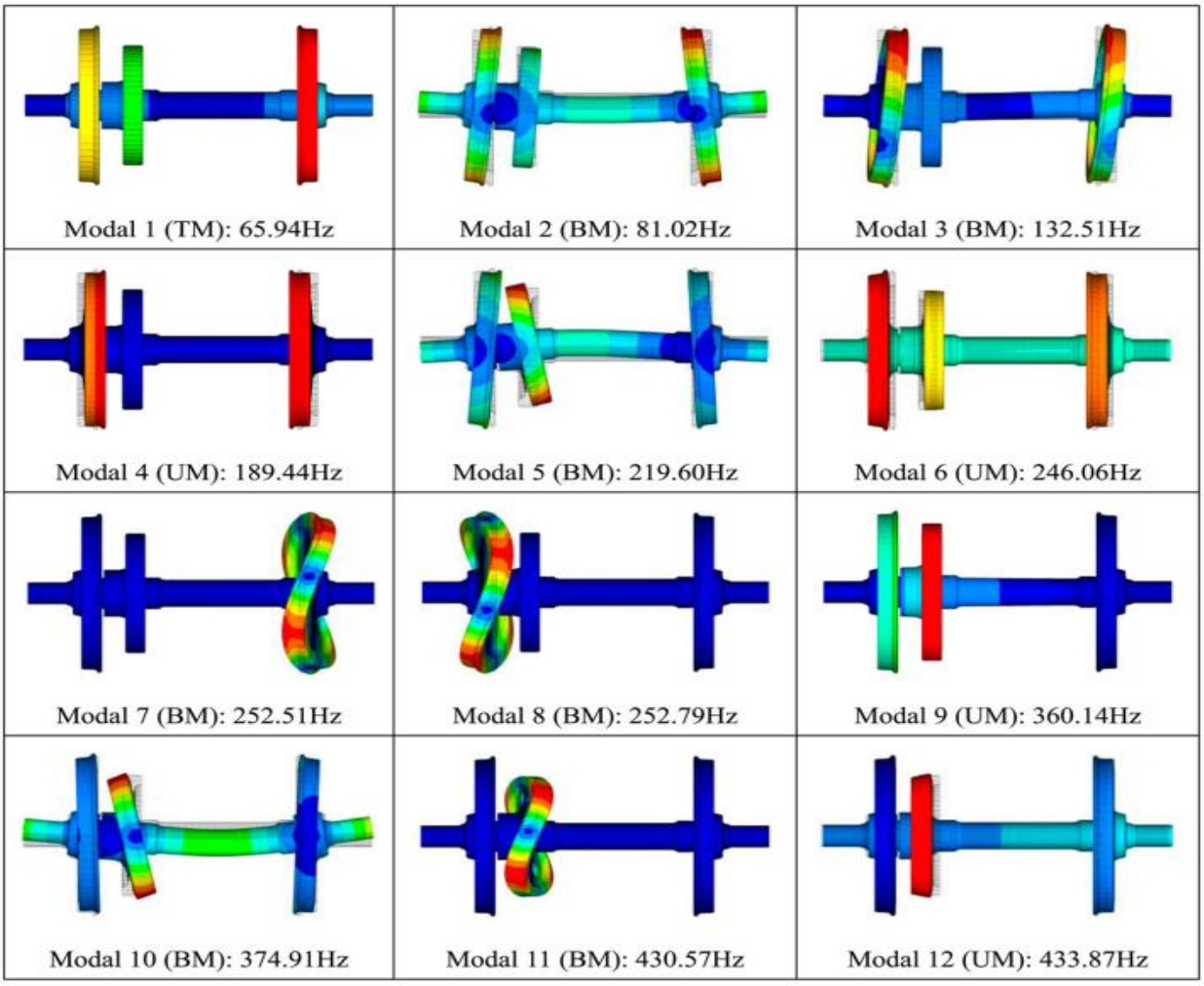

(a)

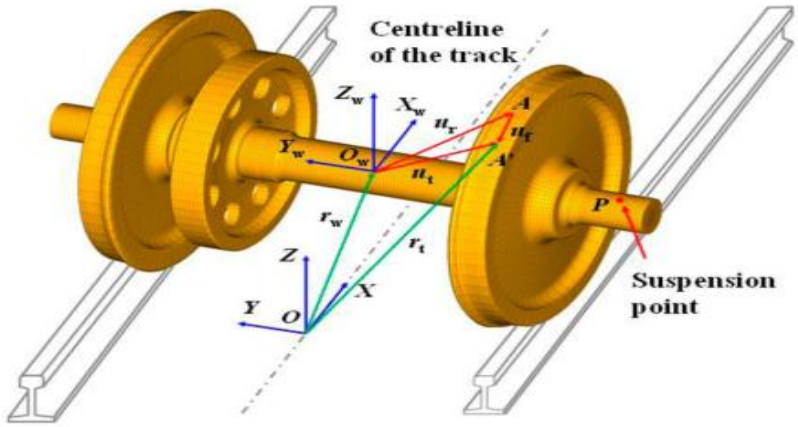

(b)

Figure 2.3: (a) Eigen modes of the wheelset and (b) Transformation of the coordinate system [45]

Figure 2.3(b) clearly depicts the technique for calculating elastic deformation. Two reference coordinate systems are specified when the running condition on a tangent track is taken into account. The global absolute coordinate system O-XYZ is fixed along the track's centerline, whereas the floating coordinate system O_w-$X_wY_wZ_w$ travels along with the wheelset. Before deformation, random point A of the wheelset has a location vector u_r in O_w-$X_wY_wZ_w$. The small elastic deformation u_f causes this point to shift to A'. As a result, the ultimate position vector r_t in O-XYZ is as follows:

$$r_t = r_w + Tu_t = r_w + T(u_r + u_f) \tag{2.7}$$

Where r_w is the rigid displacement vector of the wheelset and T is the time-dependent transformation matrix that specifies the wheelset's orientation in O-XYZ. It can be expressed as [45];

$$T = \begin{bmatrix} \cos\varphi_w & \sin\varphi_w & 0 \\ -\cos\theta_w \sin\varphi_w & \cos\theta_w \cos\varphi_w & \sin\theta_w \\ \sin\theta_w \sin\varphi_w & -\sin\theta_w \cos\varphi_w & \cos\theta_w \end{bmatrix} \tag{2.8}$$

Where θ_w is the rolling angle and φ_w is the yawing angle of the wheelset.

As a result, the velocity vector of point A' can be easily obtained by differentiating with regard to Equation (32) as follows:

$$\dot{r}_t = \dot{r}_w + \dot{T}(u_r + u_f) + T\dot{u}_f \tag{2.9}$$

Similarly, the acceleration vector of point A’ is the derivative of the velocity vector. Thus, the acceleration vector can be expressed as

$$\ddot{r}_t = \ddot{r}_w + \ddot{T}(u_r + u_f) + 2\dot{T}\dot{u}_f + T\ddot{u}_f \tag{2.10}$$

According to equation (2.7), the displacement A’ is the superposition of large rigid motion and small elastic deformation. The elastic deformation equation can be expressed below as

$$M_f\ddot{u}_f + C_f\dot{u}_f + K_fu_f = F_f \tag{2.11}$$

Where M_f, C_f and K_f are the mass, damping and stiffness matrices respectively which can be extracted using ANSYS and F_f is the total external force associated with the floating coordinate system $O_w – X_wY_wZ_w$.

2.4.2 Railway Wheels

Railway wheels are the most important component of rolling stock. Because all of the stresses and weight of rolling stock are transferred to tracks via the wheel, railway wheels are the most stressed components of railway vehicles, and optimal design and material selection must be taken into account [46]. During the train operation the wheel subjected to constant wear process because wheels are important in guide the train on tracks either on straight track or the curves, also the wheel are responsible for the train to pass through the switches and crossing safely. Figure 2.4 below shows the wheel nomenclature.

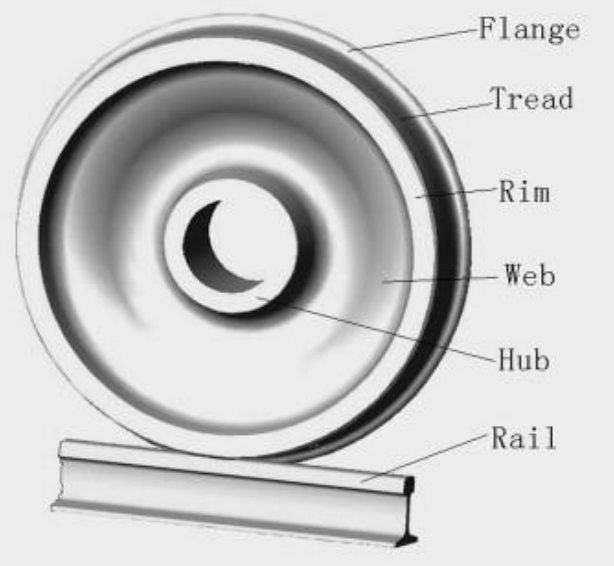

Figure 2.4: Wheel nomenclature [47]

2.4.3 Wheel-Rail Contact Mechanics

The location of the wheel-rail contact, which is usually 1 cm in size, fluctuates as a train proceeds down a section of track [48], [49], [50]. The precise location is determined by the wheel and rail profiles, as well as the track's curvature, whether the wheel is the leading or trailing wheelset on a bogie, and other characteristics specified by the bogie design. However, in straight track, the wheel tread and rail head are likely to come into contact, whereas in curved track, the wheel flange and rail gauge corner will come into contact. Three distinct locations of wheel-rail contact have been described as indicated in Figure 2.5; Region A - Wheel tread-rail head: This is where the wheel-rail contact occurs most frequently, and it generally happens when the railway vehicle is traveling on straight tracks or curves with an extremely large radius. The contact stresses and lateral forces

are the lowest in this area. Region B -Wheel flange-rail gauge corner: This region is substantially smaller than region A, and it's generally much more severe. Contact stresses and wear rates are often substantially greater. Two-point contacts, where the tread and flange make contact, may develop if there is a lot of wear and material transfer. Region C - Contact between field sides of wheel and rail: Contact is unlikely to occur here, but if it occurs, severe contact stresses are created, resulting in unfavorable wear characteristics and inaccurate steering of the wheelset.

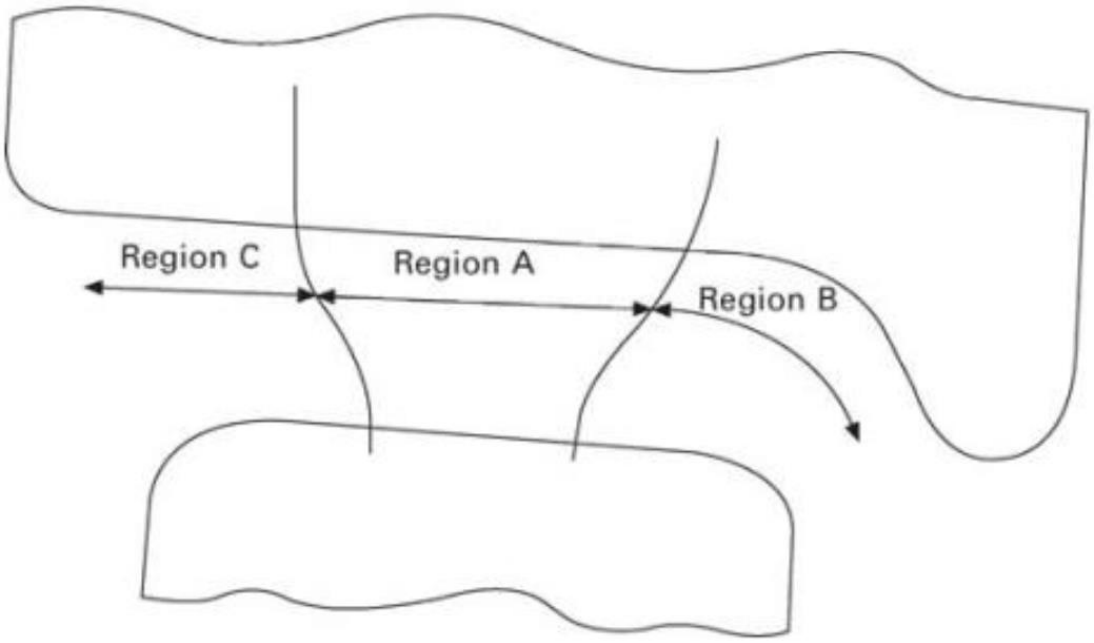

Figure 2.5: Wheel rail contact region [47]

2.4.5 Hertz Contact Theory Mathematical Equation

It is critical to measure the accurate stress analysis for rail-wheel in order to predict the fatigue of wheels. In general, the Hertz contact theory is important for predicting rolling contact stress; however, this method has less accuracy for rolling contact stress results when a large number of stresses develop [51]. To calculate a number of contact areas and pressure distributions, it is necessary to understand the main formula by Hertz theory [52]. Kim (2014) [52] stated that the Hertz contact theory takes the radius of curvature of the rail and wheel profiles in contact as a constant and assumes no plastic deformation in the contact area.

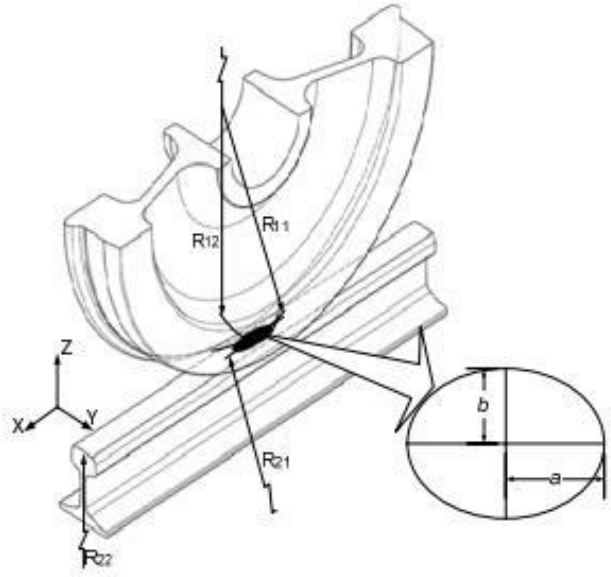

Figure 2.6: Rail-wheel contact of elliptical [51]

Figure 2.6 depicts an elliptical rail-wheel contact with labeled dimensions x,y,z. To find the value of the normal pressure distribution p(x,y), use the formula [44], [53], [54]:

$$P = p_0 \sqrt{(1 - \frac{x^2}{a^2} - \frac{y^2}{b^2})} \tag{2.12}$$

a-x longitudinal direction for half-length width contacts area and b- y lateral direction half width contact area

$$a = m(\frac{3\pi}{4} \times p \frac{K_1+K_2}{(A+B)})^{\frac{1}{3}} \tag{2.13}$$

$$b = n(\frac{3\pi}{4} \times p \frac{K_1+K_2}{(A+B)})^{\frac{1}{3}} \tag{2,14}$$

To compute the rail-wheel contact areas, it is necessary to acquire the actual measurement of geometric constants for use in the above mathematics formula. The following are the curve combinations: [44], [53], [54];

$$A+B= 0.5 \times (\frac{1}{R_{11}}+\frac{1}{R_{12}}+\frac{1}{R_{22}}+\frac{1}{R_{21}}) \tag{2.15}$$

$$B-A= 0.5 \times [(\frac{1}{R_{11}} - \frac{1}{R_{12}})^2 + (\frac{1}{R_{22}} - \frac{1}{R_{21}})^2 + (\frac{1}{R_{11}} - \frac{1}{R_{12}})(\frac{1}{R_{22}} - \frac{1}{R_{21}})^2 \times cos2\beta]^{\frac{1}{2}} \tag{2.16}$$

A and B are constant, R_{11} is the wheel curvature of rolling radius, R_{12} is the wheel profile of radius, R_{21} is the radius of runaway of infinity and R_{22} is rail curvature of the radius in the cross section[51].

2.5 Track irregularity

Track irregularities, also known as rail surface irregularities, can have a significant effect on wheel-rail forces and local stresses, causing structural deterioration and affecting the dynamics of railway systems [55], [56]. Typically, because of cyclic wheel-rail interactions, track degradations, rail wear, etc., track irregularities degrade at random in the spatial-temporal dimension. One of the focus areas is how to ensure the completeness of the system excitations in order to reveal the dynamic reliability of railway substructures with respect to safety, comfort, and stability [57].

In real-track circumstances, there are train flaws. Although these alterations are very slight, their impacts on the wheel-rail contact cannot be disregarded [58]. Therefore, for wavelengths between 1 m and 75 m, which correlate to wavelength intervals D1 and D2 specified by the European Standard EN 13848-2, rail unevenness profiles are generated. Therefore, PSD curves can be created to create artificial unevenness profiles based on real data. Mosleh et al. [59] offered more details about the creation of unevenness profiles. The horizontal and vertical irregularities on the right rail are represented by the four unevenness profiles of the rail in Figure 2.7.

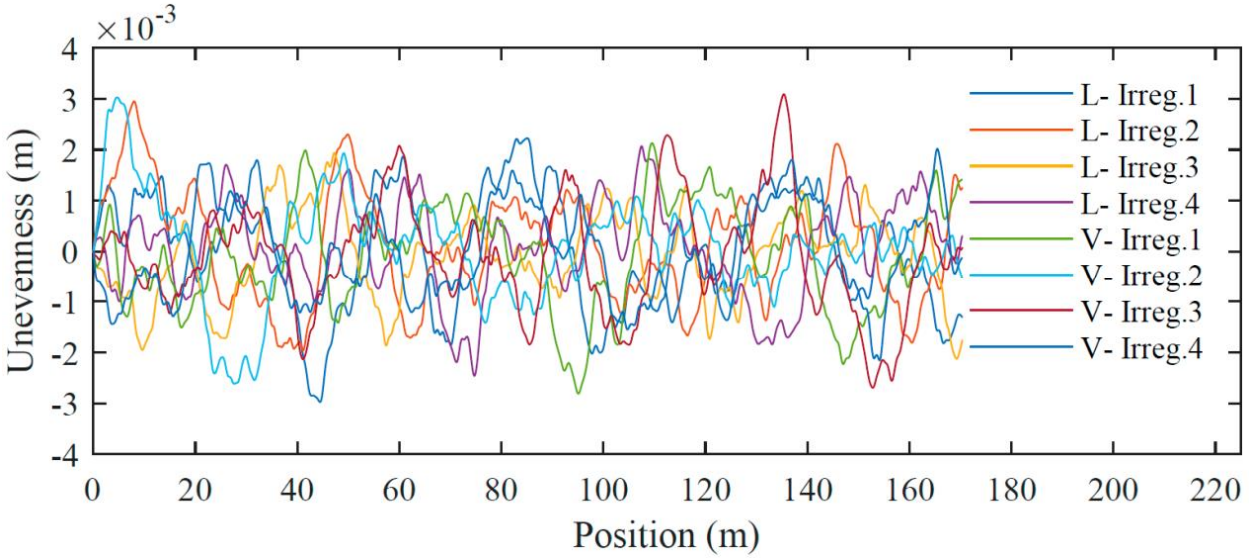

Figure 2.7: Track irregularity profile [58]

The objective of TIPM is to describe the representative vectors of track irregularity that have probabilistic properties. Typically, the track irregularity vectors can be represented as below

$$\text{Ç} = (\text{Ç}_1, \text{Ç}_2, \text{Ç}_3, \text{Ç}_4) \quad (2.17)$$

Where Ç_1, Ç_2, Ç_3, and Ç_4 are denote four types of track irregularity that is vertical profile, alignment, cross level and gauge respectively.

Track irregularities measured by a track inspection vehicle of a maintenance-of-way department may contain data accumulated from tens of thousands of kilometers denoted by S^{tot}.

$$\{\text{Ç}_i(s) = (\text{Ç}_{1,i}(s),\ \text{Ç}_{2,i}(s),\ \text{Ç}_{3,i}(s), \text{Ç}_{4,i}(s))\ i=1,2\ldots,N;\ s \in [0, S^{tot}/N\} \quad (2.18)$$

Which is assumed to pertain to a second order centered random field [55]. By assuming track irregularities as a stationary random process, the power spectral density (PSD) of $\text{Ç}_{\tilde{\Theta},i}(s)$, $\tilde{Q}$=[1,2,3,4], can be induced as the Fourier transform of the auto correlation function $R_{\tilde{\Theta},i}(\text{c})$ of $\text{Ç}_{\tilde{\Theta},i}(s)$ as;

$$P_{\tilde{\Theta}(i,\omega)} = \frac{1}{2\pi}\int_{-\infty}^{+\infty} R_{X,i}\,(\text{c}) e^{-j\omega} d\text{c},\ \omega \in [\omega_l, \omega_u] \quad (2.19)$$

Where, ω is the frequency, with ω_l and ω_u the lower and upper frequency limits respectively.

2.6 Wheel polygonization

There are three types of wheel damage that is wheel flat, wheel polygonization and out of roundness (OOR). Wheel flat caused by a blocked wheel massively sliding along the rail, wear, material transformation (Martensite), break outs and flat area. Polygonised wheel and OOR wheels caused by stick slip effects, re-profiling, dynamic wheel-set oscillations that caused by resonances in vehicle/track interaction [60]. Because of the eccentricity of the wheel motion and the rotational inertia of the wheels, a type of wear known as polygonization wear is seen on railroad wheels. This type of wear is defined by a change in the morphology of surface characteristics from circular to non-circular. However, a well-known issue for high-speed trains is the phenomena of train wheel polygons, or wheels with a certain degree of OOR. [61]. The term “wheel polygon” refers to periodic radial deviations from the ideal round shape of the circumference of the wheel [62].

In actual life, the wheels are not completely smooth and have imperfections. Despite their tiny size, these out-of-roundness irregularities can cause extreme variations in wheel-rail contact pressures, causing vibrations on the train and track components [61], [63]. The wheel

polygonization is characterized by a periodic radial tread irregularity around the perimeter. Peng [64] recommends that the uneven amplitudes for wheel polygonization be greater than 0.2 mm. Some parameters inherent in polygonization, such as the varying wavelengths (λ) as a function below of harmonic order (θ) and wheel radius (R_w), can geometrically describe the phenomenon.

$$\lambda = \frac{2\pi R_w}{\theta},\ \theta = 1, 2, 3\ldots, n \tag{2.20}$$

The sine function amplitude for each wavelength is calculated as follows:

$$a = \sqrt{2} \times 10^{\frac{L_{w\theta}}{n}} \times w_{ref} \tag{2.21}$$

Where w_{ref} = 1um, $L_{w\theta}$ can be calculated by the following function

$$L_{w\theta} = 24.7 \log_{10}(\lambda_\theta) + 8.47 \tag{2.22}$$

Figure 2.8 shows the shapes of typical polygonal wheels with different harmonic OOR orders. The technical term "harmonic order" refers to a sinusoidal radial deformation of the circumference with a specific period. The "OOR amplitude" is defined as the deviation of the radius from the nominal constant value. There is currently no explicit conclusion about the technique through which wheel polygons are produced. Nonetheless, polygonal wheels have a number of drawbacks [65], [66]. For instance, at speeds above 200 km/h, this phenomenon will result in significant vibrations that are transmitted from the wheels of the train to the compartments inside and from the rails to the track components outside, causing deterioration of the infrastructure, poor ride comfort, noise disturbance, and an increase in maintenance costs [67].

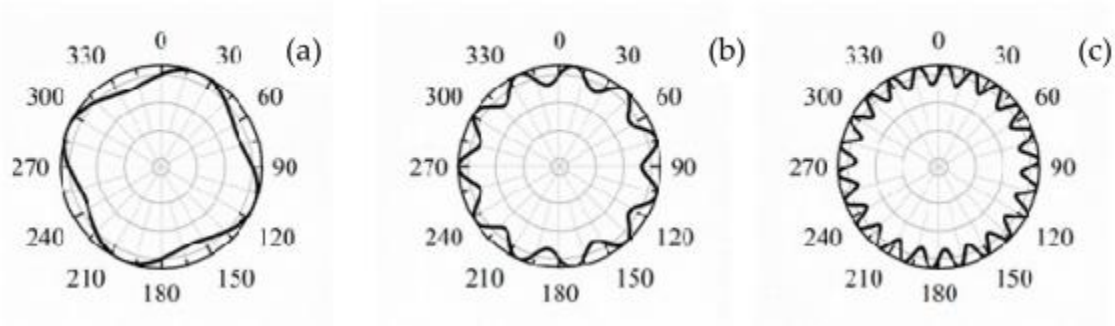

Figure 2.8: Wheel polygonizatio with different harmonic orders (a) fourth-order; (b) 11th-order; and (c) 22nd-order [67]

2.7 Articles related to research topic

In 2018, Dižo et al. studied the assessment of a rail vehicle running with the damaged wheel on a ride comfort for passengers. Through performing computer simulations of a modelled rail vehicle on a track for various excitement values and assess vehicle properties based on prescribed parameters. The passenger ride comfort was evaluated using the UIC 513 and the EN 12299:2009 standard. The ISO 2631 standard was also employed, and the grade quality running W_Z by Sperling was eventually used. Body accelerations recorded in the vertical, lateral, and finally longitudinal directions yield ride comfort criteria. However, all calculated N_{MV} indices values with the scale given in EN 12299:2009 (Table 2.1), the travelling in the analyzed passenger car is classified for as very comfortable ($N_{MV} < 1.5$) except of the case, when the wagon without the wheel-flat run at the speed of 210 km/h, where one point in front of wagon body and three in the rear part of the wagon body are classified as comfortable (values of the N_{MV} ride comfort index exceeded 1.5) [5].

Momhur et al. in 2021 studied the flexible-rigid wheelset, which introduced dynamic impacts due to the wheel tread being flat. The finite element analysis (FEA) software programme ANSYS was used to suggest the modal technique for analysing the impact of a wheel flat, which was then integrated into a multibody dynamic model of the high-speed train CRH2A (EMU) using SIMPACK. The irregularity track line emerged and was dependent on the simulation data points used. A statistical approach was also devised to examine the dynamic impact load response and effect while taking into account varying wheel flat lengths and vehicle speeds. The effect of train speed on the flat size of the vertical wheel-rail impact reaction, as well as the statistical technique, are studied using flexible and rigid wheelsets. The results imply that, in comparison to rigid wheel flats, the flexibility of the wheelset can greatly improve vertical acceleration [68].

Imran et al. in 2017 did a comparison study on the assessment of ride comfort for LRT passengers. They conducted a comparison via two possible methods which are BS EN 12299 (2009) and Sperling's Ride Index equation. BS EN 12299 standard is used to measure and evaluate the ride comfort of seating (N_{vd}) and standing (N_{va}) of train passenger in three different routes. Next, Sperling's ride comfort equation used to conduct validation and comparison between the obtained data. The outcome shows a greater degree of vibration in the vertical axis, which affects the final outcome. In all three of the evaluated routes, standing shows a higher exposure to vibration. All track sections surpass the "pronounced but not unpleasant (medium)" limit range, according to a

comparison of ride comfort assessments of passengers in a sitting and standing position for both ways. Nonetheless, the seating posture at the track portion did not exceed the restriction and remained comfortable. The highest level of pain reached for both approaches for seated position is 3.34 m/s^2 for N_{va} and 2.63 m/s^2 for S_{va}. Meanwhile, the highest level of pain achieved for both methods of standing is 3.80 m/s^2 for N_{vd} and 2.88 m/s^2 for W_z [16].

Wu et al. in 2021 carried out a numerical simulation research on ride comfort analysis using a linked track-train-seat-human model with lateral, vertical, and roll vibrations. AUTOCAD used to model the 3D and Finite element analysis was used to simulate the 3D coupled track-train-seat-human model with lateral, vertical and roll vibrations to investigate the ride comfort of high-speed trains. When employing a rigid track at high speeds, it was discovered that the overall equivalent acceleration was underestimated by over 10%, while the track flexibility had little effect on the lateral, vertical, and roll floor vibrations below 20 Hz. Because the flexibility of the carbody induced substantial floor vibration in the lateral, vertical, and roll directions above 7.5 Hz, the rigid carbody model significantly overstated the total equivalent acceleration. With an increase in speed, the total equivalent acceleration tends to rise. Equivalent accelerations for two symmetrical seat locations showed similar patterns as the speed increased. The ride comfort was lowest near the carbody ends, then at high speeds in the carbody center. Regardless of the seat position or speed, the vertical acceleration on the seat pan was the worst. The subject under examination saw a decrease in the total equivalent acceleration due to the nearby subject. The carbody damping can reduce the total equivalent acceleration effectively in the whole speed range [69].

In 2019, Suchánek et al. conducted a study to assess the comfort of passengers riding in a rail carriage using dynamic simulations. The study concentrated on the dynamic analysis in the programme SIMPACK with the rail expansion, the design of the rail vehicle in the CAD software CATIA, and the simulation analysis of a rail vehicle with an active tilting mechanism of the vehicle body. The building of standard rail vehicles is simpler than installing bodies on vehicle bogies. This kind of body mounting is used to either increase the size of the body tilt during a curve ride or so lessen the lateral unbalanced acceleration that affects the passengers, or to allow for a higher driving speed in a curve with the same radius while maintaining the lateral acceleration value. Eight different variations of velocity, vehicle occupancy, and tilting mechanism setting were examined. The vehicle's tilting mechanism was shown to have the greatest effect on passenger ride

comfort. But also, the velocity of the vehicle has the biggest impact on passenger ride comfort. The impact of the vehicle occupancy becomes evident only at higher velocities. The best passenger comfort is at the lowest speed of 87 $km \cdot h^{-1}$. From comparison of the variants, the best passenger comfort is reached in the middle of the vehicle car [7].

In 2017, Melnik et al. similar to 2018 Vaičiūnas et al. assessed the passengers ride comfort in a coach. In order to forecast ride qualities or assess proposals for ride comfort in advance, forces and accelerations in various points within the body of a rail vehicle were determined using modelling and dynamical analysis in the programme SIMPACK. Results indicated that as running pace increases, comfort quality decreases. Additionally, the location where the passenger's body is least affected by acceleration is close to the centre of the waggon (centre of gravity). Areas, which the highest values of acceleration are generated in, are in front and rear locations of the passenger car [70][71].

In 2021, Kardas et al. did an experimental study of the ride comfort of a rail vehicle passenger. Two methods were used in the study of the ride comfort of a rail vehicle passenger, based on measurements of the acceleration of mechanical vibrations. The analysis of these accelerations using the spectral method and the weighted method made it possible to assess the impact of vibrations in the tested vehicles on the sensations related to comfort. The results of experimental studies showed that low-frequency vibrations contribute to the greatest reduction in the feeling of comfort [35].

Wang et al. in 2020, did an experimental study to investigate ride comfort quality analysis for high-speed railway vehicles. The results of the tests and data processing revealed that under normal air spring conditions, the maximum values of the ride comfort index of the motor (D1) and trailer (M1) are 1.43 and 1.70, respectively, both less than 2.5, while under airless spring conditions, the maximum values of the ride comfort index of the motor (D1) and trailer (M1) are 1.94 and 2.23, both less than 3.0 [72].

Zeng et al. in 2020 investigated the effect of wheel polygonization on high-speed trains. Multi-rigid-body dynamics of a high-speed vehicle was built in SIMPACK for simulation and analysis. The findings demonstrated that high-order polygonization causes significant wheel-rail forces and vehicle vibrations, which are very damaging to safety dependability and uncomfortable ride

quality. Wheel polygonization is also influenced by the season, wheel diameter, vehicle type, and historical incidence rate, according to correlation analysis [73].

1n 2021, Dumitriu et al. conducted a study that evaluates the ride comfort at the vertical vibrations of a railway vehicle using two methods—the mean comfort technique and Sperling's method. The two systems have one thing in common: they both estimate the comfort sensation using comfort indices, particularly the ride comfort index N_{MVZ} and the ride comfort index W_z. These indexes' values are generated through numerical simulations. The given results primarily demonstrate that the two assessment methodologies produce significantly different results in terms of ride comfort under identical vehicle operating conditions [36].

Kumar et al. in 2017, investigated the impact of vibration on passenger comfort in a railroad vehicle. The study analyzed whole-body vibration in a railway vehicle by using the four-degree-of-freedom (DOF) human biodynamic model along with Sperling's index calculation. Sperling's index of a railway vehicle computed using the rigid car body model is overestimated when compared to Sperling index values derived using the flexible car body model. The acceleration response of different body sections is superimposed onto ISO curves, and it was discovered that for both flexible and stiff car body models, the reaction acceleration levels are practically below the 1 h curve up to 80 km/h [74].

Sadeghi et al. in 2019, investigated the effect of harmonic and non-harmonic rail irregularity on the rail vehicle ride comfort. A two-dimensional model of the slab-track-vehicle interaction was created. A rail, concrete slabs, concrete base layers, nonlinear wheel-rail interaction, and a vehicle comprise the model (a carbody, suspension systems, bogies, and wheels). To validate the model's outcomes, a comparison was done between the model's results and those of a comprehensive field test conducted in this study. The Sperling index (Wz) was used to represent the amount of comfort throughout the train travel. It was discovered that the wavelength of rail irregularity has a significant impact on the riding comfort of rail vehicles [75].

Chen et al. in 2021, conducted a study to evaluate ride comfort of dynamic metro vehicle considering structural flexibility. First, carbody of the vehicle and frame finite element models were created, which were subsequently reduced using substructures theory's method and the Guyan reduction method. The flexible vehicle track coupled dynamic model was developed on

this premise. The ride comfort of metro vehicles on straight and curved lines was assessed under rail random irregularity, short-wave excitation, and long-wave excitation, respectively, after a comparison of the flexible model and the conventional rigid model was examined. The results showed that the carbody accelerations calculated by the flexible model are greater than those computed by the rigid model. The flexible model clearly reflects and calculates the sensitive frequency range of humans, indicating that the ride comfort of metro vehicles may be more precisely evaluated using the flexible vehicle model [76].

2.8 Summary

Ride comfort in railway transportation is perplexing, since it is determined by a variety of dynamic performance parameters as well as subjective observations from train passengers. However, under certain circumstances, wheels on rail vehicles may sustain damage while in operation. Then, the profile of wheels is no longer circular, but it is changed depending on the type and severity of defects. When such a rail car with a damaged wheel works, the quality of a passenger's ride comfort degraded. According to the literature analysis, the research used various methodologies to analyze and evaluate the ride comfort issues. Initially, they used mathematical method (Sperling's Ride Index method). In other articles, they use finite element analysis and dynamic simulation methods.

Table 2.2: Literature summary

S/N	Authors (Year)	Objective	Methodology	Finding(s)
1.	Dižo et al. 2018 [5]	To evaluate the impact of a rail vehicle running with a damaged wheel on passenger comfort.	SIMPACK	The results revealed that the wagon running is less pleasant in wagons that do not have wheel-flats. Driving a rail vehicle with a damaged wheel at high speeds has even more detrimental consequences.
2.	Imran et al. 2017 [16]	To assess the trip comfort of LRT passengers using whole-body vibration.	Mathematical method-Sperling's Ride Index method	The ride comfort of passengers sitting and standing in both approaches suggests that all track sections surpass the pronounced but not the medium limit range.

3.	Wu et al. 2021 [69]	To investigate the ride comfort of a linked track-train-seat-human model subjected to lateral, vertical, and roll vibrations.	• CAD-AUTOCAD • FEA-ANSYS	The track flexibility was shown to have a small influence on the lateral, vertical, and roll floor vibrations below 20 Hz, but the total equivalent acceleration was overestimated by more than 10% at high speeds.
4.	Suchánek et al. 2019 [7]	Using dynamic simulations, assess the passenger riding comfort of a rail vehicle.	• CAD-CATIA • SIMPACK	Results showed that tilting mechanism of the vehicle has biggest impact on passenger ride comfort. Furthermore, it observed that, the velocity of the vehicle has also the biggest impact on ride comfort.
5.	Melnik et al. 2017 [70]	To evaluate the passenger ride comfort for a coach.	SIMPACK	The results revealed that when running speed increased, the degree of comfort decreased.
6.	Kardas et al. 2021 [35]	To study the ride comfort of a rail vehicle passenger.	• Spectral method • Weighted method	The results showed that low-frequency vibrations contribute to the greatest reduction in the feeling of comfort.
7.	Wang et al. 2020 [72]	To investigate ride comfort quality analysis for high-speed railway vehicles.	Experimental method	The results revealed that the maximum value of the ride comfort index is 1.70 under standard air spring conditions, and 2.23 under airless spring conditions.
8.	Zeng et al. 2020 [73]	To study the failure effects of wheel polygonization on high-speed trains.	SIMPACK	According to the findings, high-order polygonization causes considerable wheel-rail forces and vehicle vibrations, which are both adverse to safety reliability and ride pleasure.
9.	Dumitriu et al. 2021 [36]	To evaluates the ride comfort at the vertical vibrations of a railway.	Numerical Simulation	The given results primarily demonstrate that the two assessment methodologies produce significantly different results in terms of ride comfort under

				identical vehicle operating conditions.
10.	Kumar et at. in 2017 [74]	To investigate the impact of vibration on passenger comfort in a railroad vehicle.	Dynamic simulation	Sperling's index of a railway vehicle computed using the rigid car body model is overestimated when compared to Sperling index values derived using the flexible car body model.

2.9 Research gap

The research mentioned above makes it clear that wheels on rail vehicles might sustain damage while in use under specific circumstances. Currently, it appears that railway wheel polygonization must be a fixed-frequency issue. In particular, there must be some structural modes of the dynamic vehicle/track system that can be stimulated to start the polygonization of the wheels at specific speeds and with specific ordering. However, no study was done to investigate the effect of rail vehicles moving with wheel polygonization on AALRT passenger ride comfort by considering vehicle speed, track irregularity, and variable load. Most studies investigated the effect of wheel polygonization on high-speed trains. As a result, insufficient attention has been paid to the wheel polygonization of dynamic behaviour, particularly passenger ride comfort on the light rail train. This study addressed the role played by vehicle speed, track irregularity, flexible wheelset, vehicle carrying loads, and wheel polygonization amplitudes and orders on light rail train ride comfort.

CHAPTER THREE

3.0 METHODOLODY

3.1 Introduction

In this study, the first step was developing flexible wheelsets by SOLIDWORKS and import it in FEM. The outcome of the finite element analysis will serve as an input for SIMPACK. The flexibility is connected to the surrounding multi-body system using the master node. By specifically choosing the nodes of the reduced finite element model, this subset of the master node is determined during reduction in the FE code.

In the second stage, the commercial software program SIMPACK first presents a standard AALRT multi-vehicle model. In SIMPACK, a flexible body of wheelsets were created. For importing the flexible body into SIMPACK, the cdb file comprises the physical and structural data from finite element software (ANSYS). In order to define a flexible body in the body properties, it is necessary to transform FE output data into flexible body input (.Fbi) files.

Track irregularity data that was obtained from the AALRT maintenance office was imported into the model. The impact of flexible wheelset polygonization and track irregularity on passenger ride comfort was investigated using the aforementioned methodology. Additionally, the impact of vehicle loading case and vehicle speed on passenger comfort was studied.

The research carried out by identifying the effects of wheel polygonization, vehicle speed, and vehicle carrying load on passenger ride comfort through analysis the railway ride index. Four cases during dynamic simulation was considered. i.e., running a rail vehicle with its maximum operation speed (70km/h) without polygonal wheel, running a rail vehicle with its maximum operation speed by varying the number of wheel polygons, running a wheeled polygonal rail vehicle at different speeds and running a wheeled polygonal rail vehicle at a designed speed by varying the vehicle carrying loads. The simulation helped to analyze the railway ride index. Hence the following methods was followed as shown in Figure 3.1.

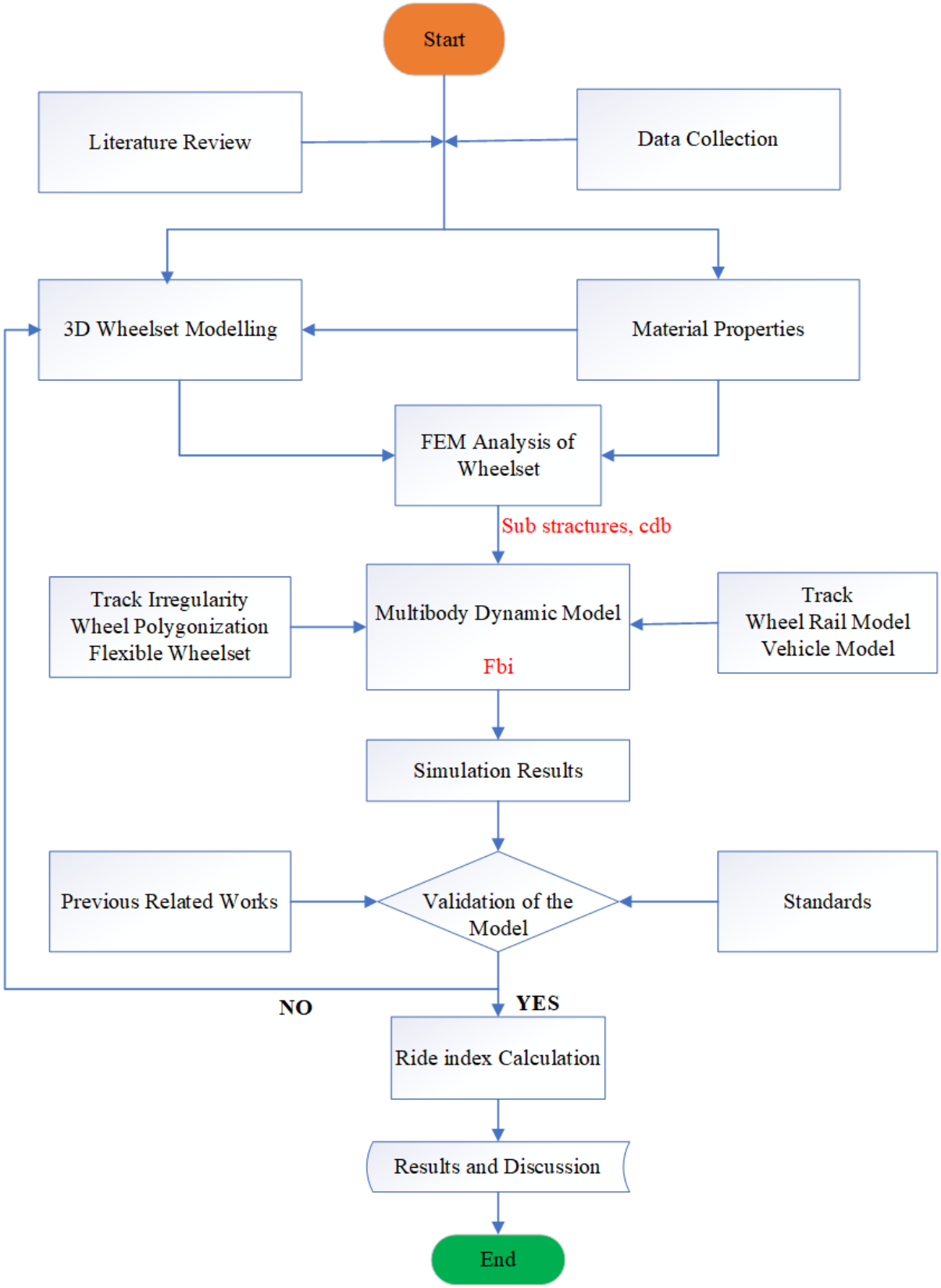

Figure 3.1: Methodology flow chart

3.2 Data collection

Primary and secondary data used in this research from Addis Ababa Light Rail Transit and literature review respectively. Primary that collected were dimensions of rail vehicle, axle load and mechanical properties. The literature review for secondary data included existing published research, conference papers, proceedings, reference book, etc. International standards also was used i.e., EN 12299:2009 and ISO 2631. See Appendix A for some of the primary data from Addis Ababa Light Rail Transit technical sheet).

Axle load and weight of the vehicle

Table 3.1: Passenger's carrying capacity of AALRT vehicle (source: Addis Ababa Light Rail Transit technical sheet).

Number of passengers	Seated	Standing	Total
Level seats	65	0	65
Rated passenger capacity (standing -6 people/m^2)	65	189	254
Overload passenger capacity (standing -8 people/m^2)	65	252	317

Table 3.2: Vehicle weight (source: Addis Ababa Light Rail Transit technical sheet).

Loads	Vehicle weight (t)	Passenger weight (t)	Total weight (t)
Empty	44	0	44
Rates passenger capacity	44	15.24	59.24
Overload passenger capacity	44	19.02	63.02

Note that, 60kg as the average of each passenger weight

Table 3.3: Axle load (source: Addis Ababa Light Rail Transit technical sheet).

	Axle load (t)	Axle load (kN)	Load at the wheel (kN)
Empty	7.33	72	36
Rates passenger capacity	9.873	96.8	48.412
Overload passenger capacity	10.5	103	51.5

3.3 Flexible wheelset model analysis

In the original multibody system approach, wheelsets are assumed to be rigid structures, which means that no body deformations are taken into account. This assumption is a useful simplification for many applications. However, an extension of the modeling may be required in some circumstances, particularly when significant deformations of the component represented by the body are expected. When the forces operating on the component are large in contrast to its structural stiffness, or when the frequency of the forces is close to the structural Eigen frequency, structural vibrations are excited, larger deformations might occur.

The 3D wheelset geometry was modeled in SOLIDWORKS, but meshing and master node selection were formulated and calculated using the finite element method. The structural flexibility of a wheelset as a flexible body in a multibody system has become well-described using FEM. The FE mesh nodes of a flexible structure's deformation serve as a representation of the structure's deformation [77]. In general, the nodes perform translations in all three directions. The flexible body is coupled to the surrounding multibody system via a subset of nodes called master nodes in SIMPACK. During the reduction phase, this subset of master nodes is determined in FE software by explicitly choosing the nodes of the reduced finite element model. Substructure analyses in ANSYS mechanical ABDL are a means to reduce the size (degrees of freedom) of the FE model so that it may be included into the MBS software.

3.3.1 Analysis of the mechanical ABDL model's substructure

A process known as sub structuring reduces a collection of finite elements into a single element that is represented as a matrix and is referred to as a "super element," which helps to save computer time and enable the solution of very complex problems using a minimal amount of computing power. Condensation is achieved by defining a group of master degrees of freedom, which are mostly employed to define the interface between the super element and other elements and to capture dynamic features for dynamic analysis [41]. The procedures for carrying out substructure analysis on a wheelset structure are shown in Figure 3.2.

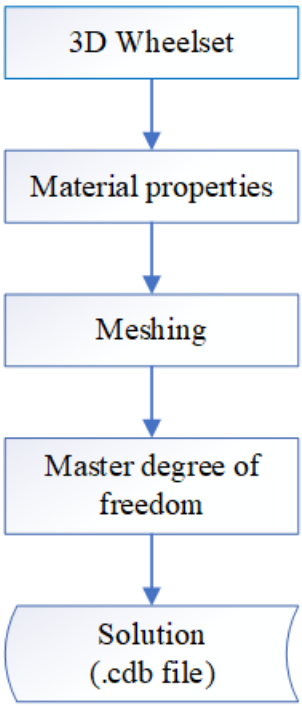

Figure 3.2: Steps for substructure analysis

i. To create wheelset geometry, a 3D model was generated in SOLDWORKS software according to the S1002 wheel profile [78], [79] as shown in Figure 3.3 (for more details, see Appendix B). It is then imported to ANSYS in parasolid format.

Figure 3.3: A 3D geometry of a wheelset

ii. The material property of the wheelset is shown in Table 3.4.

Table 3.4: Wheelset mechanical properties (source: Addis Ababa Light Rail Transit technical sheet).

	Type	**Young modulus**	**Poisson's ratio**	**Density**
Wheelset material properties	ER7	210GPa	0.3	7850kg/m

iii. The discretization of the model into elements and nodes is referred to as meshing. It should be noted that the higher the mesh density, the more accurate the results. However, this comes at a larger cost in terms of simulation time and resources. The model was meshed using 10mm solid elements of the tetrahedral type. Appendix B shows in detail that the final total element was 873821 and 1250311 nodes.

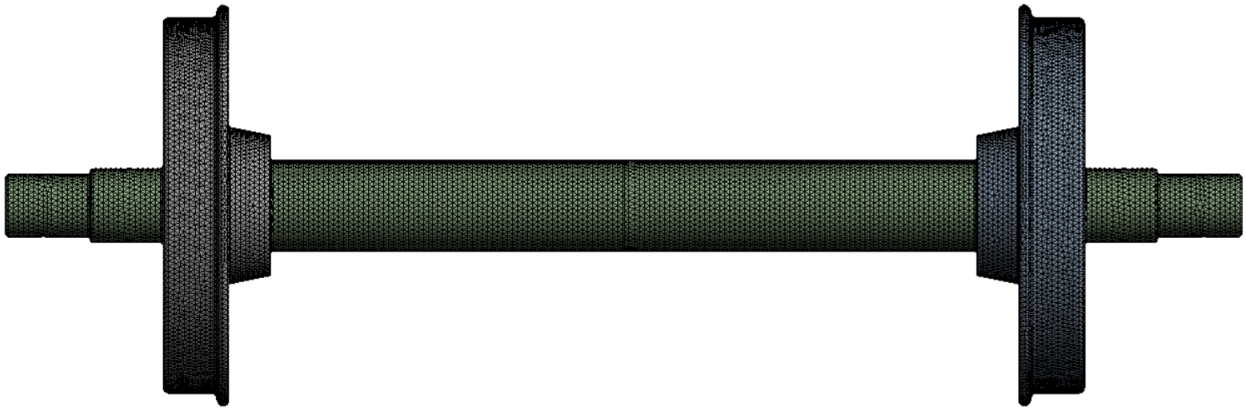

Figure 3.4: Meshing the wheelset

iv. The master degrees of freedom required in this scenario are the degrees of freedom that connect the wheel and rail to capture the dynamic features, which are located in the wheel circumference in the contact patch area, as illustrated in Figure 3.5-3.6.

v. The finite element model should then be solved. The geometry and 14376 numbers of the master meshed nodes are kept in the cdb and substructure files that are obtained from the solution output.

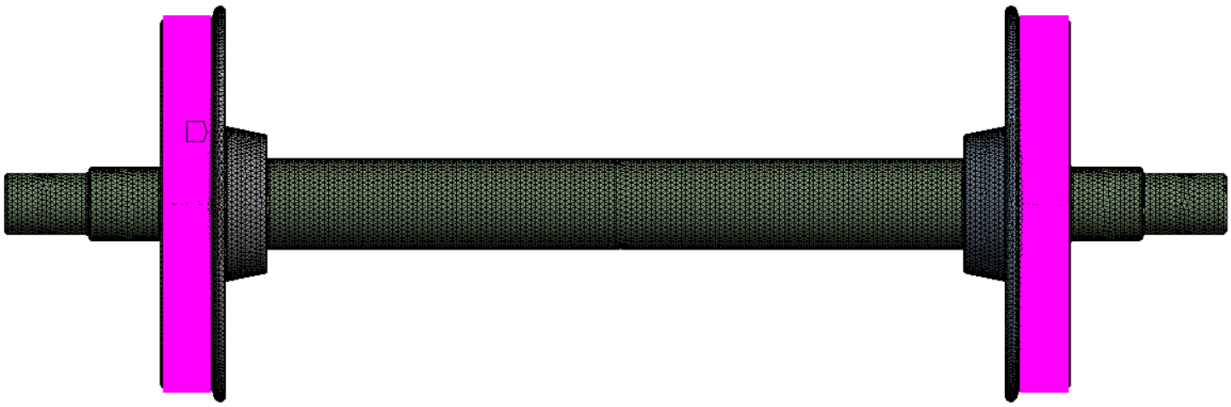

Figure 3.5: Location of master nodes in the wheel circumference

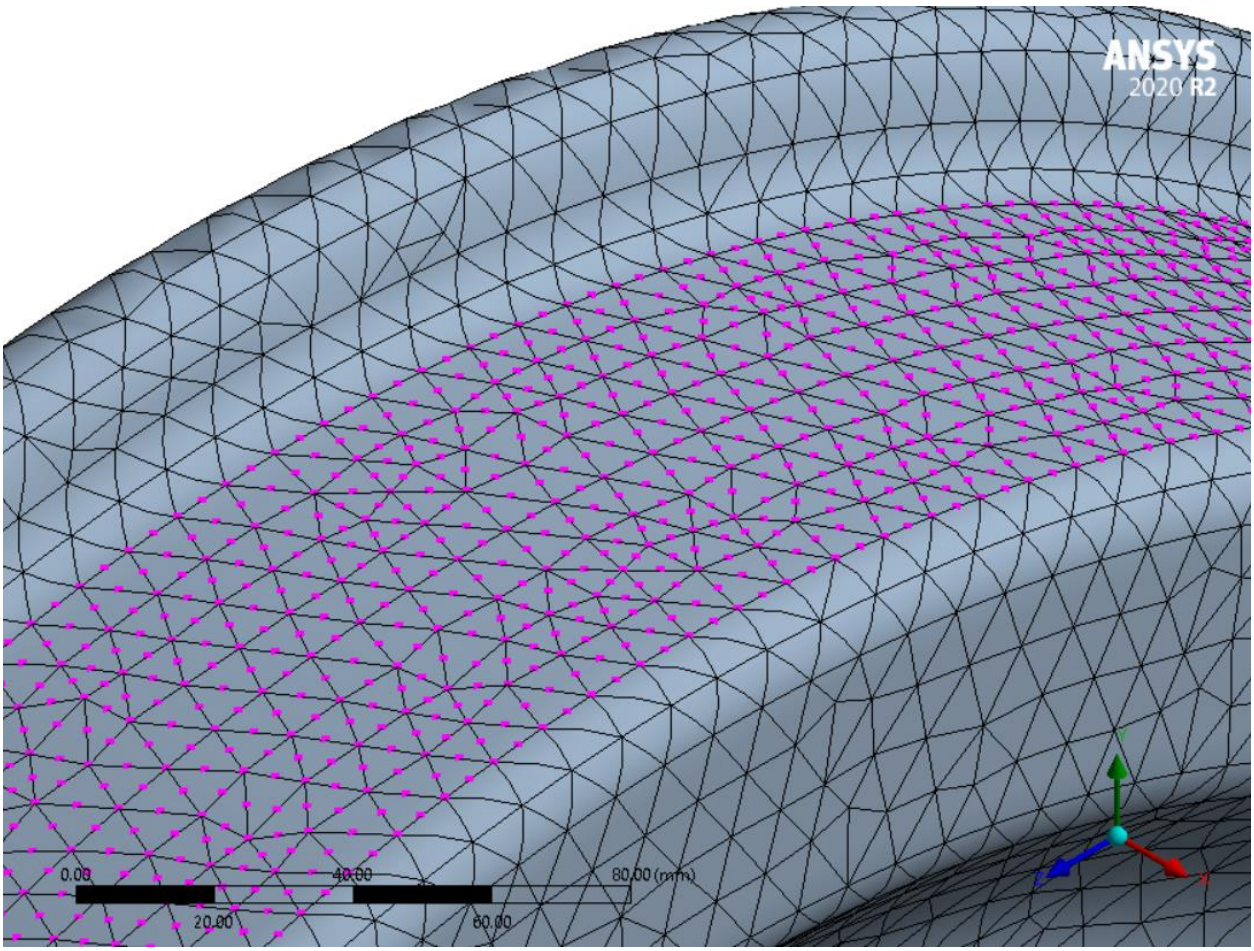

Figure 3.6: Location of master nodes on the wheel

3.4 Multibody dynamic of a rail vehicle model

The vehicle model used for this study is the Addis Ababa Light Rail Transit vehicle that is used to transport passengers in the capital city of Ethiopia. The AALRT vehicle is hinged on three car bodies and has a maximum operating speed of 70 km/h, though the designed speed is 80 km/h.

It is necessary to construct a proper model in order to carry out the computer simulations. Various Multi Body Simulation software programs could be used for this. The SIMPACK rail module program, one of the most well-known pieces of software that is widely utilized in both the academic and industry worlds, is employed in this study. It should be noticed that SIMPACK is utilized by the Pre and Post-Processor modules.

3.4.1 Mathematical model

Each vehicle of AALRT has three cars as shown in Figure 3.7. The car's body is modeled as a rigid body with mass M_c and moments of inertia I_{cx}, I_{cy}, and I_{cz} along its x, y, and z axes, respectively.

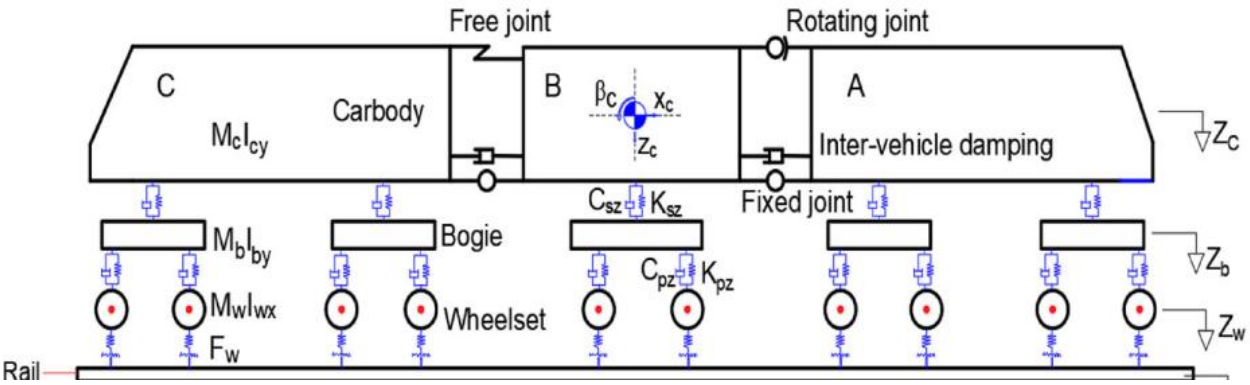

Figure 3.7: AALRT vehicle-track coupling dynamic model [42]

The vehicle is driven by the motor bogies under car bodies A and C. The car bodies are resting on the secondary springs, which are attached between the bogie and car body. The front and rare motor bogies are connected with a solid normal axle, and the trailer bogie is connected with independently rotating wheels. Double secondary suspension systems are used to attach the motor bogies and the trailing bogies. Between the wheel beam and bogie are attached cylindrical rubber springs that serve as the primary suspension. Standard coil springs and dampers are used for the secondary suspension, and they are mounted between the bogie and the car body. The wheels can freely rotate in relation to one another because each is independently fastened to a beam by a rigid journal box. Two wheels are driven by one motor via one axle. Depending on the design of the

track, a differential distributes the torque from the electric motors to the wheels in a different way [42]. Based on the theory of multi body dynamics (MBD), locomotive differential equations can be represented as uniform expressions [45].

$$M\ddot{u} + C\dot{u} + Ku = F_t \tag{3.1}$$

Where M, C, and K are the locomotive system's mass, damping, and stiffness matrices, respectively, u is the rigid displacement vector, and F_t represents the generalized forces exerted on the locomotive.

The bounce z_c and pitch θ_c represent the carbody vibration modes, while the mass m_c and inertia moment J_c show how inert the carbody is in comparison to these modes. The bogies have two degrees of freedom: pitch θ_{bi} and bounce z_{bi}, for i = 1 and 2 [80].

The mass m_b and inertia moment J_b are both present in each bogie. A Kelvin-Voigt system with the elastic constant $2k_{zc}$ and the damping constant $2c_{zc}$ that operates during translation is used to describe the elastic and damping components of each bogie's secondary suspension. A Kelvin-Voigt system with the elastic constant $2k_{zb}$ and the damping constant $2c_{zb}$ is used to represent the primary suspension corresponding to an axle during translation.

The following are the formulae for the bounce and pitch carbody motions:

$$m_c\ddot{z}_c + 2c_{zc}(2\dot{z}_c - \dot{z}_{b1} - \dot{z}_{b2}) + 2k_{zc}(2z_c - z_{b1} - z_{b2}) = 0 \tag{3.2}$$

$$J_c\ddot{\theta}_c + 2a_cc_{zc}(2a_c\dot{\theta}_c - \dot{z}_{b1} + \dot{z}_{b2}) + 2a_ck_{zc}(2a_c\theta_c - z_{b1} + z_{b2}) = 0 \tag{3.3}$$

Where $2a_c$ is wheelbase of the carbody.

The equation for the front bogie's bounce motion is

$$m_b\ddot{z}_{b1}+2c_{zc}(2\dot{z}_{b1}-\dot{z}_c-a_c\dot{\theta}_c) + 2k_{zc}(2z_{b1}-z_c-a_c\theta_c) +2c_{zb}(2\dot{z}_{b1}-\dot{\eta}_1-\dot{\eta}_2) + 2k_{zb}(2z_{b1}-\eta_1-\eta_2) = 0 \tag{3.4}$$

$$m_b\ddot{z}_{b2}+2c_{zc}(2\dot{z}_{b2}-\dot{z}_c-a_c\dot{\theta}_c) + 2k_{zc}(2z_{b2}-z_c-a_c\theta_c) +2c_{zb}(2\dot{z}_{b2}-\dot{\eta}_3-\dot{\eta}_4) + 2k_{zb}(2z_{b2}-\eta_3-\eta_4) = 0 \tag{3.5}$$

and for the rear bogie is;

Similarly, the pitch motion equation for the two bogies are;

For the front bogie

$$J_b\ddot{\theta}_{b1} + 2a_bc_{zb}(2a_b\dot{\theta}_{b1} -\dot{\eta}_1-\dot{\eta}_2) + 2a_bk_{zb}(2a_b\theta_{b1} - \eta_1-\eta_2) = 0 \tag{3.6}$$

For the rear bogie

$$J_b\ddot{\theta}_{b2} + 2a_bc_{zb}\,(2a_b\dot{\theta}_{b2} - \dot{\eta}_3 - \dot{\eta}_4) + 2a_bk_{zb}\,(2a_b\theta_{b2} - \eta_3 - \eta_4) = 0 \quad (3.7)$$

Where $2a_b$ is the wheelbase of the bogie

The bounce motion of the bogies is observed to be connected with the pitch carbody motions. However, they can be separated after the first four equations are processed properly and a convenient set of motion coordinates is chosen. To achieve this, the coordinates are modified as follows:

For the symmetrical motions

$$z_c^{+} = z_c;\ z_b^{+} = z_{b1} + z_{b2} \quad (3.8)$$

For the antisymmetrical motions

$$z_c^{-} = \theta_c;\ z_b^{-} = z_{b1} + z_{b2} \quad (3.9)$$

According to the latest equations, the relations of equation 3.2-3.5 can be written as;

$$m_c\ddot{z}_c^{+} + 4c_{zc}\,(\dot{z}_c^{+} - \dot{z}_b^{+}) + 4k_{zc}\,(z_c^{+} - z_b^{+}) = 0 \quad (3.10)$$

$$J_c\ddot{z}_c^{-} + 4a_cc_{zc}\,(a_c\ddot{z}_c^{-} - \dot{z}_b^{-}) + 4a_ck_{zc}\,(a_cz_c^{-} - z_b^{-}) = 0 \quad (3.11)$$

$$m_b\ddot{z}_b^{+} + 2c_{zc}\,(\dot{z}_b^{+} - \dot{z}_c^{+}) + 2k_{zc}\,(z_b^{+} - z_c^{+}) + 4c_{zb}\,(\dot{z}_b^{+} - \dot{\eta}^{+}) + 4k_{zb}\,(z_b^{+} - \eta^{+}) = 0 \quad (3.12)$$

$$m_b\ddot{z}_b^{-} + 2c_{zc}\,(\dot{z}_b^{-} - a_c\dot{z}_c^{-}) + 2k_{zc}\,(z_b^{-} - a_cz_c^{-}) + 4c_{zb}\,(\dot{z}_b^{-} - \dot{\eta}^{-}) + 4k_{zb}\,(z_b^{-} - \eta^{-}) = 0 \quad (3.13)$$

Where

$$\eta^{+} = \frac{\eta_1 + \eta_2 + \eta_3 + \eta_4}{4} \text{ and } \eta^{-} = \frac{\eta_1 + \eta_2 - \eta_3 - \eta_4}{4} \quad (3.14)$$

represent the functions corresponding to the excitation modes caused by the symmetrical and antisymmetrical bounce of the axle designs for the vehicle [14].

The assumptions made in formulating the model are as follows:

- Bogie and car body component masses are rigid.
- Axle box was assumed as a wheel set's integral part, hence its weight was combined with the wheel set's mass

- The springs and dampers of the suspension system elements have linear characteristics.
- Friction does not exist between axle and bearing.
- All wheel profiles are identical from left to right on a given axle and from axle to axle and all wheel remains in contact with the rails.
- The track irregularity mode in vertical direction is symmetrical for both left and right rail is considered.
- The dynamic simulation was made on straight track with no supper elevation and curve radius

The procedure for modeling a multibody dynamic rail vehicle in the SIMPACK software is shown in Figure 3.8 below.

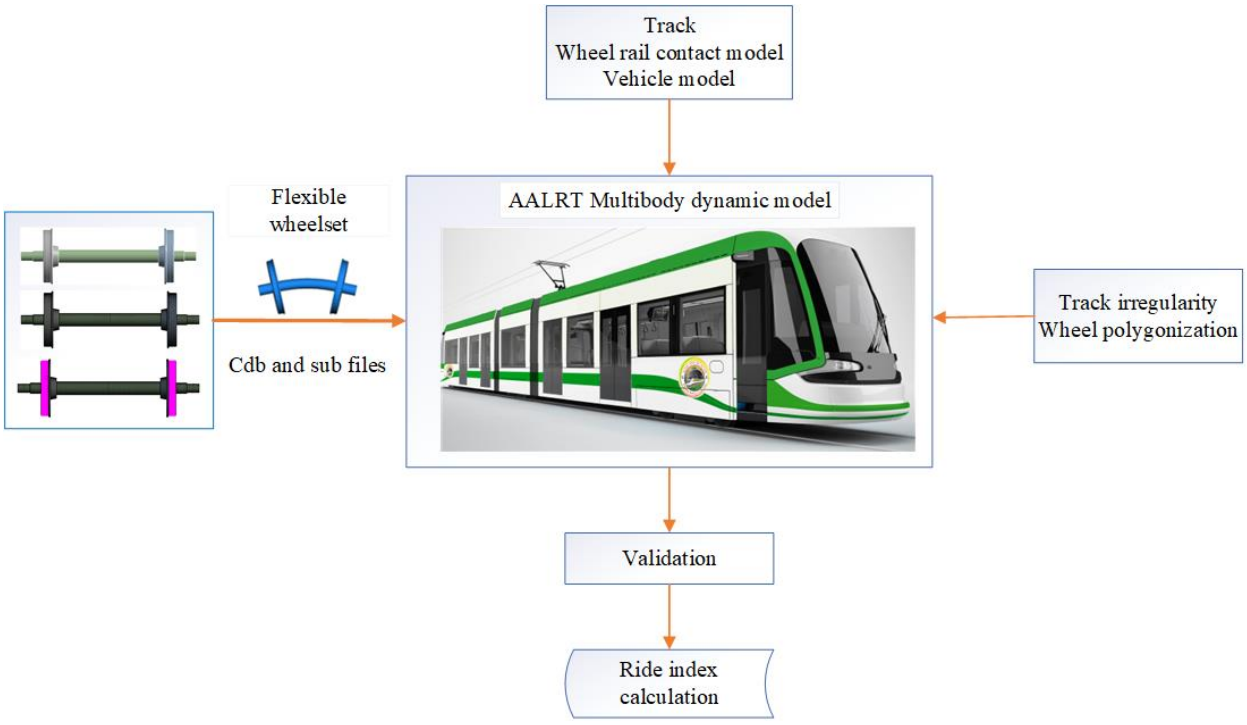

Figure 3.8: Modeling a multibody dynamic rail vehicle procedure

3.4.2 Wheelset and rail modeling

The guided wheelset was created by selecting from the general rail track joint of an existing rail wheelset module and then edited according to the data and specifications obtained from AALRT as shown in Figure 3.9. The parameters for the wheelset and rail are shown in Table 3.5.

Table 3.5: Wheelset parameters and values from AALRT (source: Addis Ababa Light Rail Transit technical sheet).

Parameters	**Value**
Wheelset mass - m_w	880 kg
Wheel diameter - D_w	660 mm
Flange height	28 mm
Flange thickness	21.21 mm
Wheelset shaft diameter - d_s	176 mm
Wheel profile type	S1002
Rail profile	UIC50
Rail cant	0.0694444
Young's modulus - E	202GN/m^2
Wheelset base - W_b	Variable
Friction coefficient	0.4
Vehicle center distance	18000 mm
Track gauge	1435 mm
Rail head width	70 mm
Rail tread width	48 mm
Rail base thickness	49.4 mm
Rail base width	125 mm
Rail height	152 mm
Rail web thickness	15 mm
Rail base thickness	28 mm
Wheelset roll moment of inertia I_{xx}	1130 kgm^2
Wheelset pitch moment of inertia I_{yy}	176 kgm^2
Wheelset yaw moment of inertia I_{zz}	1130 kgm^2

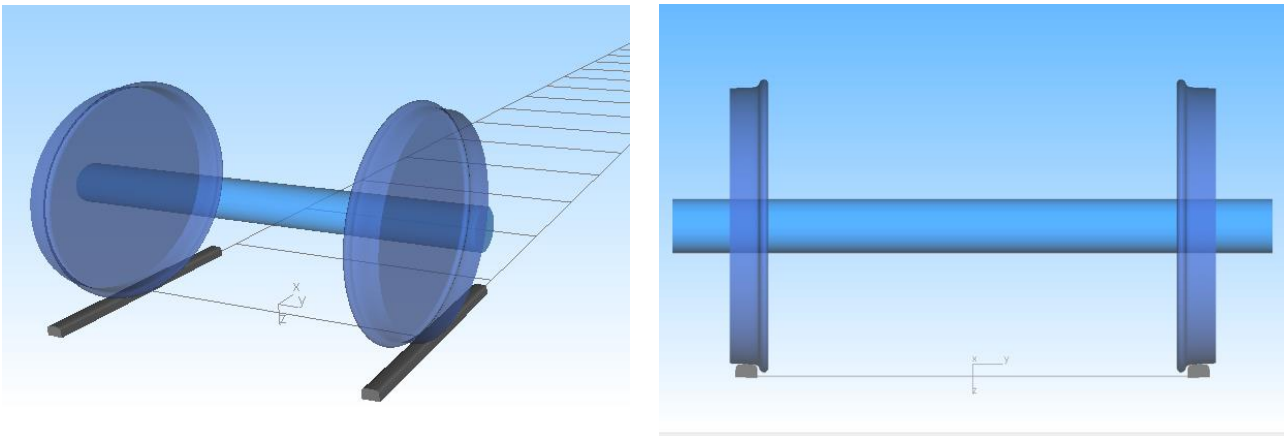

Figure 3.9: Modeling of wheelset and rail

3.4.3 Bogie frames modeling

The bogie frame was created by the following procedures: First, go to the body toolbar and then change the type of 3D geometry of the body to wheel rail bogie. Then modify it according to the AALRT body type. The AALRT bogie parameters are shown in Table 3.6 below.

Table 3.6: Bogie frame parameter and values from AALRT (source: Addis Ababa Light Rail Transit technical sheet).

Parameters	**Value**
Bogie frame mass	2615 kg
Axle base	2400 mm
Bolster mass	220 kg
Bolster dimension X-Y-Z	0.7m × 2.3m × 0.12m
Bogie roll moment of inertia J_{xx}	1250 kgm^2
Bogie pitch moment of inertia J_{yy}	1870 kgm^2
Bogie yaw moment of inertia J_{zz}	1250 kgm^2

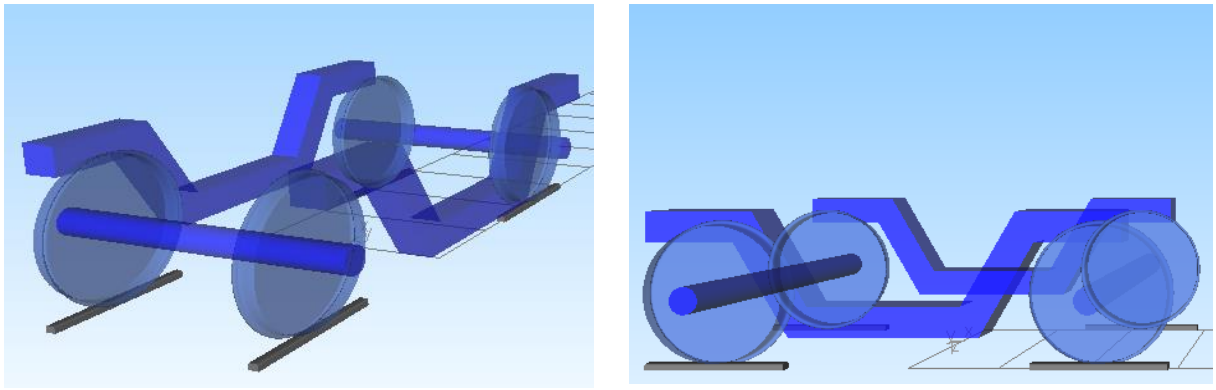

Figure 3.10: Modeling of bogie frame

3.4.5 Suspension element modeling

To create the primary spring suspension, insert Type 1 markers on the frame and wheelset at the attachment points of the primary suspension. Insert force element type 86: Spring Damper Ser/Par cmp between the two markers. Again, insert the same type of marker in the same places. Then insert force element type 6 (spring damper serial CMP) between the two markers. To create the secondary suspension, follow the same step using force types 79 (shear spring cmp) and 6 (spring damper serial ptp) by inserting markers between the car body and bogie frame. Table 3.7 shows the data required for the creation of the suspension system obtained from AALRT.

Table 3.7: Suspension elements parameters and values from AALRT (source: Addis Ababa Light Rail Transit technical sheet).

Parameters	Notation	Value
Longitudinal primary suspension spring stiffness	k_{px}	600000 N/m
Lateral primary suspension spring stiffness	k_{py}	75000 N/m
Vertical primary suspension spring stiffness	k_{pz}	600000 N/m
Longitudinal primary damping coefficient	c_{px}	15000 Ns/m
Lateral primary damping coefficient	c_{py}	2000 Ns/m
Vertical primary damping coefficient	c_{pz}	17000 Ns/m
Longitudinal secondary suspension spring stiffness	k_{sx}	160000 N/m
Lateral secondary suspension spring stiffness	k_{sy}	160000 N/m
Vertical secondary suspension spring stiffness	k_{sz}	430000 N/m
Longitudinal secondary damping coefficient	c_{sx}	20000 N/m
Lateral secondary damping coefficient	c_{sy}	17500 Ns/m
Vertical secondary damping coefficient	c_{sz}	21000 Ns/mm

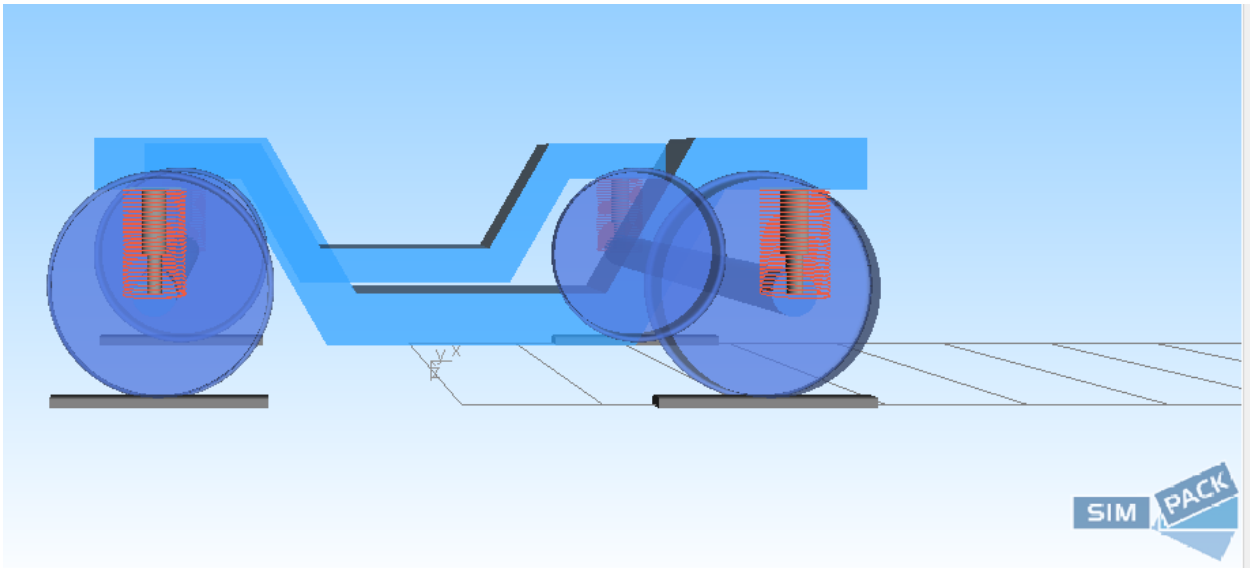

Figure 3.11: Modeling of suspension elements

3.4.6 Car body model

Creating the car body in SIMPACK is slightly different than the others. It needs the SIMPACK documentation (3D-primitive): Wheel Rail Vehicle Cab This 3D primitive represents the approximated geometry for standard wheel-rail vehicles. The car body model dimension parameter refers to the 3D primitive and is then modified according to the AALRT car body specifications. The AALRT car body specifications are tabulated in Table 3.8 below.

Table 3.8: Car body parameters and values from AALRT (source: Addis Ababa Light Rail Transit technical sheet).

Parameters	Notation	Value
Car body mass	m_c	44000 kg
Car body length	L_c	25500 mm
Car body width	w_c	3105 mm
Car body axle base	$2a_c$	18000 mm
Car body roll moment of inertia	J_{xx}	4375 kgm^2
Car body pitch moment of inertia	J_{yy}	8750 kgm^2
Car body pitch moment of inertia	J_{zz}	8750 kgm^2

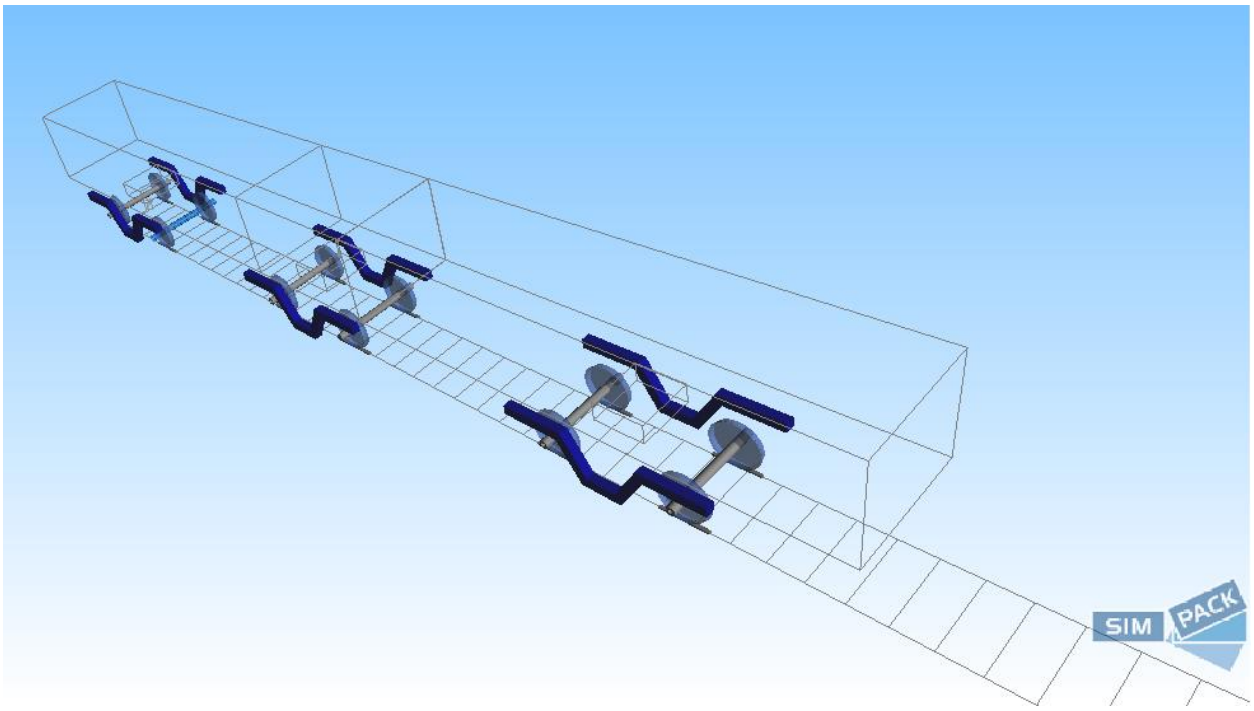

Figure 3.12: Modeling of car body

3.4.7 Wheel-rail contact model

A crucial component of the vehicle-track coupled dynamics model is the wheel-rail contact that connects the vehicle subsystem to the ballastless track subsystem. The wheel-rail contact model assists in studying the geometrical relationship between the wheel and the rail and calculating the amount of contact force on the wheel and rail surface. It is assumed that the wheel and rail have a 0.4 coefficient of friction. According to the Hertzian nonlinear elastic contact theory, the normal and tangential contact forces F_{wi} (t) between the wheel and rail are computed and expressed as follows [42], [77]:

$$F_{wi}(t) = \begin{cases} 0 \\ C_H[Z_{wi}(t) - Z_{ri}(x,t)]^{\frac{3}{2}} \end{cases} \begin{matrix} Z_{wi}(t) - Z_{ri}(x,t) < 0 \\ Z_{wi}(t) - Z_{ri}(x,t) > 0 \end{matrix} \quad (3.15)$$

$Z_{wi}(t)$ represents the vertical displacement of the ith wheelset, $Z_{ri}(x, t)$ represents the vertical displacement of the rail at the ith wheelset's location, and C_H represents the Hertzian constant, which is equal to 9.37×10^{10} N/m$^{3/2}$.

3.5 Formation of track irregularity

Track irregularities are defined as the discrepancy between the measurements received from inspection vehicles and the nominal geometry of the track, and are often characterized by lateral and vertical rail displacements.

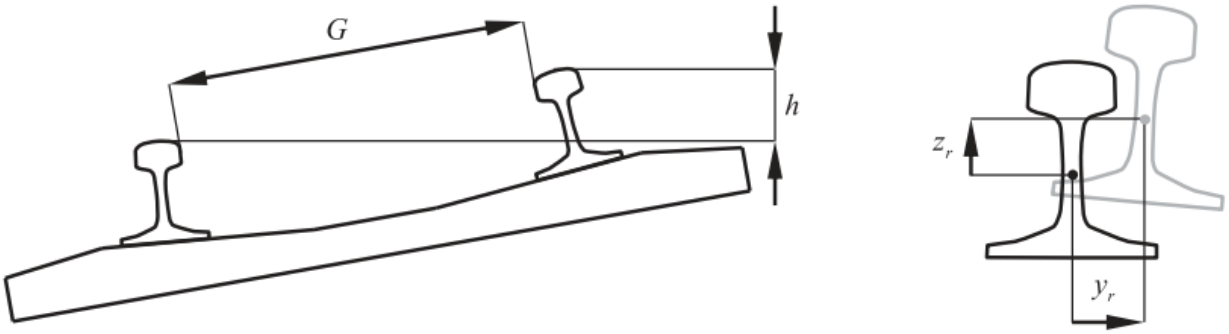

Figure 3.13: Parameters describing the track geometry and its irregularities

As indicated in Figure 3.13, the longitudinal level z_r and the alignment y_r are the vertical and lateral displacements of the rail relative to its design geometry [81]. To refer to the left or right rail, the subscript *r* is either l or *r*. The variations between the measured and nominal cross-level and gauge are represented by the cross-level variation Δh and the gauge variation ΔG, respectively. Track abnormalities are measured and stored as a function of track arc-length by inspection vehicles.

3.6 Coupling the flexible wheelset with the rigid dynamic rail vehicle model

The FEMBS preprocessing module in SIMPACK reads the substructure analysis output files, which contain the physical and structural data of the wheelset. Applying Eigen mode computations requires the usage of flexible body input files (.fbi), which are produced by FEMBS.

Eigen modes are a flexible structure's natural oscillations. The matching Eigen mode deformation will be triggered when a flexible structure is excited at a frequency that matches one of its Eigen frequencies, as shown in Figure 3.14. Appendix H shows the wheel's flexible wheelset markers in SIMPACK.

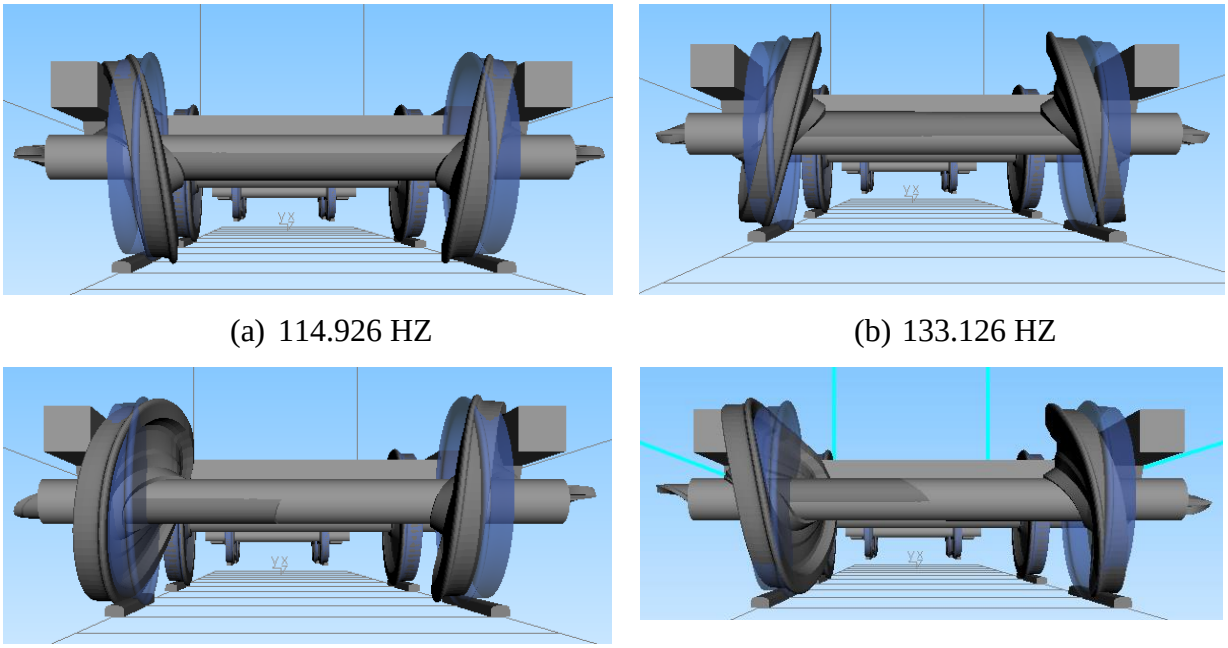

(a) 114.926 HZ (b) 133.126 HZ

(c) 200.218 HZ (d) 297.626 HZ

Figure 3.14: The wheelset's Eigen modes at frequencies between 100 and 300HZ

3.7 Wheel polygons mathematical model

Wheel polygons are classified into two types; periodic and nonperiodic [82]. Periodic discontinuity occurs when a given order polygon dominates; it does not occur when there is no dominance. When the order components of a polygon are widely scattered, it is called nonperiodic discontinuity, and this sort of polygon is generated by the superposition of harmonics with varying amplitudes, wear lengths, and phases. The method of simple harmonic functions is utilized in this research to define the periodic discontinuity of the wheel circumference. The difference in circumferential irregularities is viewed as a harmonic function, as shown below.

$$\begin{Bmatrix} \Delta r(\beta) = A\,sin(n(\beta + \beta_0)) \\ r = R - \Delta r \end{Bmatrix} \quad (3.16)$$

Where β is the wheel rotation angle, β_0 is the initial phase angle, Δr is the wheel diameter difference, A is the uncircular smooth wear depth, n is the wheel polygon order, R is the nominal rolling circle radius, r is the actual rolling circle radius.

The number of orders and degree of polygonal wheel wear are determined by the fixed wavelength principle, which is given by [83]:

$$\lambda_p = \frac{2\pi r}{N} \tag{3.17}$$

Where λ_p is the wavelength of wheel polygonization, r is the radius of the wheel, and N is the order of the wheel polygonization.

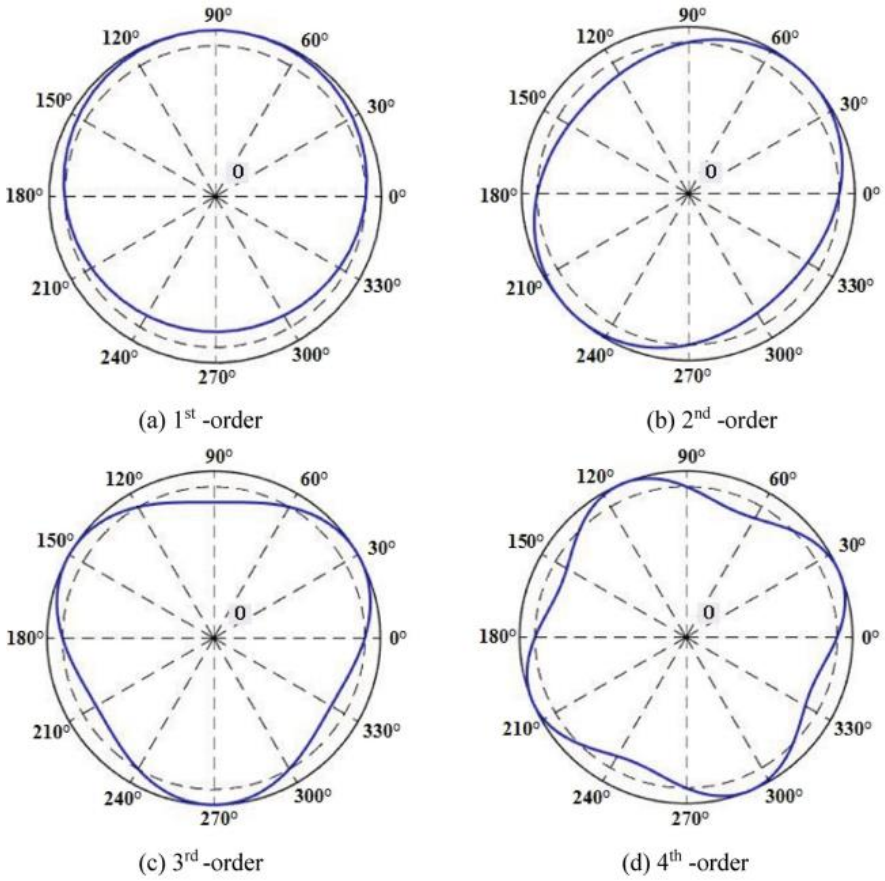

Figure 3.15: Diagram showing periodic wheel polygonizations of various orders [83].

Figure 3.15(a-d) shows the 1st, 2nd, 3rd, and 4th-order periodic wheel polygonizations, each with an amplitude of A = 0.1 mm, with the wheel OOR amplitudes enlarged 200 times for ease of inspection. The 1st-order periodic wheel polygonization (N = 1) indicates that the wheel is eccentric as a result of machining or wear (Figure 8(a)); to some extent, this is an issue that all railway wheels experience. For the 2nd-order periodic polygonization situation (N = 2), the wheel is elliptic, as illustrated in Figure 8(b), and for the 3rd-order periodic polygonization example (N = 3), it tends to be triangulated. Figure 8 (d) illustrates the wheel's quadrilateral polygonization for N = 4. (See Appendix J for wheel polygonization amplitudes of 0.1, 0.2 and 0.3mm).

3.8 Validation of the model

SIMPACK was used to perform static equilibrium and preload calculations. The preload load solver aids in calculating the vertical force at the wheel-rail contact area, which should be consistent across all wheels. The only factor considered is the gravity of different components of the vehicle. The preload solver determines the preloads so that the system is in equilibrium, i.e., the residual accelerations (joint body accelerations) are zero or so minimal that they can be close to zero. The vehicle travelled 17 kilometres at 70 km/h without experiencing any track irregularities. While the joint body acceleration was 3.357×10^{-07} as shown in Appendix E, which is very small and near zero, the peak dynamic vertical force obtained was 50.423 kN for each wheel, as shown in Figure 3.16, which was the same as the static force under preload conditions. See Appendix E for more details.

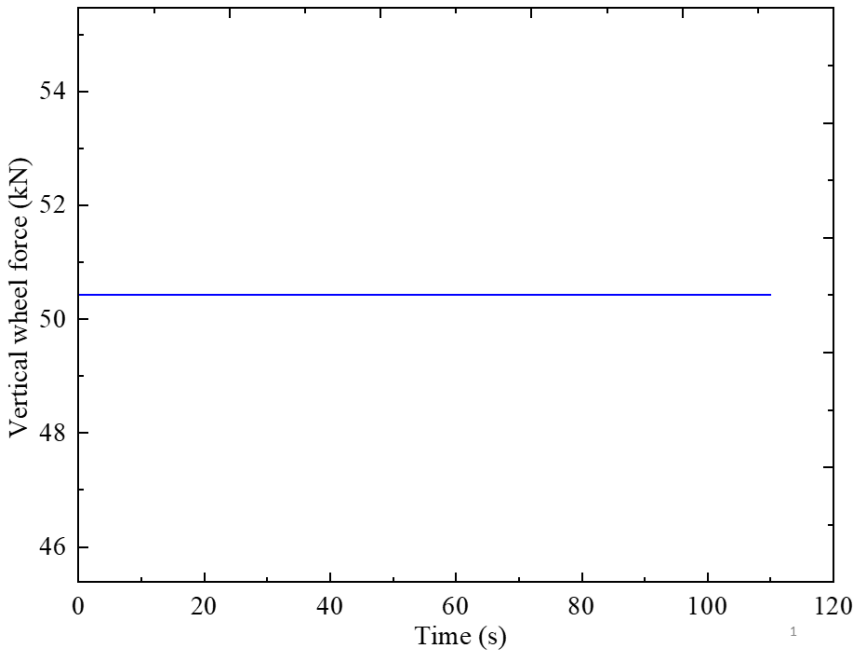

3.16: Preload static force

The model was also validated by conducting two further simulations: the rigid-flexible coupled dynamic model with a polygonal wheel and the rigid-flexible coupled dynamic model without a polygonal wheel with track irregularities. The speed used for validation was 40 km/h, and it was used according to the wheel defect manual recommendation [84]. The study done by Bethel et al. in 2022 [42], which comprised an experimental method and a simulation method, was used for

validation of the model of the present work through comparison of the vertical acceleration and lateral acceleration results. The results of vertical acceleration and lateral acceleration are plotted in Appendix I and J, respectively, and are below the standard limit of 2.5 m/s^2 as specified by UIC518.

As can be seen in Appendix I, the peak vertical accelerations calculated with and without the polygonal wheel are 1.43 and 1.1 m/s^2, respectively. Similarly to the one obtained from Bethel et al. in 2022 [42], the peak vertical accelerations calculated with and without the polygonal wheel are 1.4 and 0.85 m/s^2.

3.9 Ride comfort index calculation

For the evaluation and assessment of passenger ride comfort, it is necessary to know the accelerations in individual directions x, y, and z. Therefore, the sensors were defined in the front wheelset of the multibody dynamics system. The indexes were extracted from the results tool of the sensor.

The computation of the passenger ride comfort index at the rail car floor level consists of multiple steps [5]. Procedure outputs are frequency weighted RMS-values of acceleration $a_{XP95}^{W_d}$, $a_{YP95}^{W_d}$ and $a_{ZP95}^{W_b}$ respectively, where a is RMS-values of acceleration X, Y and Z are directions of acceleration, p is measured position, 95 signifies the 95th percentile, W_d is weighted in the x and y directions at the floor level, and W_b is weighted in the z direction at the floor level.

$$W_z = 6\times\sqrt{(a_{XP95}^{W_d})^2 + (a_{YP95}^{W_d})^2 + (a_{ZP95}^{W_b})^2} \tag{3.18}$$

Equation 3 was used to calculate the ride indexes, and the scale in Table 2.1 was used to compare the estimated comfort indexes to the passenger ride comfort according to EN 12299:2009.

CHAPTER FOUR

4.0 RESULTS AND DISCUSSION

In this chapter, the effect of a polygonized wheel on passenger ride comfort was investigated. In addition, the effects of flexible wheelsets with track irregularities were addressed. The results for the study were obtained after performing a dynamic simulation by considering straight tracks. To determine the impact of wheel polygonization amplitude and orders, vehicle speed, and load on ride comfort, the ride comfort index was calculated during simulation and various graphs plotted. Moreover, wheel polygonization was introduced to the right wheel of the first wheelset of the front bogie. Only the right wheel of the front bogie's first wheelset was taken into account for simplicity.

First the effect of the flexible wheelset on the polygonal wheel, two simulations were performed, one of the vehicle model with flexible wheelset and other with rigid wheelset. Both simulations were run on a 2.5-kilometer straight track at a speed of 70 km/h. Because of wheel radius deviations and presence of track irregularities, the highest peak rail/wheel vibration results vary. The rail/wheel vertical forces obtained due to the flexible wheelset and rigid wheelset are 172.9 kN and 226.87 kN, respectively. The findings are consistent with those of Awel [68], Baeza [84], Wu [84], Yifan ,and others who looked at the dynamic responses of a flexible wheelset in response to a damaged wheel. See appendix L.

4.1 Influence of wheel polygonization amplitude

The impact of the wheel polygonization amplitudes was addressed by running the model with the maximum operating speed of AALRT (70 km/h) on a 2.5-kilometer straight track. Three simulations were performed with different polygonization amplitudes of 0.1mm, 0.2 mm, and 0.3mm. Only the first order of polygonization was considered.

Figure 4.1 shows the obtained results of the ride comfort index due to different polygonization amplitudes, while Figures 4.2, 4.3 and 4.4 show the results of vertical and lateral acceleration, with polygonization of 0.1 mm, 0.2 mm, and 0.3 mm amplitudes, respectively. The findings show that the amplitude of 0.3 mm has the highest value of the ride comfort index, i.e., 3.01. It implies that with increasing the polygonization amplitude, the ride index also increases.

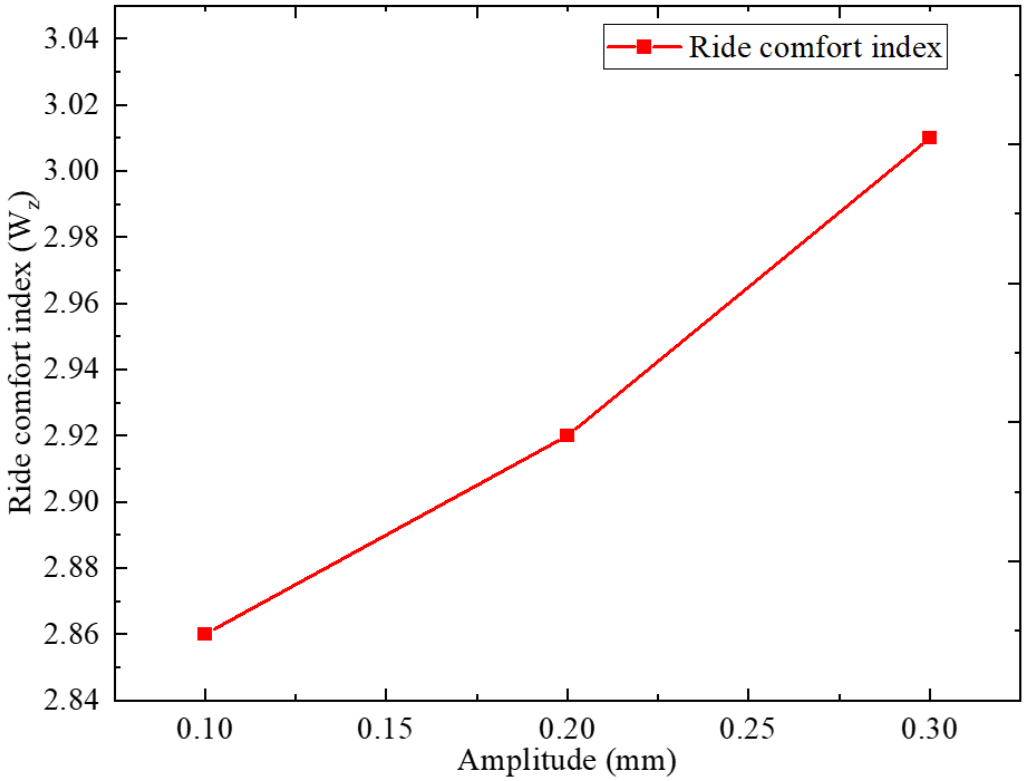

Figure 4.1: Ride comfort index due to wheel polygonization amplitudes

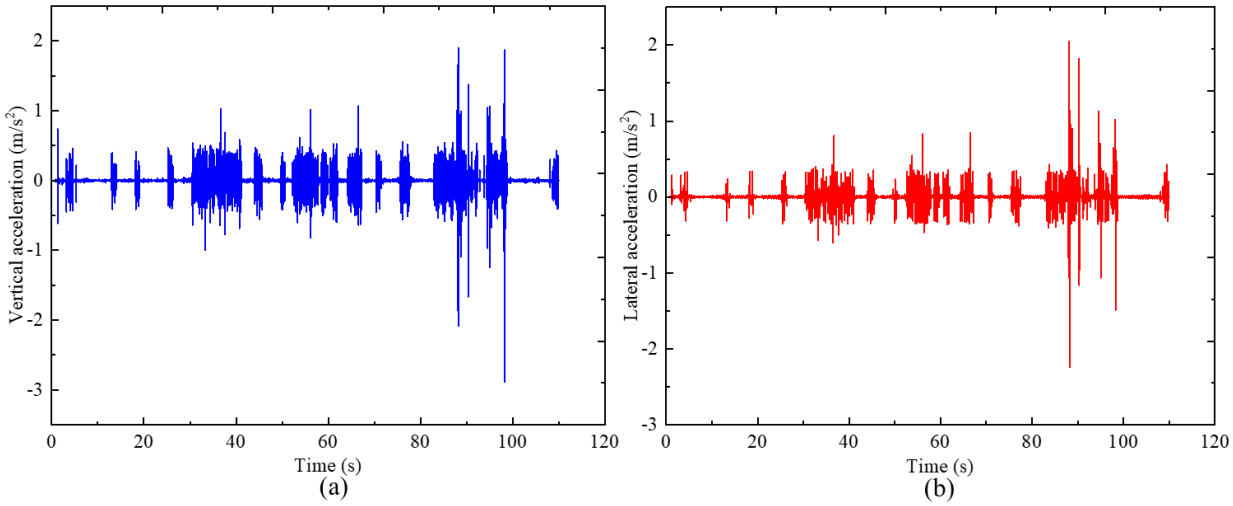

Figure 4.2: Vertical and lateral acceleration due to the 0.1 mm wheel polygonization amplitude

As summarized in Table 4.1, wheel polygonization of 0.3 mm amplitude has more impact on ride comfort compared to the other amplitudes; however, the results show that an amplitude of 0.1 mm leads to high vertical acceleration and lateral acceleration.

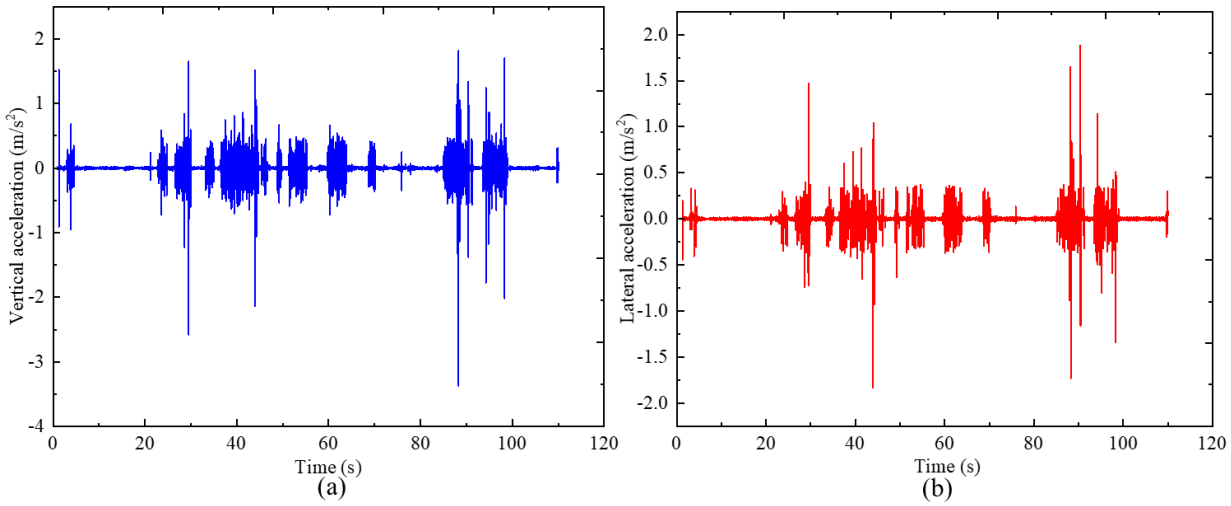

Figure 4.3: Vertical and lateral acceleration due to the 0.1 mm wheel polygonization amplitude

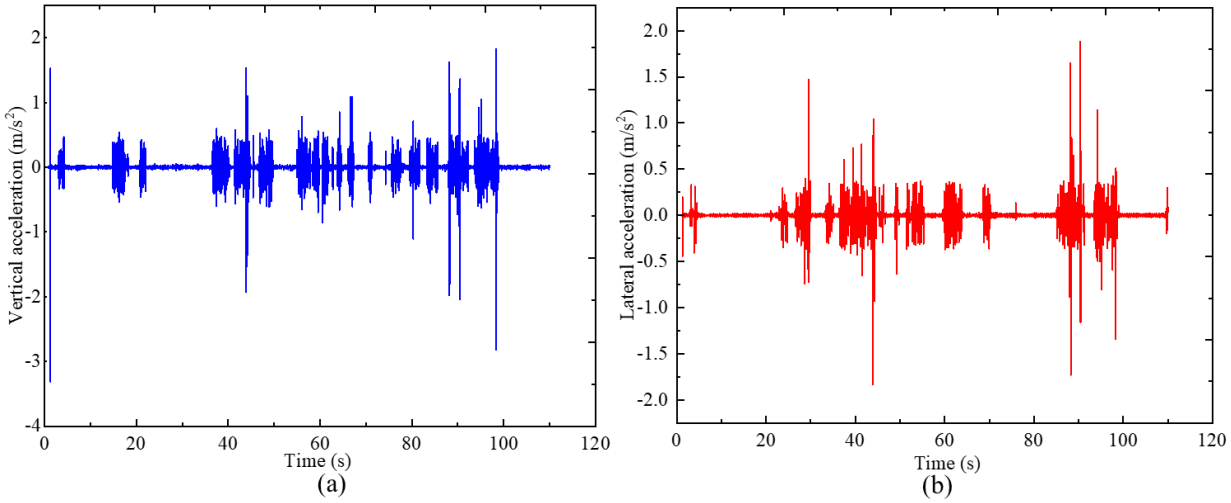

Figure 4.4: Vertical and lateral acceleration due to the 0.1 mm wheel polygonization amplitude

Table 4.1: Results due to different wheel polygonization amplitudes

Outcomes	0.1 mm amplitude	0.2 mm amplitude	0.3 mm amplitude
Ride comfort index	2.86	2.92	3.01
Vertical acceleration	1.9 m/s^2	1.81 m/s^2	1.82 m/s^2
Lateral acceleration	2.04 m/s^2	1.88 m/s^2	1.85 m/s^2

4.2 Effect of vehicle loads

Three simulation cases were performed to investigate the influence of vehicle carrying loads on ride comfort and the acceleration dynamic response of the vehicle when the wheel is polygonized. The first simulation considered the empty vehicle with 44 tons, the second simulation considered the rated passenger carrying capacity with 59.24 tons, and the last simulation considered the passenger overload carrying capacity with 63.02 tons. The model was run at a speed of 70 km/h on a 2.5-kilometer straight track.

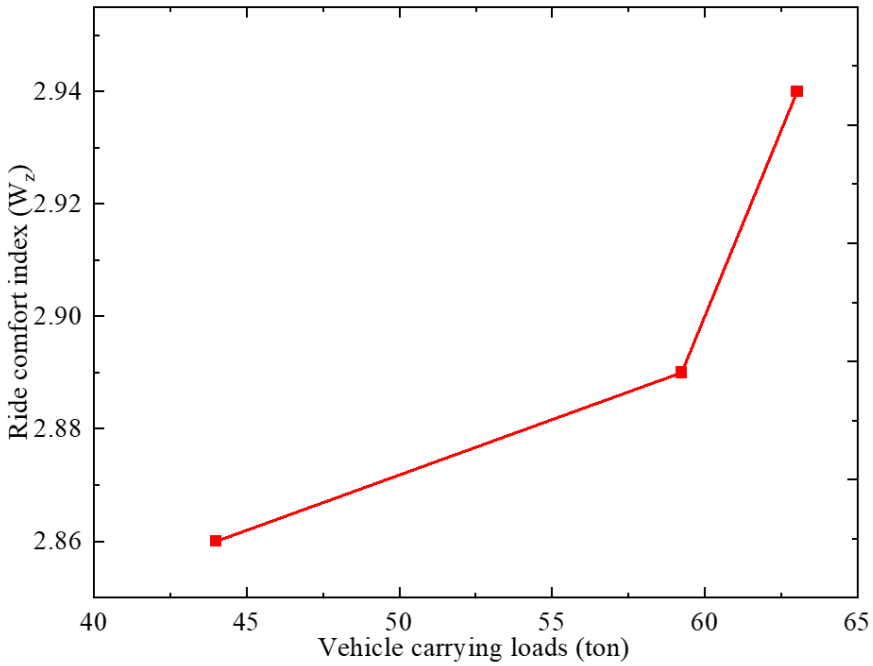

Figure 4.5: Ride comfort index due to the vehicle carrying loads

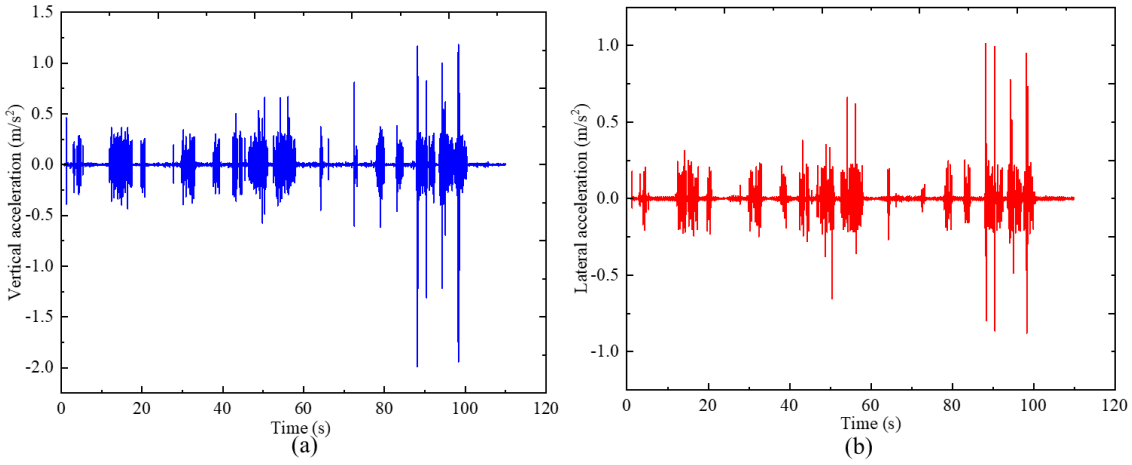

Figure 4.6: Vertical and lateral acceleration due to the empty vehicle load

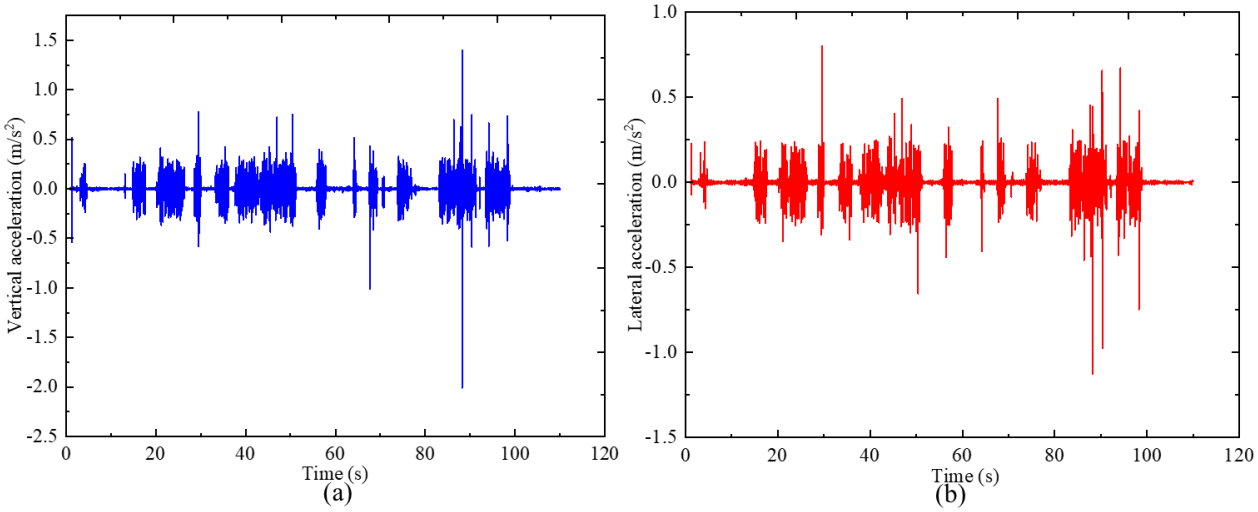

Figure 4.7: Vertical and lateral acceleration due to the rated carrying load

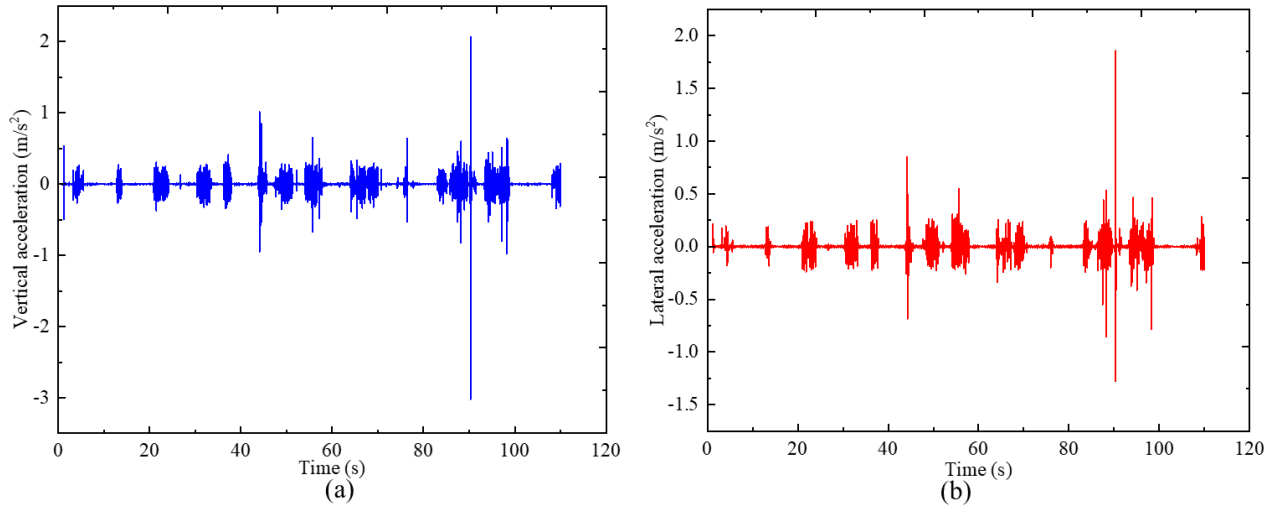

Figure 4.8: Vertical and lateral acceleration due to the overload carrying load

As shown in Figure 4.5, the ride comfort obtained due to overload carrying capacity load is 2.94, while for empty and rated carrying capacity load, it is 2.86 and 2.89, respectively. But also, the obtained vertical and lateral acceleration of the overload carrying capacity load is higher compared to the empty and rated carrying capacity load, as shown in Figures 4.6, 4.7 and 4.8. This implies that running an overloaded carrying capacity vehicle has minimal comfort compared to an empty and rated carrying capacity vehicle when the wheel has a polygonization defect. The results are tabulated in Table 4.2 for all cases.

Table 4.2: Results due to different vehicle loads

Loads	Ride index	Vertical acceleration (m/s^2)	Lateral acceleration (m/s^2)
Empty	2.86	1.18	1.01
Rated carrying capacity	2.89	1.4	0.8
Overload carrying capacity	2.94	2.06	1.86

4.3 Influence of vehicle speed

The effect of train speed on ride comfort was determined by considering six cases:

Case I: Running a vehicle having a rated carrying load with a polygonized wheel and without a polygonized wheel.

At first, the vehicle with a 59.24-tonne load was run at speeds of 30 km/h, 40 km/h, 50 km/h, 60 km/h, and 70 km/h without a polygonal wheel, and then the same runs were done with a polygonal wheel. Figure 4.9 shows the ride comfort index versus vehicle speeds. It was observed that ride comfort varies at different speeds. The highest speed (70 km/h) has a greater effect on ride comfort, whether the wheel is polygonized or unpolygonized, as shown in Figure 4.9 and summarized in Table 4.3. With a polygonal wheel, the maximum ride comfort index is 2.81 caused by a speed of 70 km/h and the minimum ride comfort index is 1.87 caused by a speed of 30 km/h, while without a polygonal wheel, the maximum ride comfort index is 2.79 caused by a speed of 70 km/h and the minimum ride comfort index is 1.85 caused by a speed of 30 km/h.

Table 4.3: Results due to different vehicle speeds and the rated passenger's carrying load

S/N	Vehicle speed (km/ h)	Ride index	
		With Polygonal wheel	Without Polygonal wheel
1.	30	1.87	1.85
2.	40	2.04	2.03
3.	50	2.33	2.28
4.	60	2.52	2.51
5.	70	2.81	2.79

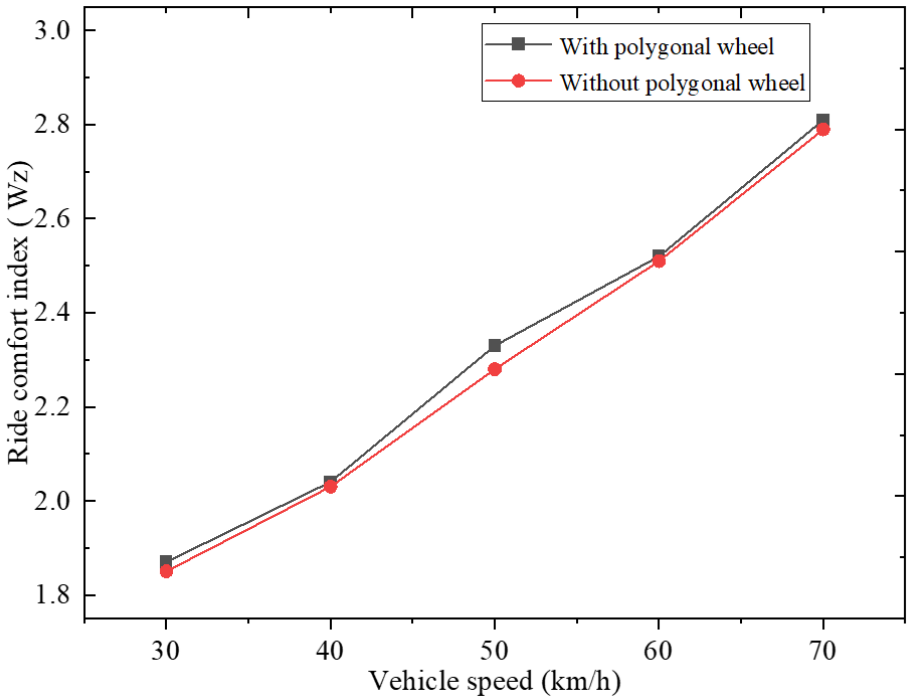

Figure 4.9: Influence of vehicle speed with and rated passenger's carrying load on ride comfort

Case II: Running a vehicle carrying an overload with a polygonized wheel and without a polygonized wheel.

The vehicle with a 63.02-tonne load was run at speeds of 30 km/h, 40 km/h, 50 km/h, 60 km/h, and 70 km/h without a polygonal wheel, and then the same runs were done with a polygonal wheel. Figure 4.10 shows the ride comfort index versus vehicle speeds. It was observed that ride comfort varies at different speeds. The highest speed (70 km/h) has a greater effect on ride comfort, whether the wheel is polygonized or unpolygonized, as shown in Figure 4.10 and tabulated in Table 4.4. With a polygonal wheel, the maximum ride comfort index is 2.86 caused by a speed of 70 km/h and the minimum ride comfort index is 1.87 caused by a speed of 30 km/h, while without a polygonal wheel, the maximum ride comfort index is 2.84 caused by a speed of 70 km/h and the minimum ride comfort index is 1.85 caused by a speed of 30 km/h.

See appendices F and G for the obtained rail-wheel vertical and lateral forces due to rated carrying loads and overload carrying loads, respectively, for a minimum speed and a maximum speed of 30 km/h and 70 km/h, respectively.

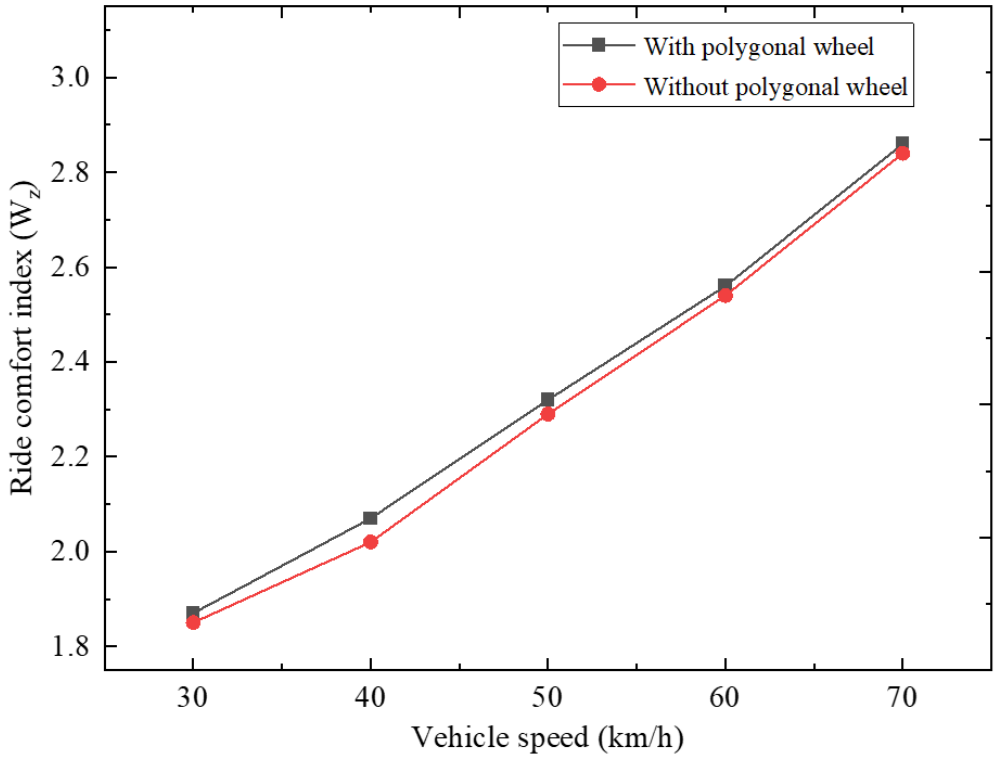

Figure 4.10: Influence of vehicle speed with overloaded loads on ride comfort

Table 4.4: Results due to different vehicle speeds with overloaded passenger carrying capacity

S/N	Vehicle speed (km/ h)	Ride index	
		With Polygonal wheel	Without Polygonal wheel
1.	30	1.87	1.85
2.	40	2.07	2.02
3.	50	2.32	2.29
4.	60	2.55	2.54
5.	70	2.86	2.84

Case III: Running a vehicle with a rated carrying load with two polygonized wheels from different bogies

The vehicle with a 59.24-tonne load was run at speeds of 30 km/h, 40 km/h, 50 km/h, 60 km/h, and 70 km/h with polygonized wheels on the first and second bogies. Figure 4.11 shows the ride comfort index versus vehicle speeds. It was observed that ride comfort varies at different speeds.

The highest speed (70 km/h) has a greater effect on ride comfort; see Table 4.5. The maximum ride comfort index is 2.84 at a speed of 70 km/h, and the minimum ride comfort index is 1.86 at a speed of 30 km/h.

Table 4.5: Ride comfort index due to vehicle speed with a rated passenger's carrying load and two polygonized wheels.

Vehicle speed (km/h)	Ride comfort index
30	1.86
40	2.04
50	2.32
60	2.56
70	2.84

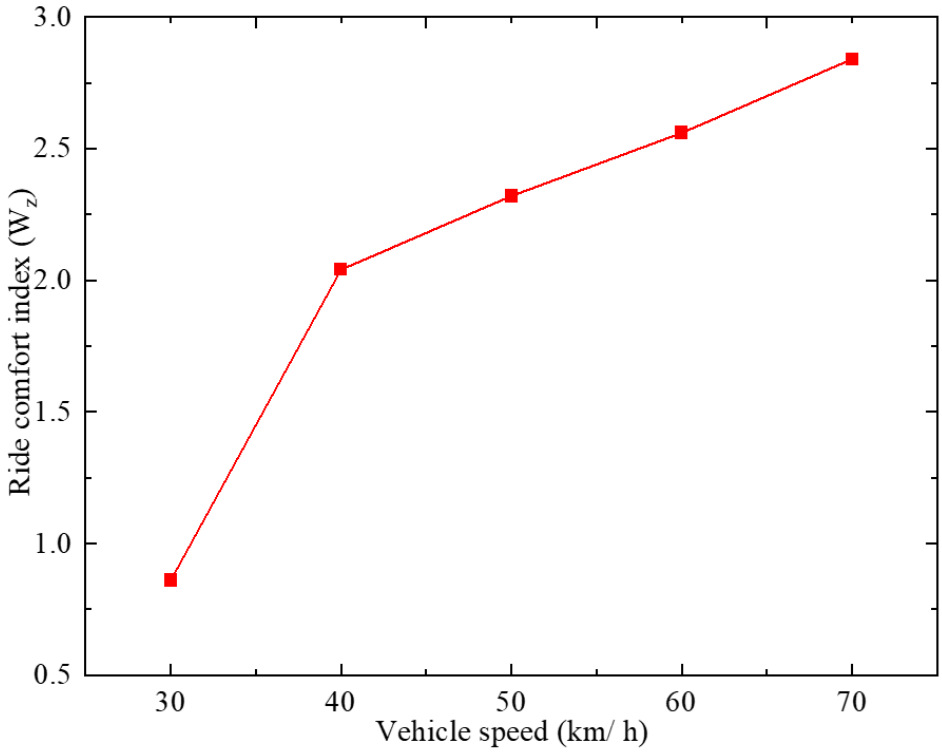

Figure 4.11: Ride comfort index due to vehicle speed with a rated passenger's carrying load and two polygonized wheels.

Case IV: Running a vehicle carrying an overload with two polygonized wheels from different bogies

The vehicle with a 63.02-tonne load was run at speeds of 30 km/h, 40 km/h, 50 km/h, 60 km/h, and 70 km/h with polygonized wheels on the first and second bogies. Figure 4.12 shows the ride comfort index versus vehicle speeds. It was observed that ride comfort varies at different speeds. The highest speed (70 km/h) has a greater effect on ride comfort; see Table 4.6. The maximum ride comfort index is 2.85 at a speed of 70 km/h, and the minimum ride comfort index is 1.86 at a speed of 30 km/h.

Table 4.6: Ride comfort index due to vehicle speed with overload passenger's carrying load and two polygonized wheels.

Vehicle speed (km/h)	Ride comfort index
30	1.86
40	2.05
50	2.34
60	2.58
70	2.85

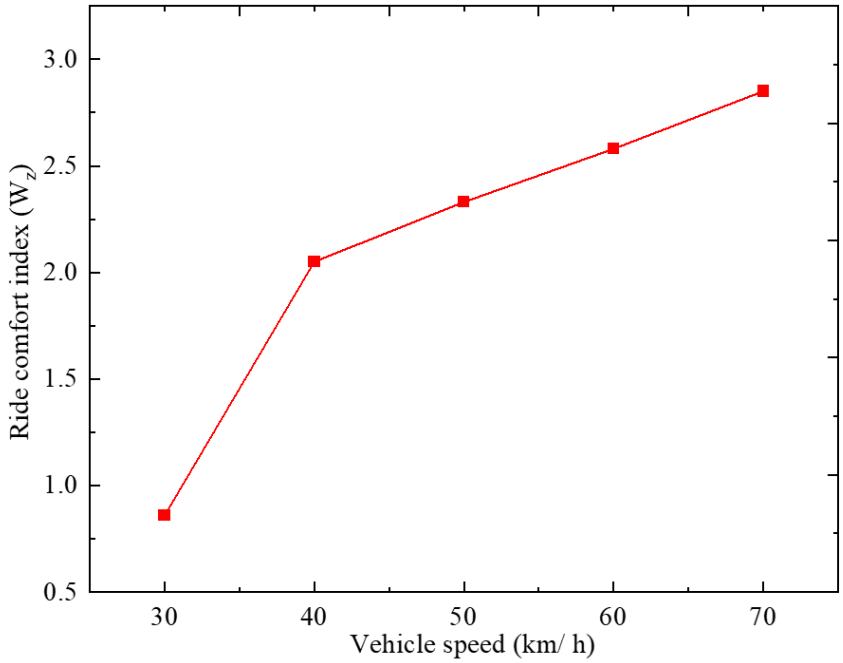

Figure 4.12: Ride comfort index due to vehicle speed with overload passenger's carrying load and two polygonized wheels.

Case V: Running a vehicle with a rated carrying load with three polygonized wheels from different bogies

The vehicle with a 59.24-tonne load was run at speeds of 30 km/h, 40 km/h, 50 km/h, 60 km/h, and 70 km/h with one polygonized wheel on each bogie. Figure 4.13 shows the ride comfort index versus vehicle speeds. It was observed that ride comfort varies at different speeds. The highest speed (70 km/h) has a greater effect on ride comfort; see Table 4.7. The maximum ride comfort index is 2.86 at a speed of 70 km/h, and the minimum ride comfort index is 1.88 at a speed of 30 km/h.

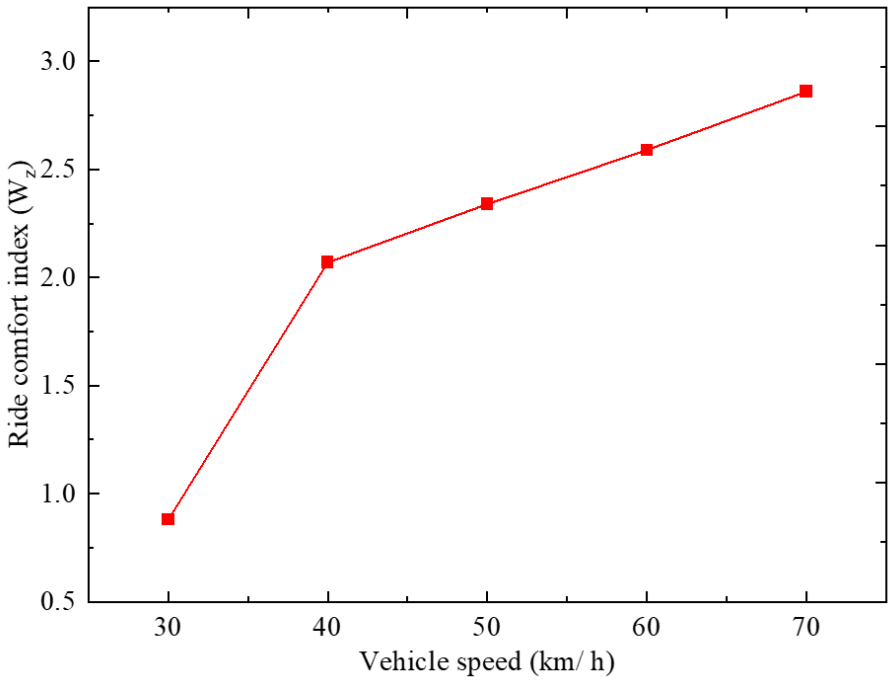

Figure 4.13: Ride comfort index due to vehicle speed with a rated passenger's carrying load and three polygonized wheels.

Table 4.7: Ride comfort index due to vehicle speed with a rated passenger's carrying load and three polygonized wheels.

Vehicle speed (km/h)	Ride comfort index
30	1.88
40	2.07
50	2.34
60	2.59
70	2.86

Case VI: Running a vehicle carrying an overload with three polygonized wheels from different bogies

The vehicle with a 63.02-tonne load was run at speeds of 30 km/h, 40 km/h, 50 km/h, 60 km/h, and 70 km/h with one polygonized wheel on each bogie. Figure 4.14 shows the ride comfort index versus vehicle speeds. It was observed that ride comfort varies at different speeds. The highest speed (70 km/h) has a greater effect on ride comfort; see Table 4.8. The maximum ride comfort index is 2.89 at a speed of 70 km/h, and the minimum ride comfort index is 1.88 at a speed of 30 km/h.

Table 4.8: Ride comfort index due to vehicle speed with overload passenger's carrying load and tthree polygonized wheels.

Vehicle speed (km/h)	Ride comfort index
30	1.88
40	2.07
50	2.34
60	2.6
70	2.89

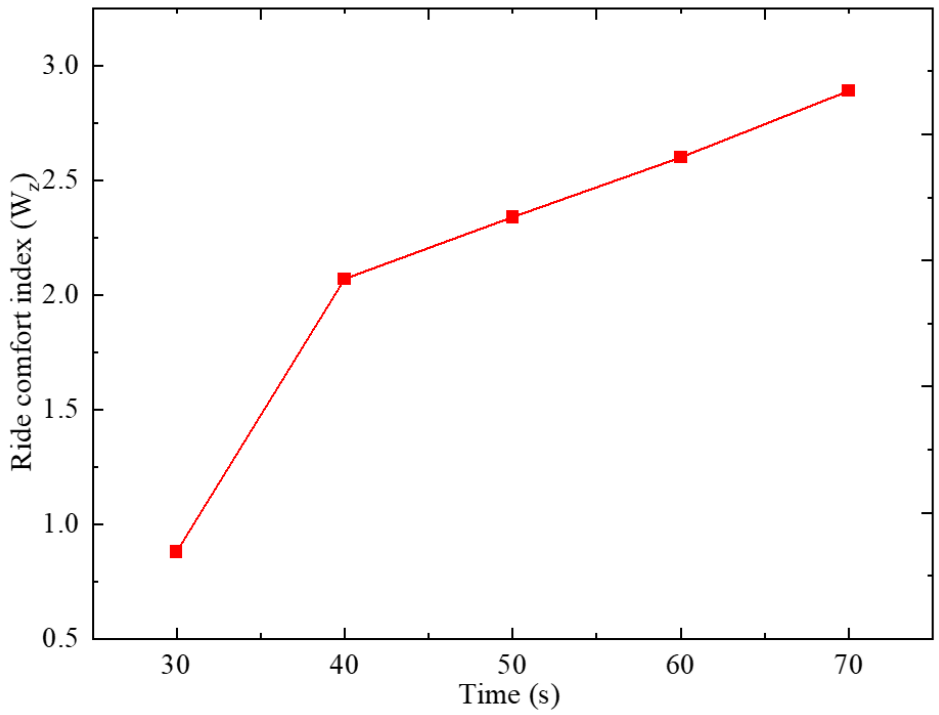

Figure 4.14: Ride comfort index due to vehicle speed with overload passenger's carrying load and three polygonized wheels.

4.4 Influence of polygonization orders with different speeds

For determining the effect of polygonization harmonic orders with different train speed on ride comfort, three cases were considered:

Case I: Running a vehicle having 2nd order of polygonization with different speeds

The vehicle with a 59.24-tonne load was run at speeds of 30 km/h, 40 km/h, 50 km/h, 60 km/h, and 70 km/h with a polygonal wheel having 2nd order. The highest speed (70 km/h) has a greater effect on ride comfort, as shown in Figure 4.15. The maximum ride comfort index is 3.14 caused by a speed of 70 km/h and the minimum ride comfort index is 2.00 caused by a speed of 30 km/h.

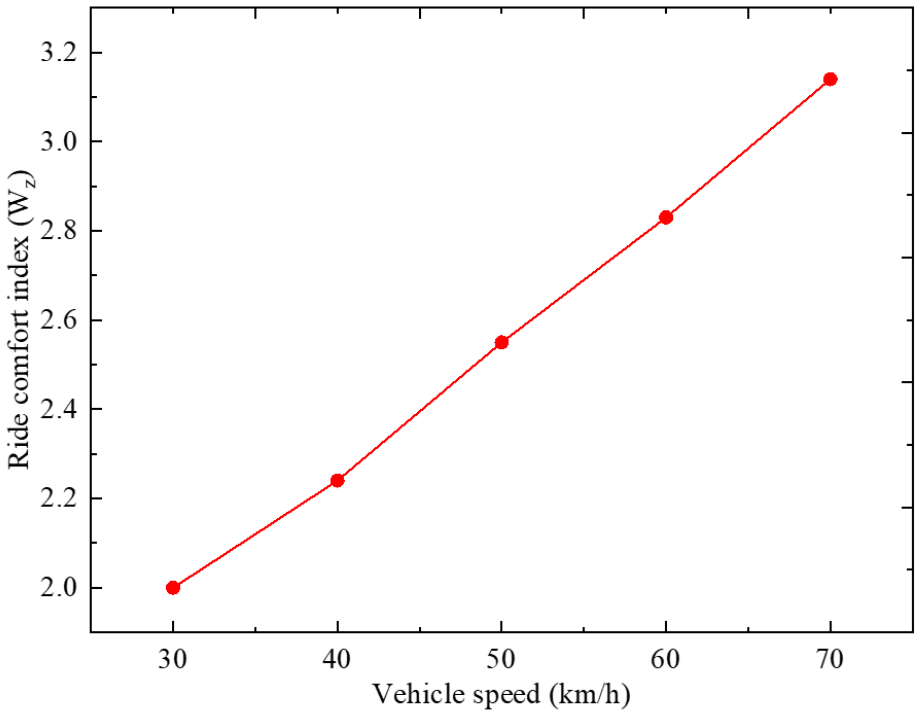

Figure 4.15: Ride comfort index due to 2nd order of polygonization

Case 2: Running a vehicle having 4th order of polygonization with different speeds

The vehicle with a 59.24-tonne load was run at speeds of 30 km/h, 40 km/h, 50 km/h, 60 km/h, and 70 km/h with a polygonal wheel having 4th order. The highest speed (70 km/h) has a greater effect on ride comfort, as shown in Figure 4.16. The maximum ride comfort index is 3.67 caused by a speed of 70 km/h and the minimum ride comfort index is 2.57 caused by a speed of 30 km/h.

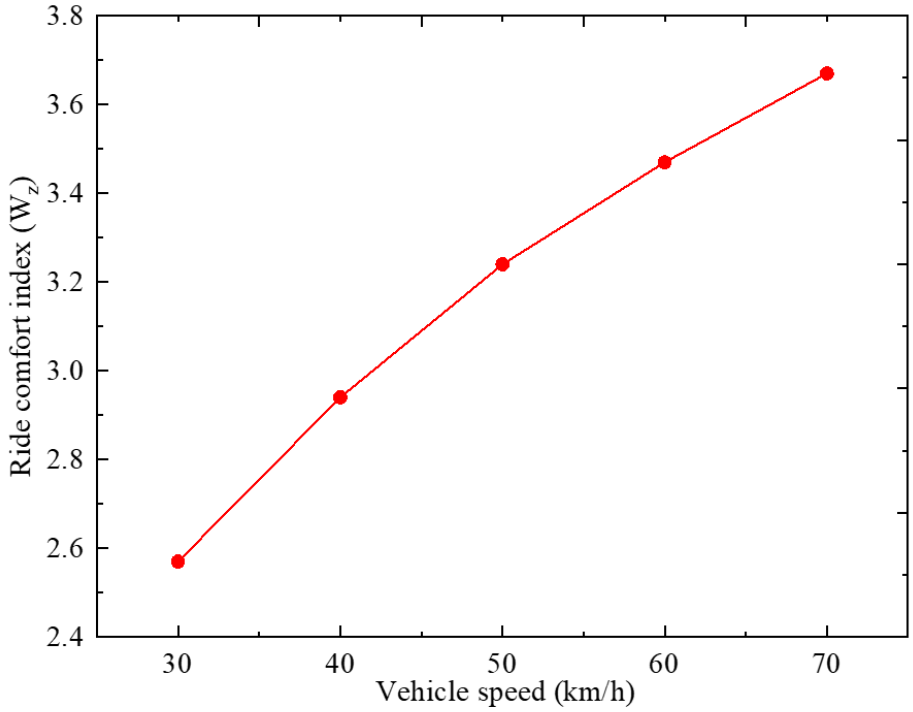

Figure 4.16: Ride comfort index due to 4th order of polygonization

Case 3: Running a vehicle having 6th order of polygonization with different speeds

The vehicle with a 59.24-tonne load was run at speeds of 30 km/h, 40 km/h, 50 km/h, 60 km/h, and 70 km/h with a polygonal wheel having 6th order. The highest speed (70 km/h) has a greater effect on ride comfort, as shown in Figure 4.17. The maximum ride comfort index is 4.07 caused by a speed of 70 km/h and the minimum ride comfort index is 3.07 caused by a speed of 30 km/h. The effect of polygonization on harmonic orders is summarized in Table 4.9.

Table 4.9: Ride comfort index due to different orders of polygonization

	Ride comfort index		
Vehicle speed (km/h)	2nd order	4th order	6th order
30	2.00	2.57	3.07
40	2.24	2.94	3.42
50	2.55	3.24	3.67
60	2.83	3.47	3.89
70	3.14	3.67	4.07

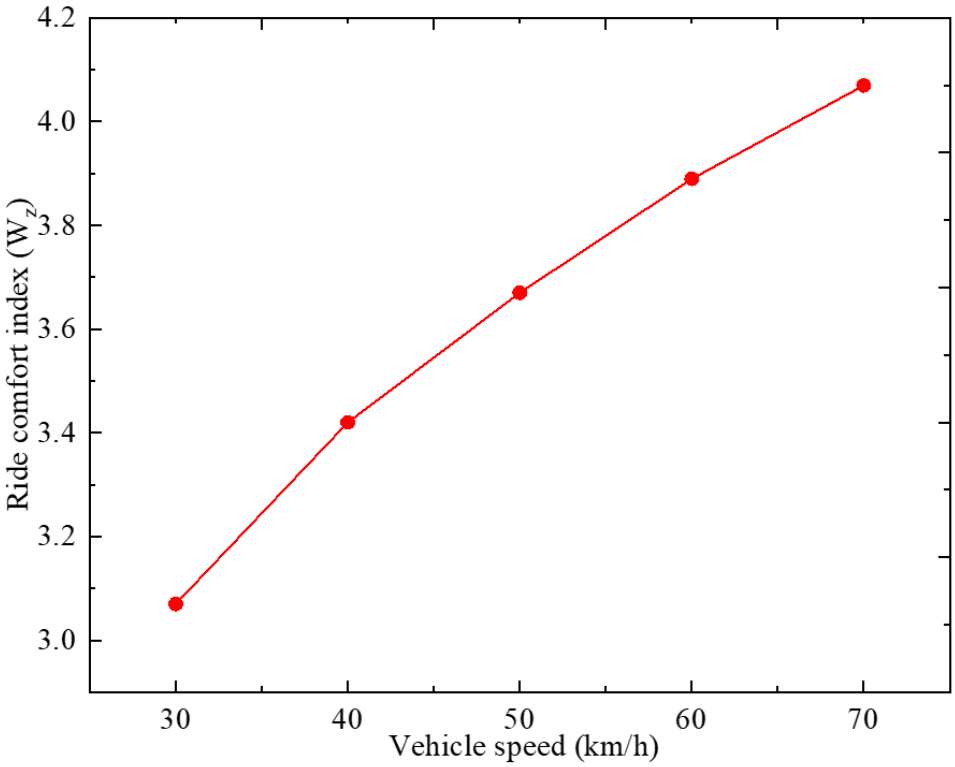

Figure 4.17: Ride comfort index due to 6th order of polygonization

4.5 Summary

For the case of wheel polygonization amplitude, the findings show that the amplitude of 0.3 mm has the highest value of the ride comfort index compared to the one obtained from 0.1 mm and 0.2 mm amplitude, i.e., 3.01. This means that the higher the polygonization amplitude, the higher the vibrations on rail-wheel contact.

Running a vehicle with polygonal wheels, the ride comfort index obtained was higher compared to the unpolygonal wheel effect in all cases of rated carrying capacity and overload carrying capacity. Moreover, with the increasing order of polygonization, the ride index also increases.

Vehicle speed seems to have a big effect on ride comfort in all cases, although it has been observed that running a vehicle at a high speed has a more negative effect on ride comfort compared to running at a low speed. This has also been proved by published works [5], [83]. So, operation at a high speed of 70 km/h will reduce the comfort of passengers. Refer to Table 2.1 for the ride comfort index evaluation scale.

CHAPTER FIVE

5.0 CONCLUSION AND RECOMMENDATION

5.1 Conclusion

In this research work, ANSYS and the SIMPACK platform were established. The multibody system of the AALRT vehicle model was integrated with FEM to study the effects of vehicle speed, vehicle carrying loads, and wheel polygonization amplitude on ride comfort when wheels experience polygonal defects. The following conclusions were drawn upon completion of the study:

- Wheel polygonization of 0.3 mm amplitude has more impact on ride comfort compared to the other amplitudes (0.1mm and 0.2mm). This implies that with an increase in polygonization amplitude, the ride index will also increase.
- Running an overloaded carrying capacity vehicle has minimal comfort compared to an empty and rated carrying capacity vehicle when the wheel has a polygonization defect.
- With increasing vehicle speed, the ride index also increases, which means that at high speeds, the ride comfort will be diminished.
- Oders of wheel polygonization also found that they have an effect on ride comfort. With the increasing order of polygonization, the ride index also increases.

5.2 Recommendation

This study has a significant impact on the maintenance planning for wheels and rails as well as operation management.

- For the operation team, when the rail vehicle wheel is polygonized before reprofilling the wheel, they can operate the vehicle with a rated carrying load at a speed of not more than 60 km/h and the vehicle with an overload carrying load at a speed of not more than 50 km/h.
- For the maintenance team, when the rail vehicle wheel is polygonized with a high amplitude from 0.3 mm to above, it is better to reprofile the wheel because the passengers will be uncomfortable.

5.3 Future works

The present study attempted to investigate the effect of a polygonized wheel on passenger ride comfort by considering a flexible wheelset and rigid carbody. The following suggestions for future investigation are provided as an extension and continuation of this study.

- Evaluate the effect of wheel polygonization on passenger ride comfort by considering curved track.
- Asses the effect of higher polygonization amplitudes on passenger ride comfort.
- Examine the effect of a higher number of harmonic-order polygons and out of roundness on passenger ride comfort.

REFERENCES

[1] Y. Peng *et al.*, "A review of passenger ride comfort in railway: assessment and improvement method," *Transp. Saf. Environ.*, vol. 4, no. 2, 2022, doi: 10.1093/tse/tdac016.

[2] M. Loulová, A. Suchánek, and J. Harušinec, "Evaluation of the Parameters Affecting Passenger Riding Comfort of a Rail Vehicle," *Manuf. Technol.*, vol. 17, no. 2, pp. 224–231, 2017, [Online]. Available: https://doi.org/10.xxxx/mft.2017.041

[3] G. Wang, C. Xie, J. H. Park, W. H. Kim, and C. Soo, "Critical points numerical analysis of ride comfort of the flexible railway carbody Critical points numerical analysis of ride comfort of the flexible railway carbody," 2019, doi: 10.1088/1757-899X/682/1/012004.

[4] L. Jing, K. Wang, and W. Zhai, "Impact vibration behavior of railway vehicles: a state-of-the-art overview," *Acta Mech. Sin. Xuebao*, vol. 37, no. 8, pp. 1193–1221, 2021, doi: 10.1007/s10409-021-01140-9.

[5] J. Dižo, M. Blatnický, S. Steišunas, and B. Skočilasová, "Assessment of a rail vehicle running with the damaged wheel on a ride comfort for passengers," *MATEC Web Conf.*, vol. 157, pp. 1–11, 2018, doi: 10.1051/matecconf/201815703004.

[6] A. Guizani, M. Hammadi, J. Choley, T. Soriano, M. S. Abbes, and M. Haddar, "Multiphysics Modelling and Simulation for Systems Design and Monitoring," *Multiphysics Model. Simul. Syst. Des. Monit.*, pp. 189–198, 2015, doi: 10.1007/978-3-319-14532-7.

[7] A. Suchánek, M. Loulová, and J. Harušinec, "Evaluation of passenger riding comfort of a rail vehicle by means dynamic simulations," *MATEC Web Conf.*, vol. 254, p. 03009, 2019, doi: 10.1051/matecconf/201925403009.

[8] G. Wang, C. Xie, J. H. Park, W. H. Kim, and C. Soo, "Ride comfort enhancement in railway vehicle by the reduction of the car body structural flexural vibration Ride comfort enhancement in railway vehicle by the reduction of the car body structural flexural vibration," 2017, doi: 10.1088/1757-899X/227/1/012042.

[9] J. Dižo *et al.*, "Evaluation of ride comfort in a railway passenger car depending on a change

of suspension parameters," *Sensors*, vol. 21, no. 23, 2021, doi: 10.3390/s21238138.

[10] Y. Ye, D. Shi, P. Krause, Q. Tian, and M. Hecht, "Wheel flat can cause or exacerbate wheel polygonization," *Veh. Syst. Dyn.*, vol. 58, no. 10, pp. 1575–1604, 2020, doi: 10.1080/00423114.2019.1636098.

[11] U. Olofsson and K. Sundvall, "Influence of leaf, humidity and applied lubrication on friction in the wheel-rail contact: Pin-on-disc experiments," *Proc. Inst. Mech. Eng. Part F J. Rail Rapid Transit*, vol. 218, no. 3, pp. 235–242, 2004, doi: 10.1243/0954409042389364.

[12] D. W. Barke and W. K. Chiu, "A review of the effects of out-of-round wheels on track and vehicle components," *Proc. Inst. Mech. Eng. Part F J. Rail Rapid Transit*, vol. 219, no. 3, pp. 151–175, 2005, doi: 10.1243/095440905X8853.

[13] B. Peng, S. Iwnicki, P. Shackleton, and Y. Song, "General conditions for railway wheel polygonal wear to evolve," *Veh. Syst. Dyn.*, vol. 59, no. 4, pp. 568–587, 2021, doi: 10.1080/00423114.2019.1697458.

[14] M. Dumitriu and M. A. Gheti, "Evaluation of the ride quality and ride comfort in railway annals of Faculty Engineering Hunedoara; Huneodoara – International Journal of Engineering," vol. 13, no. 3, pp. 123-132, January, 2016, doi: https://www.proquest.com/openview/f289e7175753130d51ff9f0ff804dbe7/1.pdf?pq-origsite=gscholar&cbl=616472.

[15] M. Dumitriu, "Numerical analysis on the influence of suspended equipment on the ride comfort in railway vehicles," *Arch. Mech. Eng.*, vol. 65, no. 4, pp. 477–496, 2018, doi: 10.24425/ame.2018.125438.

[16] T. Imran, T. Munawir, A. Abqari, A. Samah, and M. Afiq, "A Comparison Study on the Assessment of Ride Comfort for LRT Passengers," vol. 012039, 2017, doi: 10.1088/1757-899X/226/1/012039.

[17] E. Dumitriu, "Evaluation of the comfort index in railway vehicles depending on the vertical suspension," pp. 23–32, 2019, https://www.researchgate.net/publication/281092175_Evaluation_of_the_comfort_index_i

n_railway_vehicles_depending_on_the_vertical_suspension_features

[18] W. Huang and B. Shuai, "A methodology for calculating the passenger comfort benefits of railway travel," *J. Mod. Transp.*, vol. 26, no. 2, pp. 107–118, 2018, doi: 10.1007/s40534-018-0157-y.

[19] Y. Kim, H. Kwon, S. Kim, C. Park, and T. Park, "Correlation of ride comfort evaluation methods for railway vehicles," *J. rail rapid transit*, vol. 217, pp. 73–88, 2015, doi: 10.1243/095440903765762823.

[20] Y. Jiang, B. K. Chen, and C. Thompson, "A comparison study of ride comfort indices between Sperling's method and EN 12299," *Int. J. Rail Transp.*, vol. 7, no. 4, pp. 279–296, 2019, doi: 10.1080/23248378.2019.1616329.

[21] M. Nastac, S., Picu, "Whole-Body-Vibration Exposure in Trains," *Fascicle XIV Mech. Eng.*, vol. 6841, no. 2010, pp. 55–60, 2010, doi.org/10.3844/ajassp.2010.352.359.

[22] P. Filipa Pinheiro da Silva and J. Mendes, "Passengers Comfort Perception and Demands on Railway Vehicles: A Review," *KnE Eng.*, vol. 2020, pp. 257–270, 2020, doi: 10.18502/keg.v5i6.7039.

[23] D. J. Oborne and M. J. Clarke, "The development of questionnaire surveys for the investigation of passenger comfort," *Ergonomics*, vol. 16, no. 6, pp. 855–869, 2013, doi: 10.1080/00140137308924577.

[24] J. Huang and S. Kaewunruen, "Evaluation of Railway Passenger Comfort with Machine Learning," *IEEE Access*, vol. 10, pp. 2372–2381, 2022, doi: 10.1109/ACCESS.2021.3139465.

[25] K. V. Gangadharan, C. Sujatha, and V. Ramamurti, "Dynamic response of railroad vehicles: A frequency domain approach," *Int. J. Heavy Veh. Syst.*, vol. 15, no. 1, pp. 65–81, 2008, doi: 10.1504/IJHVS.2008.017984.

[26] R. C. Sharma, "Evaluation of passenger ride comfort of Indian rail and road vehicles with ISO 2631-1 standards: Part 2 - simulation," *Int. J. Veh. Struct. Syst.*, vol. 8, no. 1, pp. 7–10, 2016, doi: 10.4273/ijvss.8.1.02.

[27] J. Winter, I. Windemut, N. Kevlishvili, D. Schmeling, and J. Maier, "Passenger comfort for the next generation train: Subject trials for ventilation and lighting," *Civil-Comp Proc.*, vol. 110, pp. 1–12, 2016, doi: 10.4203/ccp.110.196.

[28] P. D. Cand *et al.*, "Ride Comfort Analysis with Physiological," pp. 1010–1021, doi: 10.1089/tmj.2009.0040.

[29] Z. Tang and J. Xu, "Research on the physiological and psychological factors' evaluation index framework of train ride comfort," *2013 IEEE Conf. Anthol. Anthol. 2013*, no. January 2013, 2013, doi: 10.1109/ANTHOLOGY.2013.6784702.

[30] H. Ciloglu, M. Alziadeh, A. Mohany, and H. Kishawy, "Assessment of the whole body vibration exposure and the dynamic seat comfort in passenger aircraft," *Int. J. Ind. Ergon.*, vol. 45, pp. 116–123, 2015, doi: 10.1016/j.ergon.2014.12.011.

[31] P. Filipa Pinheiro da Silva and J. Mendes, "Passengers Comfort Perception and Demands on Railway Vehicles: A Review," *KnE Eng.*, no. June, 2020, doi: 10.18502/keg.v5i6.7039.

[32] F. Han, Z. Liu, and C. Wang, "Research on a Comfort Evaluation Model for High-Speed Trains Based on Variable Weight Theory," *Appl. Sci.*, vol. 13, no. 5, 2023, doi: 10.3390/app13053144.

[33] I. Haladin, S. Lakušić, and M. Bogut, "Overview and analysis of methods for assessing ride comfort on tram tracks," *Gradjevinar*, vol. 71, no. 10, pp. 901–921, 2019, doi: 10.14256/JCE.2731.2019.

[34] A. Rodríguez, R. Sañudo, M. Miranda, A. Gómez, and J. Benavente, "Smartphones and tablets applications in railways, ride comfort and track quality. Transition zones analysis," *Meas. J. Int. Meas. Confed.*, vol. 182, 2021, doi: 10.1016/j.measurement.2021.109644.

[35] E. Kardas-cinal, "Analysis of ride comfort in selected types of rail vehicles," vol. 51, no. 4, pp. 157–183, 2021, doi: 10.2478/jok-2021-0049.

[36] M. Dumitriu and D. I. Stănică, "Study on the evaluation methods of the vertical ride comfort of railway vehicle—mean comfort method and sperling's method," *Appl. Sci.*, vol. 11, no. 9, 2021, doi: 10.3390/app11093953.

[37] J. Yang, J. Wang, and Y. Zhao, "Simulation of nonlinear characteristics of vertical vibration of railway freight wagon varying with train speed," *Electron. Res. Arch.*, vol. 30, no. 12, pp. 4382–4400, 2022, doi: 10.3934/era.2022222.

[38] F. R. Vehicle and C. Resonant, "Flexible-Rigid Rail Vehicle Carbody Resonant Vibration," pp. 1–17, 2022, doi.org/10.1080/00423114.2022.2150233.

[39] J. L. Escalona, H. Sugiyama, and A. A. Shabana, "Modelling of structural flexiblity in multibody railroad vehicle systems," *Veh. Syst. Dyn.*, vol. 51, no. 7, pp. 1027–1058, 2013, doi: 10.1080/00423114.2013.786835.

[40] P. Carlbom, "Carbody and passengers in rail vehicle dynamics," 2019, [Online]. Available: http://urn.kb.se/resolve?urn=urn:nbn:se:kth:diva-3029

[41] B. Peng, S. Iwnicki, P. Shackleton, D. Crosbee, and Y. Zhao, "The influence of wheelset flexibility on polygonal wear of locomotive wheels," *Wear*, vol. 432–433, no. January, 2019, doi: 10.1016/j.wear.2019.05.032.

[42] G. Bethel Lulu, R. Chen, P. Wang, J. Xu, J. Chen, and J. Fang, "Random vibration analysis of tram-track interaction on a curve due to the polygonal wheel and track irregularity," *Veh. Syst. Dyn.*, vol. 60, no. 4, pp. 1125–1147, 2022, doi: 10.1080/00423114.2020.1847299.

[43] L. Baeza, J. Giner-Navarro, D. J. Thompson, and J. Monterde, "Eulerian models of the rotating flexible wheelset for high frequency railway dynamics," *J. Sound Vib.*, vol. 449, pp. 300–314, 2019, doi: 10.1016/j.jsv.2019.03.002.

[44] B. Jagadeep, P. Kiran Kumar, and K. V. Subbaiah, "Stress Analysis on Rail Wheel Contact," *Int. J. Res. Eng.*, no. 1, pp. 47–52, 2018, [Online]. Available: www.ijresm.com

[45] Y. Yang, L. Ling, Y. Yang, S. Chen, and K. Wang, "Effects of wheelset flexibility on locomotive–track interaction due to rail weld irregularities," *Veh. Syst. Dyn.*, vol. 60, no. 9, pp. 3088–3108, 2022, doi: 10.1080/00423114.2021.1939063.

[46] A. Kumar and K. Sreenivas, "Design dan Analysis of Railwheel Failure," *Int. Res. J. Eng.*

Technol., vol. 04, no. 12, pp. 36–40, 2017, [Online]. Available: www.irjet.net

[47] Y. D. Jelila and H. G. Lemu, *Study of Wheel-Rail Contacts at Railway Turnout Using Multibody Dynamics Simulation Approach*, vol. 737, no. February. Springer Singapore, 2021. doi: 10.1007/978-981-33-6318-2_46.

[48] H. Shi, F. Gan, F. Li, and J. Guo, "Numerical and experimental investigation of the wheel/rail interaction and dynamics for a high-speed gauge-changeable railway vehicle," *Veh. Syst. Dyn.*, vol. 60, no. 9, pp. 3198–3214, 2022, doi: 10.1080/00423114.2021.1942506.

[49] M. W. Y. Hu, "Experimental study on wear properties of wheel and rail materials with different hardness values," 2021.

[50] Y. Hu *et al.*, "Experimental study on wear properties of wheel and rail materials with different hardness values," *Wear*, vol. 477, no. February, 2021, doi: 10.1016/j.wear.2021.203831.

[51] M. N. Tawfik, M. M. Padzi, Shahrum, H. Hapaz, M. Zahar, and M. Nur Firdaws, "Approaches of Finite Element Analysis to Study Fatigue Analysis of Rail-Wheel Contact for Light Rail Transit," *Int. J. Integr. Eng.*, vol. 14, no. 8, pp. 86–91, 2022, doi: 10.30880/ijie.2022.14.08.011.

[52] T. Y. Kim and H. K. Kim, "Three-dimensional elastic-plastic finite element analysis for wheel-rail rolling contact fatigue," *Int. J. Eng. Technol.*, vol. 6, no. 3, pp. 1593–1600, 2014.

[53] H. M. El-sayed, M. Lotfy, H. N. El-din Zohny, and H. S. Riad, "Prediction of fatigue crack initiation life in railheads using finite element analysis," *Ain Shams Eng. J.*, vol. 9, no. 4, pp. 2329–2342, 2018, doi: 10.1016/j.asej.2017.06.003.

[54] J. P. Srivastava, P. K. Sarkar, and V. Ranjan, "Contact Stress Analysis in Wheel–Rail by Hertzian Method and Finite Element Method," *J. Inst. Eng. Ser. C*, vol. 95, no. 4, pp. 319–325, 2014, doi: 10.1007/s40032-014-0145-x.

[55] L. Xu and W. Zhai, "Probabilistic assessment of railway vehicle-curved track systems considering track random irregularities," *Veh. Syst. Dyn.*, vol. 56, no. 10, pp. 1552–1576, 2018, doi: 10.1080/00423114.2018.1424916.

[56] J. N. Costa, P. Antunes, H. Magalhães, J. Pombo, and J. Ambrósio, "A novel methodology to automatically include general track flexibility in railway vehicle dynamic analyses," *Proc. Inst. Mech. Eng. Part F J. Rail Rapid Transit*, vol. 235, no. 4, pp. 478–493, 2021, doi: 10.1177/0954409720945420.

[57] B. Peng, S. Iwnicki, P. Shackleton, and D. Crosbee, "Comparison of wear models for simulation of railway wheel polygonization," *Wear*, vol. 436–437, no. May, p. 203010, 2019, doi: 10.1016/j.wear.2019.203010.

[58] A. Guedes *et al.*, "Detection of Wheel Polygonization Based on Wayside Monitoring and Artificial Intelligence," *Sensors*, vol. 23, no. 4, 2023, doi: 10.3390/s23042188.

[59] A. Mosleh, P. A. Costa, and R. Calçada, "A new strategy to estimate static loads for the dynamic weighing in motion of railway vehicles," *Proc. Inst. Mech. Eng. Part F J. Rail Rapid Transit*, vol. 234, no. 2, pp. 183–200, 2020, doi: 10.1177/0954409719838115.

[60] G. Tao, "Polygonisation of railway wheels : a critical review," *Railw. Eng. Sci.*, vol. 28, no. 4, pp. 317–345, 2020, doi: 10.1007/s40534-020-00222-x.

[61] B. Fu, S. Bruni, and S. Luo, "Study on wheel polygonization of a metro vehicle based on polygonal wear simulation," *Wear*, p. 203071, 2019, doi: 10.1016/j.wear.2019.203071.

[62] G. Tao, Z. Wen, X. Jin, and X. Yang, "Polygonisation of railway wheels: a critical review," *Railw. Eng. Sci.*, vol. 28, no. 4, pp. 317–345, 2020, doi: 10.1007/s40534-020-00222-x.

[63] V. Gonçalves, A. Mosleh, C. Vale, and P. A. Montenegro, "Wheel Out-of-Roundness Detection Using an Envelope Spectrum Analysis," *Sensors*, vol. 23, no. 4, 2023, doi: 10.3390/s23042138.

[64] B. Peng, S. Iwnicki, and P. Shackleton, "Mechanisms of Railway Wheel Polygonization," 2020, https://core.ac.uk/reader/384446060.

[65] H. Wu, P. Wu, F. Li, H. Shi, and K. Xu, "Fatigue analysis of the gearbox housing in high-speed trains under wheel polygonization using a multibody dynamics algorithm," *Eng. Fail. Anal.*, vol. 100, no. February, pp. 351–364, 2019, doi: 10.1016/j.engfailanal.2019.02.058.

[66] Z. Chi, J. Lin, R. Chen, and S. Huang, "Data-driven approach to study the polygonization of high-speed railway train wheel-sets using field data of China's HSR train," *Meas. J. Int. Meas. Confed.*, vol. 149, p. 107022, 2020, doi: 10.1016/j.measurement.2019.107022.

[67] Y. Song, Y. Du, X. Zhang, and B. Sun, "Evaluating the Effect of Wheel Polygons on Dynamic Track Performance in High-Speed Railway Systems Using Co-Simulation Analysis," 2019, doi.org/10.3390/app9194165.

[68] A. Momhur, Y. X. Zhao, W. Q. Li, Y. Z. Sun, and X. L. Zou, "Flexible-Rigid Wheelset Introduced Dynamic Effects due to Wheel Tread Flat," *Shock Vib.*, vol. 2021, pp. 13–23, 2021, doi: 10.1155/2021/5537286.

[69] J. Wu and Y. Qiu, "Modelling and ride comfort analysis of a coupled track-train-seat-human model with lateral , vertical and roll vibrations," no. May, 2021, doi: 10.1080/00423114.2021.1933088.

[70] J. Dižo, M. Blatnický, and R. Melnik, "Assessment of the Passenger Ride Comfort for a Coach by Means of Simulation Computations," vol. 8, no. 2, pp. 24–32, 2017, doi: 10.1515/logi-2017-0013.

[71] J. Dižo, M. Blatnický, S. Steišūnas, and G. Vaičiūnas, "Evaluation of the Influence of a Rail Vehicle Running with Wheel-flat on the Railway Track," vol. 9, no. 1, pp. 24–31, 2018, doi: 10.2478/logi-2018-0004.

[72] G. Wang, C. Xie, Q. Zhou, and P. Yuan, "Experimental Analysis of Ride Comfort Quality for High-speed Railway Vehicles Experimental Analysis of Ride Comfort Quality for High-speed Railway Vehicles," 2020, doi: 10.1088/1742-6596/1653/1/012065.

[73] Y. Zeng, D. Song, and W. Zhang, "Risk assessment of wheel polygonization on high-speed trains based on Bayesian networks," pp. 1–11, 2020, doi: 10.1177/1748006X20972574.

[74] V. Kumar, V. Rastogi, and P. M. Pathak, "Simulation for whole-body vibration to assess ride comfort of a low-medium speed railway vehicle," *Simulation*, vol. 93, no. 3, pp. 225–236, 2017, doi: 10.1177/0037549716679254.

[75] J. Sadeghi, S. Rabiee, and A. Khajehdezfuly, "Effect of Rail Irregularities on Ride Comfort

of Train Moving over Ballast-Less Tracks," *Int. J. Struct. Stab. Dyn.*, vol. 19, no. 6, 2019, doi: 10.1142/S0219455419500603.

[76] Z. Chen and G. Zhu, "Dynamic evaluation on ride comfort of metro vehicle considering structural flexibility," *Arch. Civ. Mech. Eng.*, vol. 21, no. 4, pp. 1–16, 2021, doi: 10.1007/s43452-021-00310-7.

[77] G. Tao, M. Liu, Q. Xie, and Z. Wen, "Wheel–rail dynamic interaction caused by wheel out-of-roundness and its transmission between wheelsets," *Proc. Inst. Mech. Eng. Part F J. Rail Rapid Transit*, vol. 236, no. 3, pp. 247–261, 2022, doi: 10.1177/09544097211016582.

[78] "International standard travel and traversing tracks —," vol. 2004, https://cdn.standards.iteh.ai/samples/34547/c26fdf39ca9946c3be37d6a72f96e376/ISO-12488-1-2005.

[79] S. White and M. Uhlig, "Wheel & axle reference manual," *Transp. RailCorp*, vol. 1, no. 1, pp. 1–62, 2013, https://extranet.artc.com.au/docs/eng/rolling-stock/maintain/RSS0031.

[80] M. Dumitriu, "Numerical study of the inuence of suspended equipment on ride comfort in high-speed railway vehicles," *Sci. Iran.*, vol. 27, no. 4 B, pp. 1897–1915, 2020, doi: 10.24200/sci.2019.50946.1930.

[81] J. N. Costa, J. Ambrósio, D. Frey, and A. R. Andrade, "A multivariate statistical representation of railway track irregularities using ARMA models," *Veh. Syst. Dyn.*, vol. 60, no. 7, pp. 2494–2510, 2022, doi: 10.1080/00423114.2021.1912365.

[82] Y. Dai and C. Ye, "Influence of Wheel Polygons on Dynamic Performance of Trains," vol. 5, no. 2, 2023, doi: 10.54097/ajst.v5i2.5928.

[83] L. Jing, Z. Liu, and K. Liu, "A mathematically-based study of the random wheel-rail contact irregularity by wheel out-of-roundness," *Veh. Syst. Dyn.*, vol. 60, no. 1, pp. 335–370, 2022, doi: 10.1080/00423114.2020.1815809.

[84] Baeza L, Fayos J, Roda A, "High frequency railway vehicle-track dynamics through flexible rotating wheelsets," *Veh. Syst. Dyn.*, vol. 46, no. 7, pp. 647–659, 2008, doi: 10.1080/00423110701656148.

Appendices

Appendix A: AALRT vehicle weight and carrying capacity data

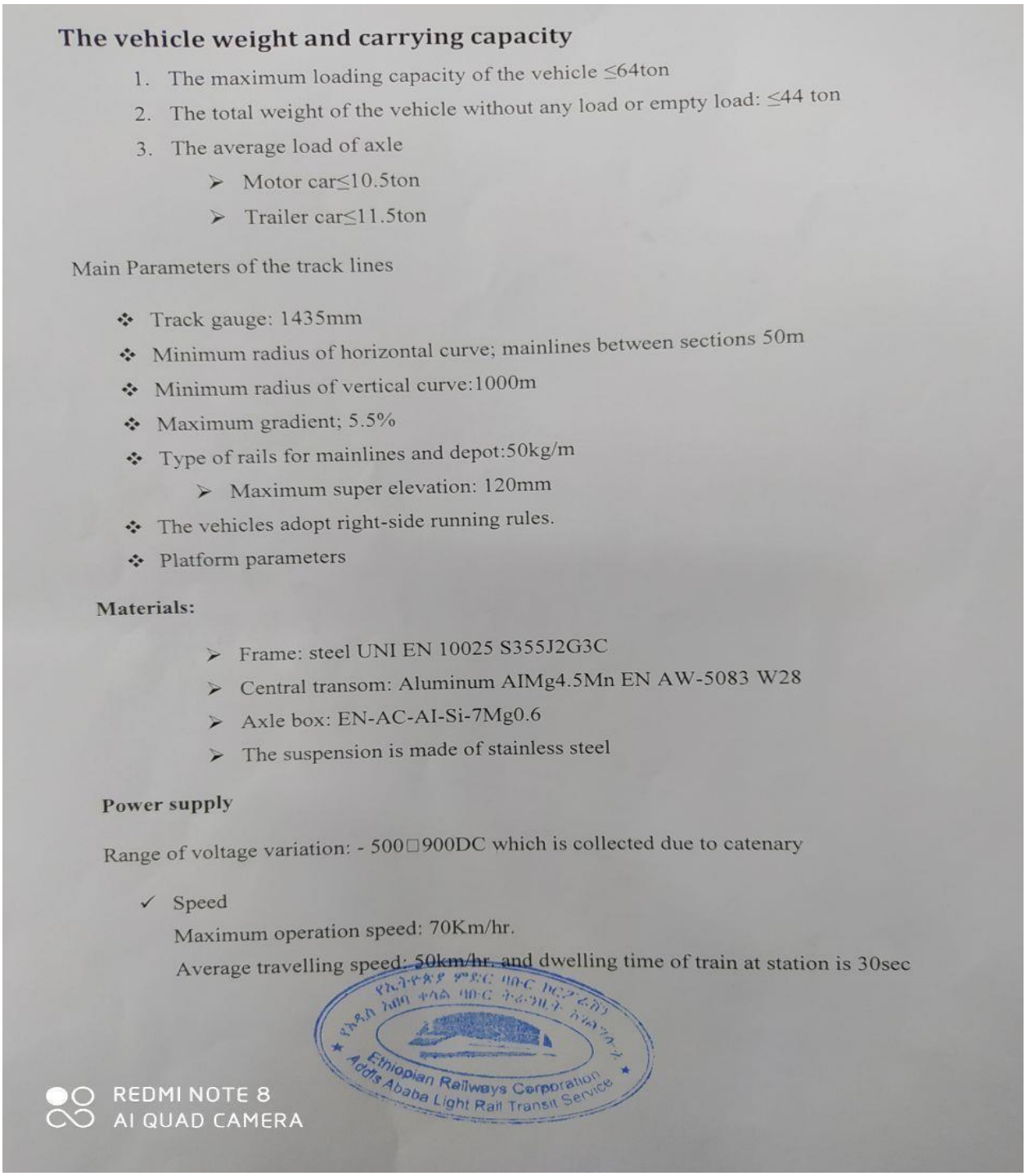

The vehicle weight and carrying capacity

1. The maximum loading capacity of the vehicle ≤64ton
2. The total weight of the vehicle without any load or empty load: ≤44 ton
3. The average load of axle
   - Motor car≤10.5ton
   - Trailer car≤11.5ton

Main Parameters of the track lines

- Track gauge: 1435mm
- Minimum radius of horizontal curve; mainlines between sections 50m
- Minimum radius of vertical curve:1000m
- Maximum gradient; 5.5%
- Type of rails for mainlines and depot:50kg/m
  - Maximum super elevation: 120mm
- The vehicles adopt right-side running rules.
- Platform parameters

Materials:

- Frame: steel UNI EN 10025 S355J2G3C
- Central transom: Aluminum AIMg4.5Mn EN AW-5083 W28
- Axle box: EN-AC-AI-Si-7Mg0.6
- The suspension is made of stainless steel

Power supply

Range of voltage variation: - 500□900DC which is collected due to catenary

- ✓ Speed

  Maximum operation speed: 70Km/hr.

  Average travelling speed: 50km/hr. and dwelling time of train at station is 30sec

Ethiopian Railways Corporation
Addis Ababa Light Rail Transit Service

REDMI NOTE 8
AI QUAD CAMERA

Appendix B: Modelling and assembling of wheelset in Solidworks

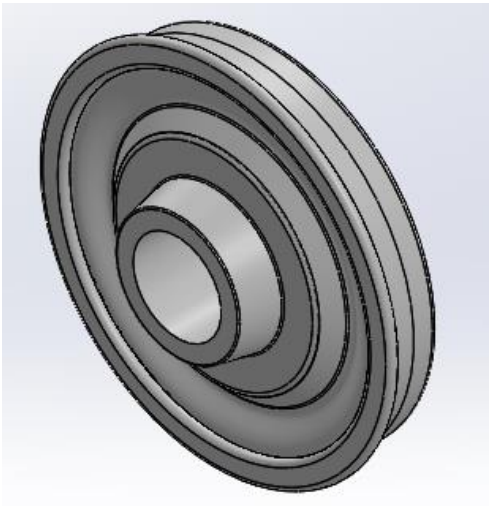

(a) Wheel

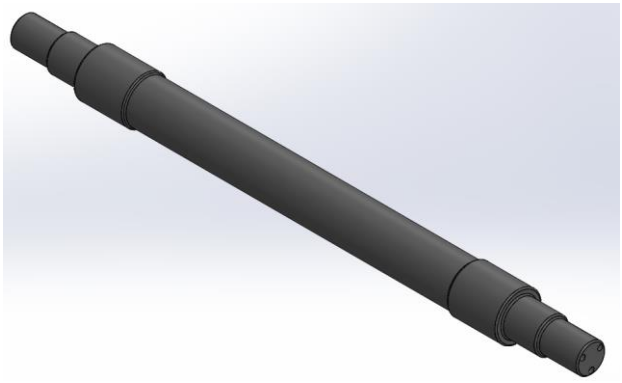

(b) Wheelset axle

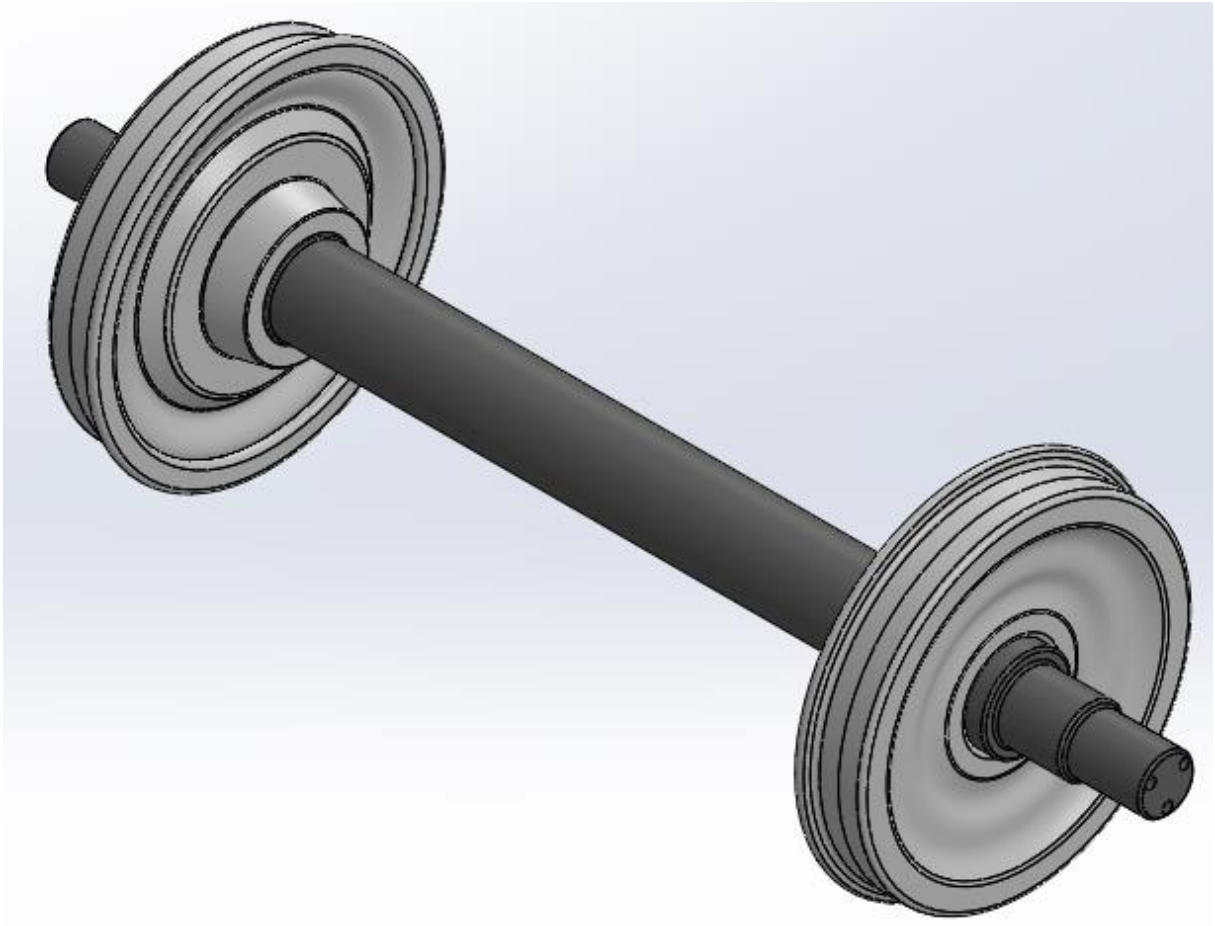

(c) 3D Wheelset

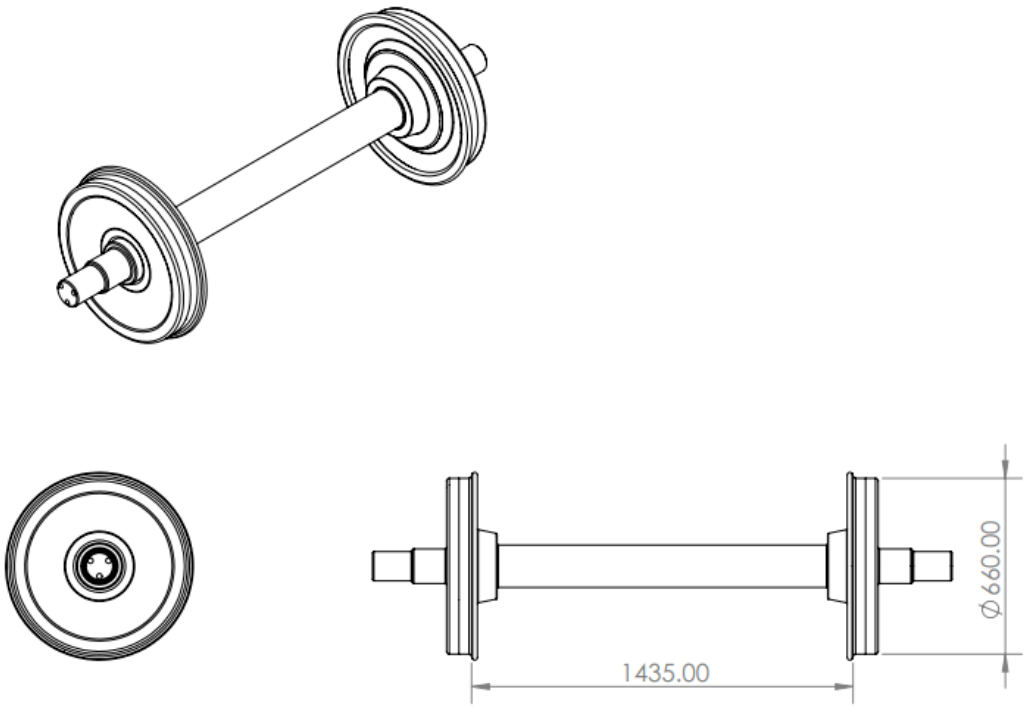

(d) 2D Wheelset

Appendix C: Meshing of wheelset in Asnys

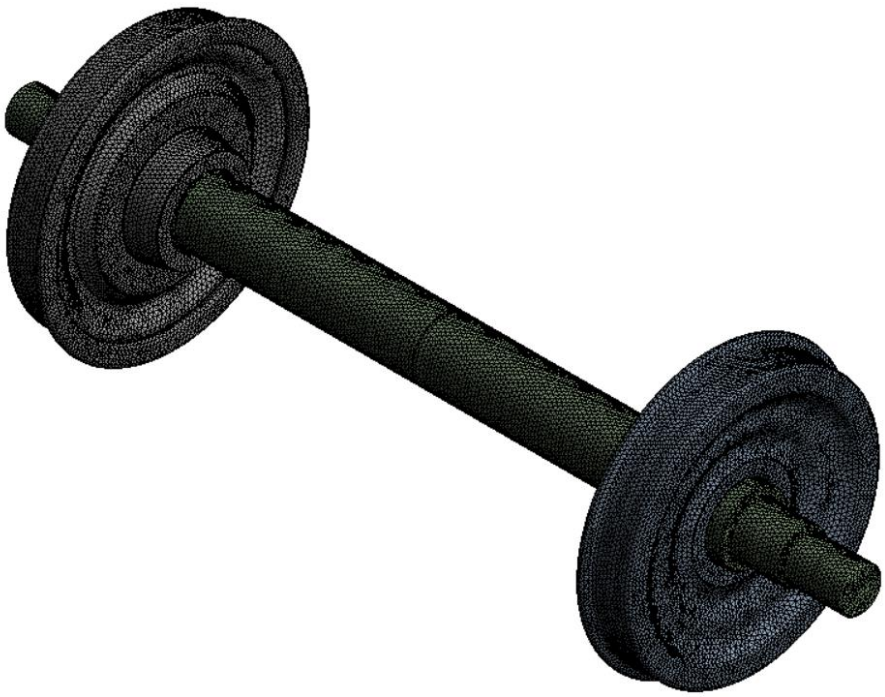

Details of "Mesh"

Display	
Display Style	Use Geometry Setting
Defaults	
Physics Preference	Mechanical
Element Order	Program Controlled
Element Size	Default
Sizing	
Use Adaptive Sizi...	Yes
Resolution	Default (2)
Mesh Defeaturing	Yes
Defeature Size	Default
Transition	Fast
Span Angle Center	Coarse
Initial Size Seed	Assembly
Bounding Box Di...	2539.6 mm
Average Surface ...	38541 mm²
Minimum Edge L...	62.832 mm
Quality	
Inflation	
Advanced	
Statistics	
Nodes	1250311
Elements	873821

(a) Meshed wheelset

(b) Section view of the meshed wheelset

Appendix D: Selection of master nodes

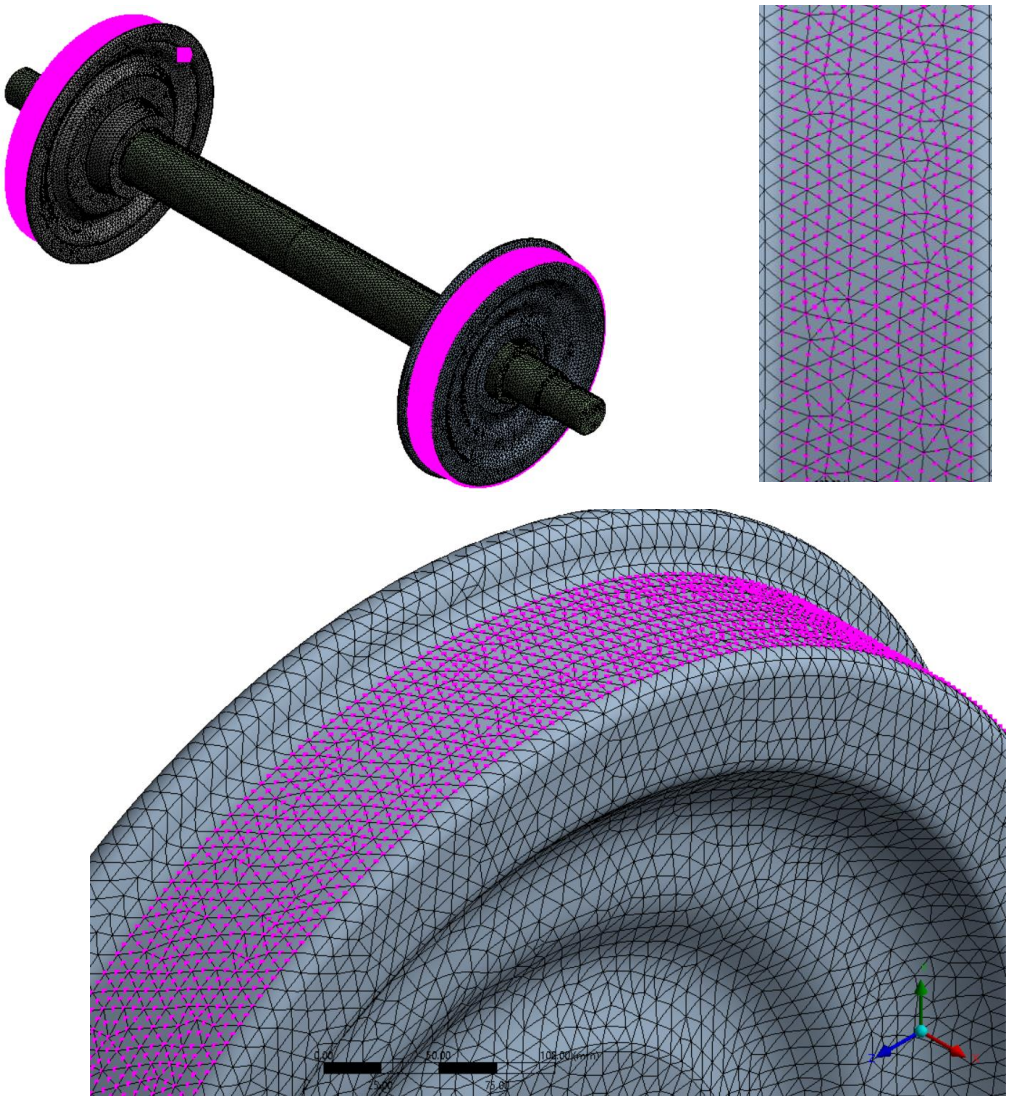

Selection of master nodes from the wheelset

Appendix E: Validation of the dynamic model of a multibody system

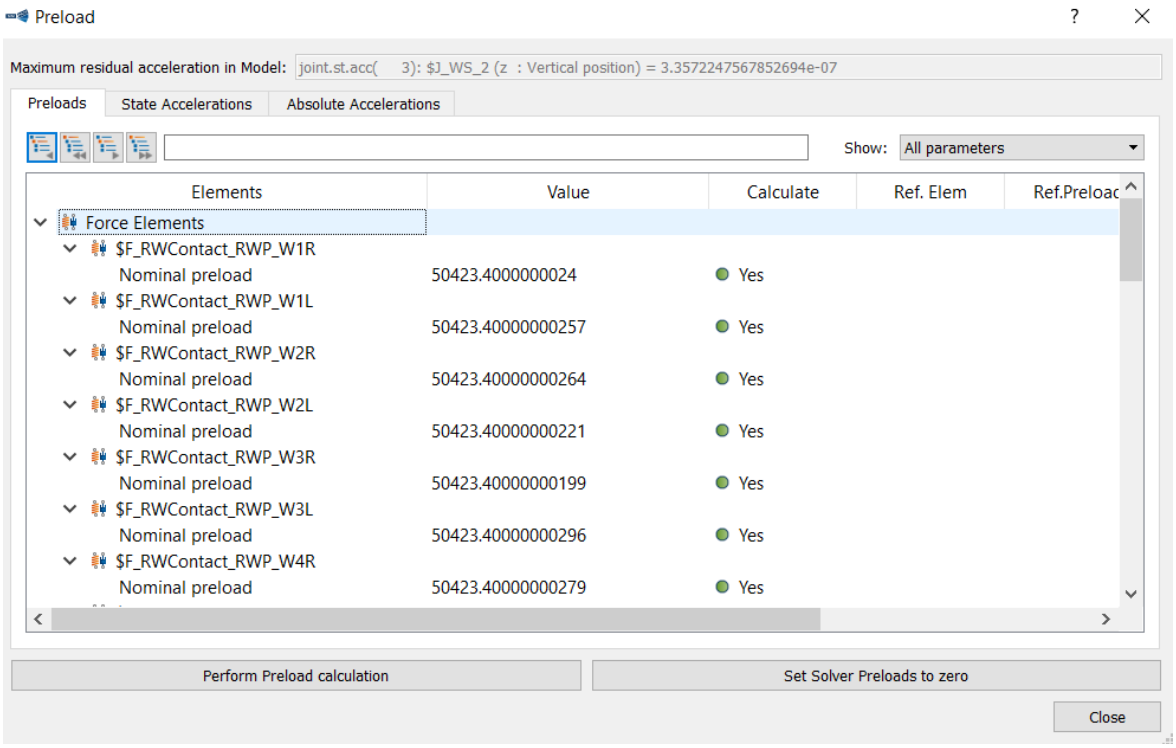

(a) Preload static force

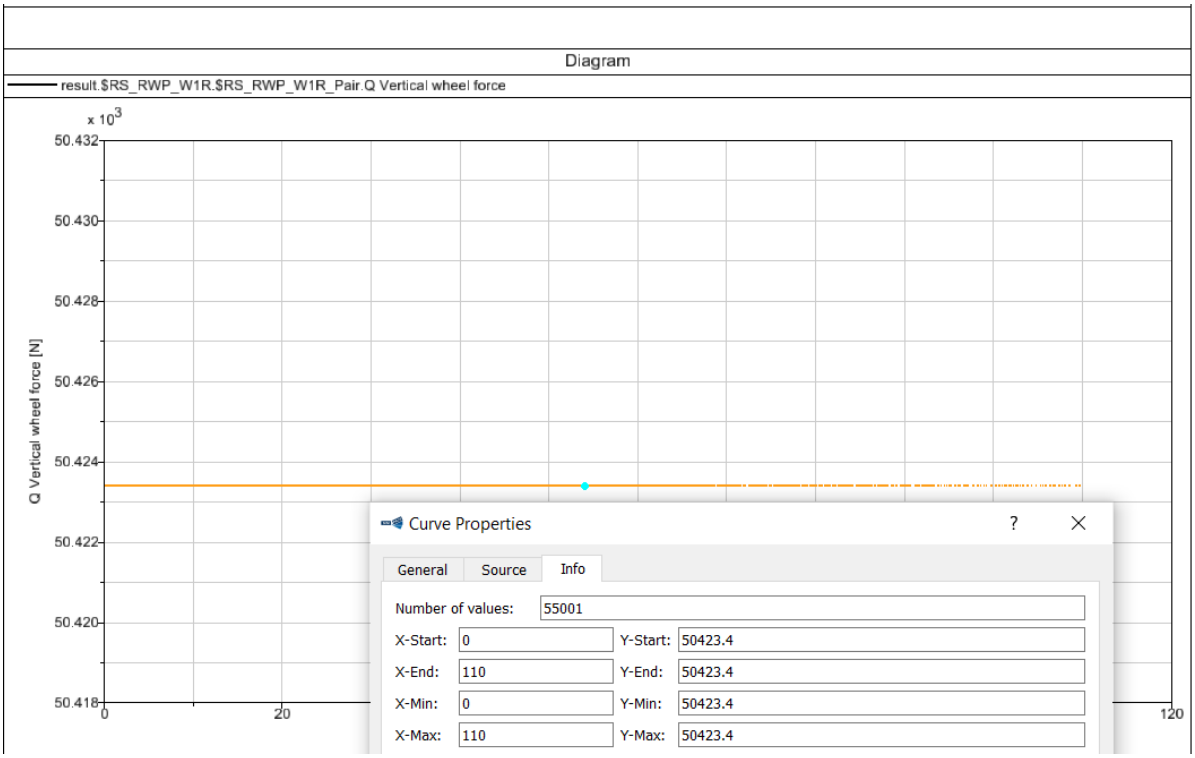

(b) Maximum vertical dynamic force without irregularities

Appendix F: Rail-wheel force obtained due to rated carrying load

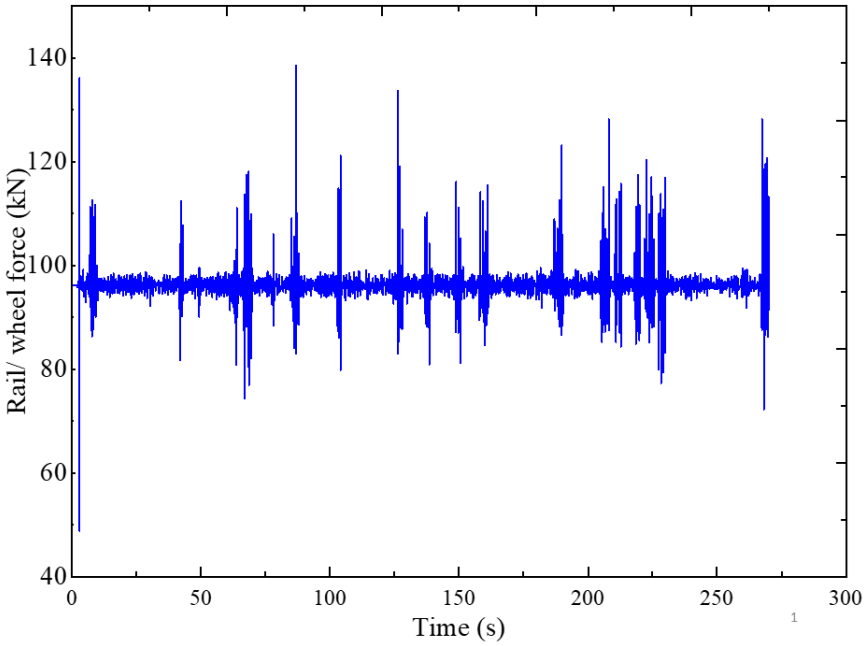

(a) Rail-wheel vertical force at 30 km/h

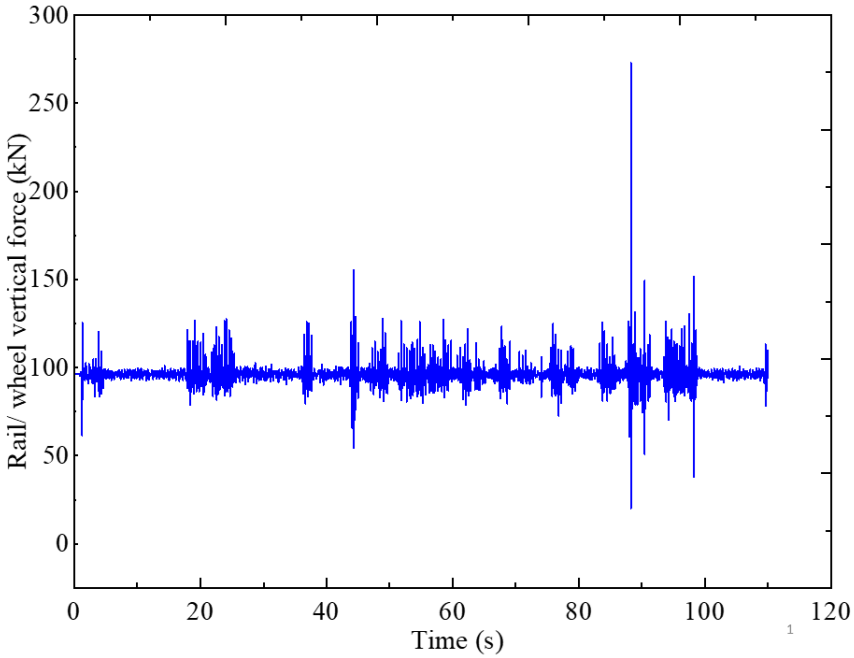

(b) Rail-wheel vertical force at 70 km/h

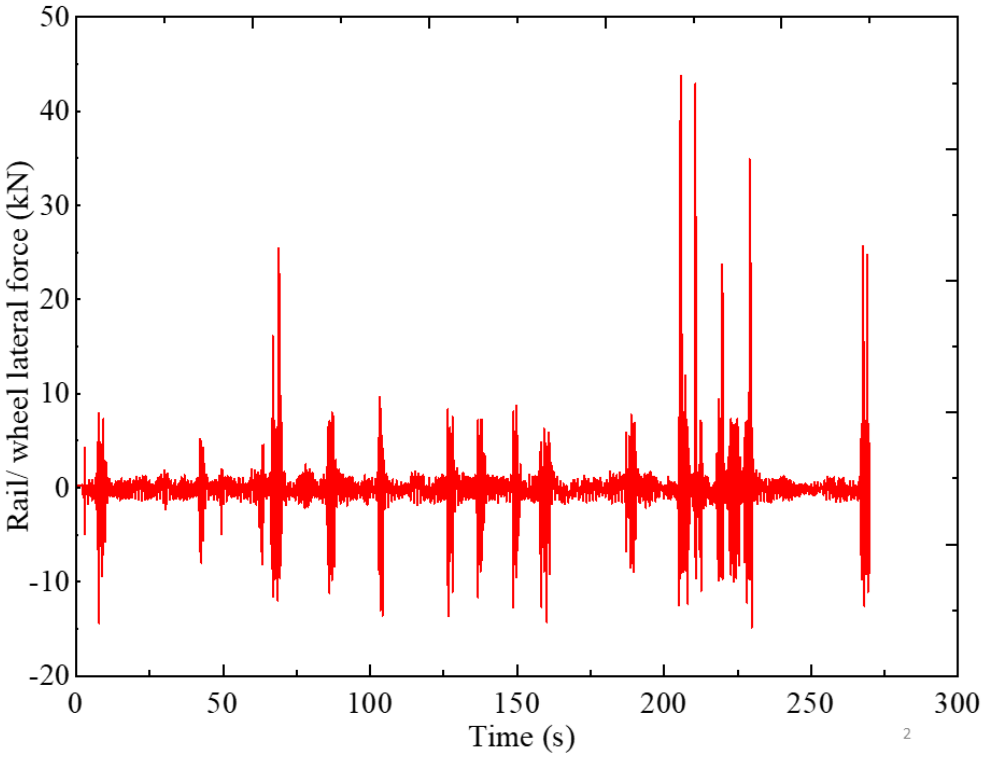

(c) Rail-wheel Lateral force at 30 km/h

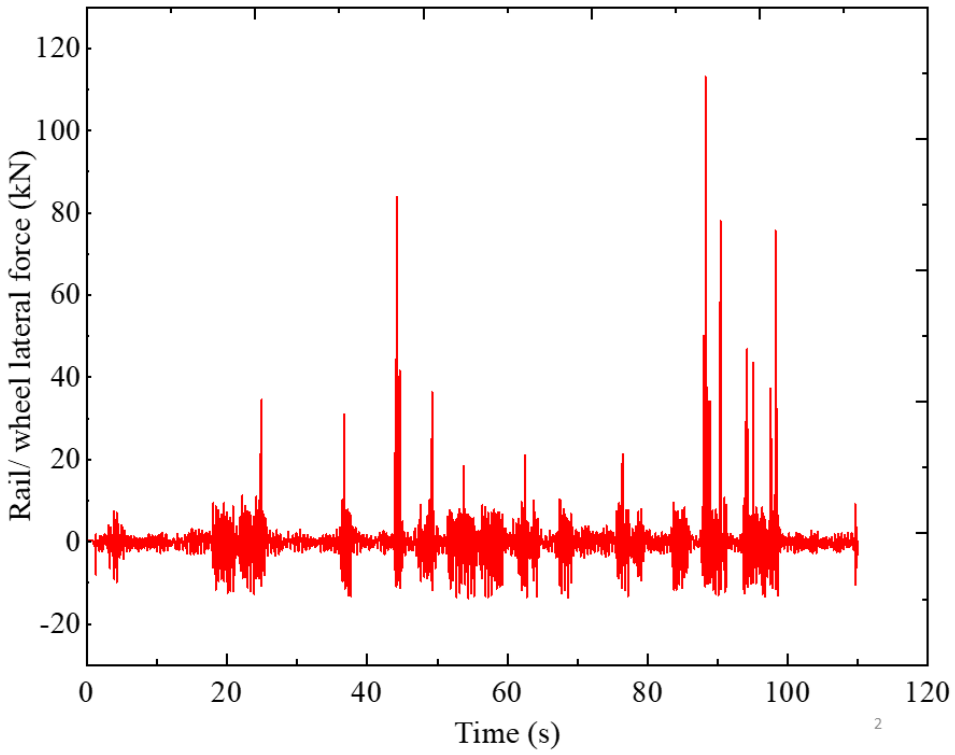

(d) Rail-wheel vertical force at 70 km/h

Appendix G: Rail-wheel force obtained due to overload carrying load

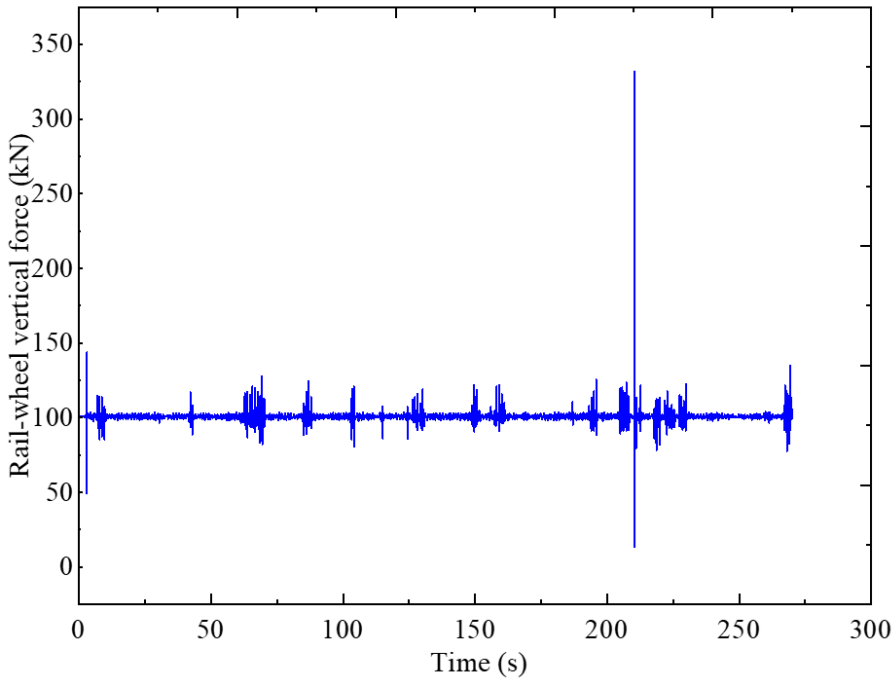

(a) Rail-wheel vertical force at 30 km/h

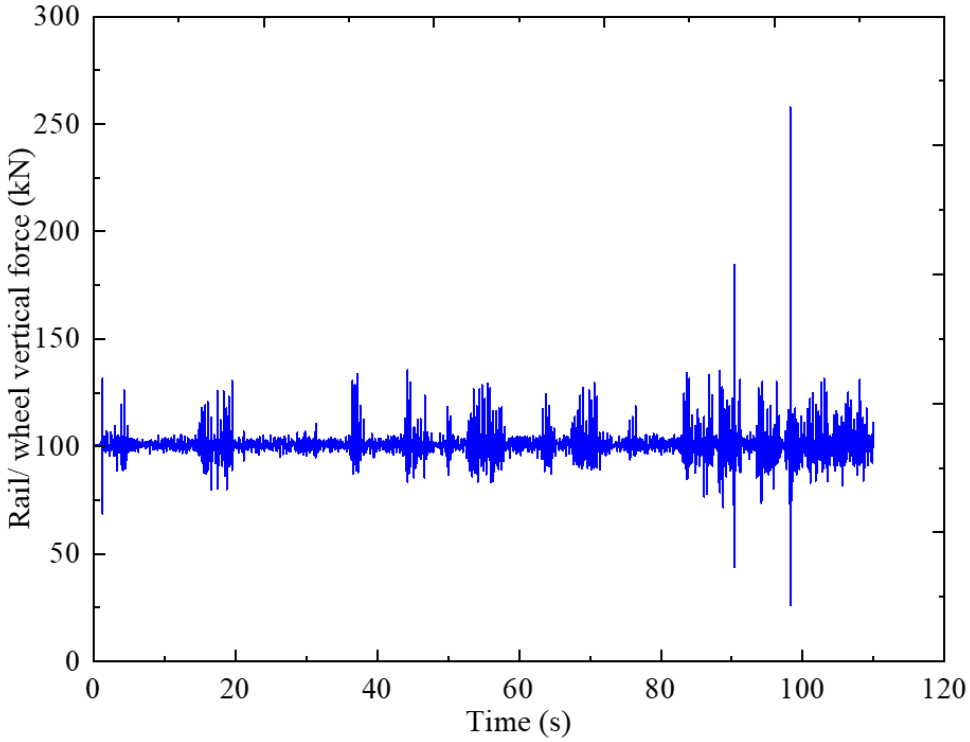

(b) Rail-wheel vertical force at 70 km/h

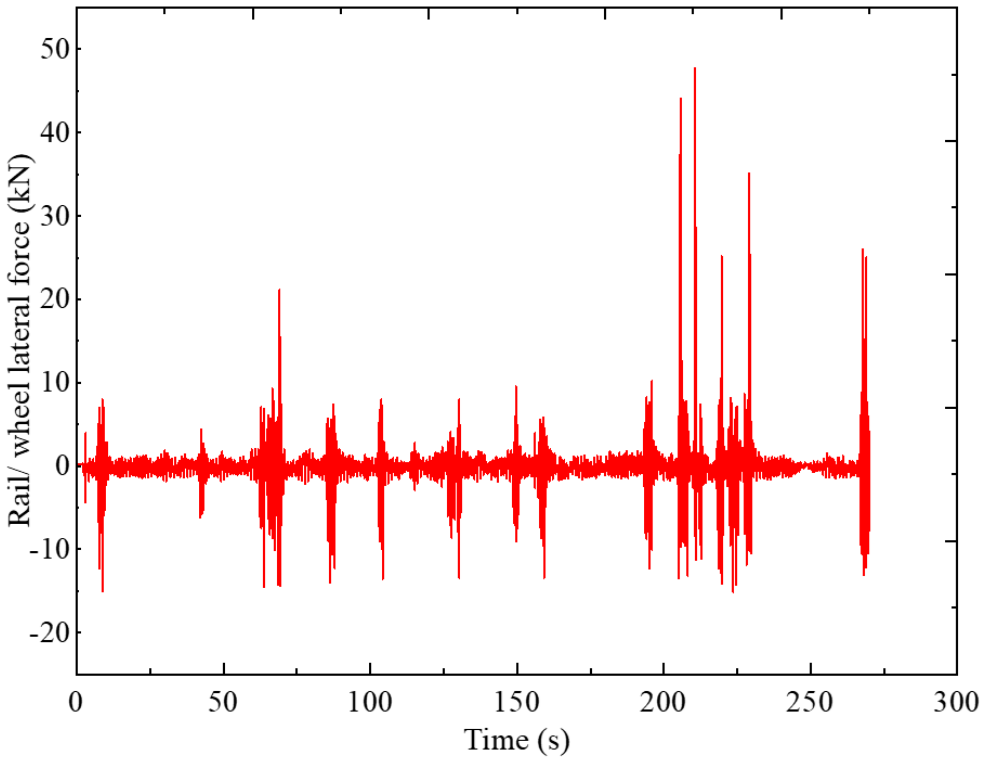

(a) Rail-wheel Lateral force at 30 km/h

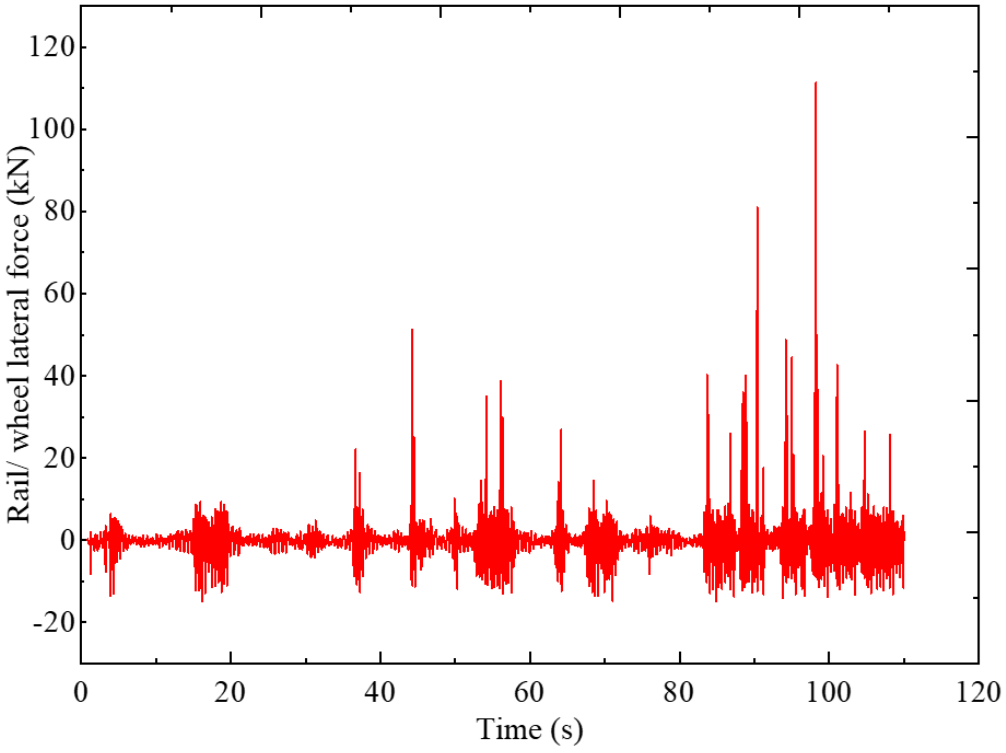

(b) Rail-wheel vertical force at 70 km/h

Appendix H: Flexible wheelset

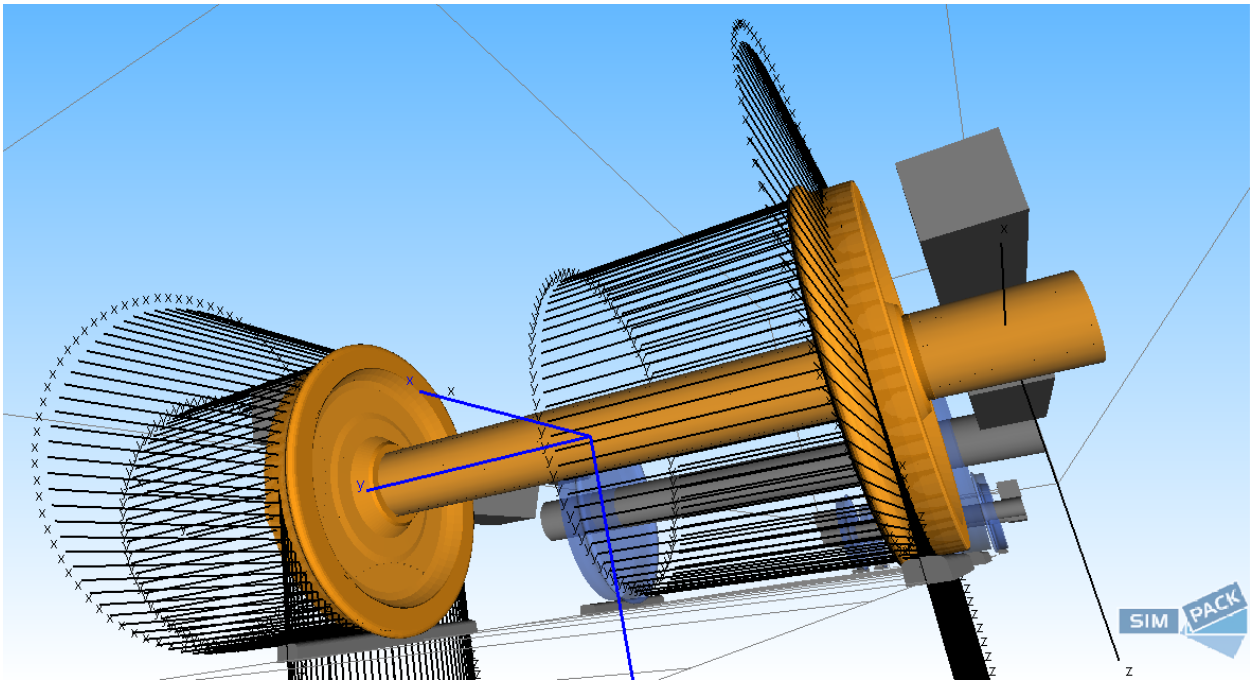

Appendix I: Vertical accelerations

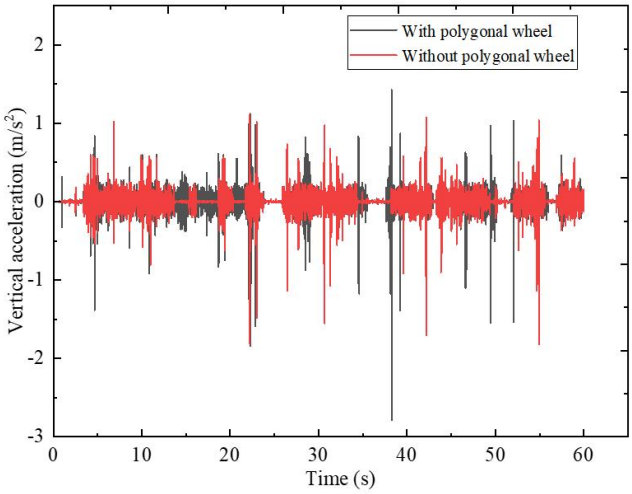

(a) Present work

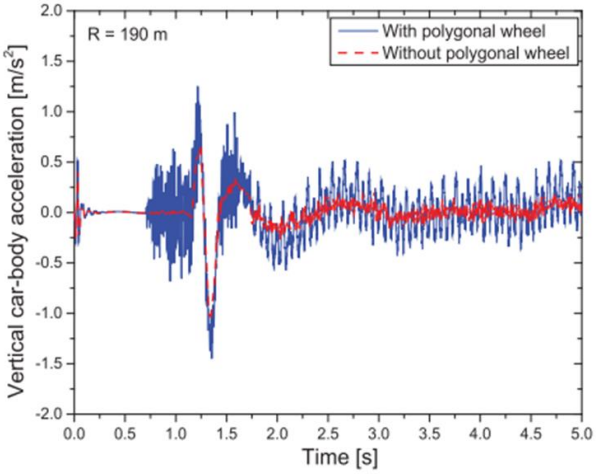

(b) Verification results [42]

Appendix J: Polygonization amplitudes

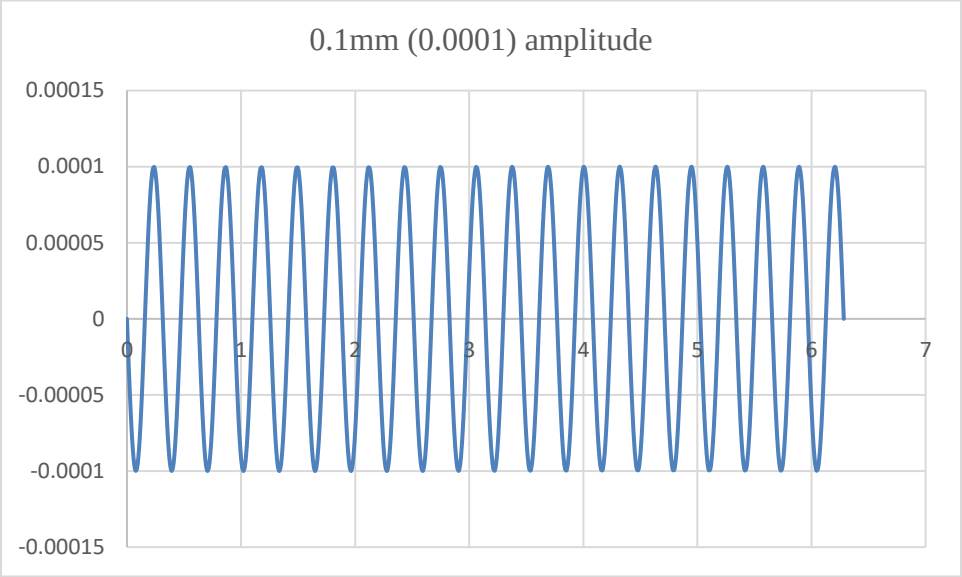

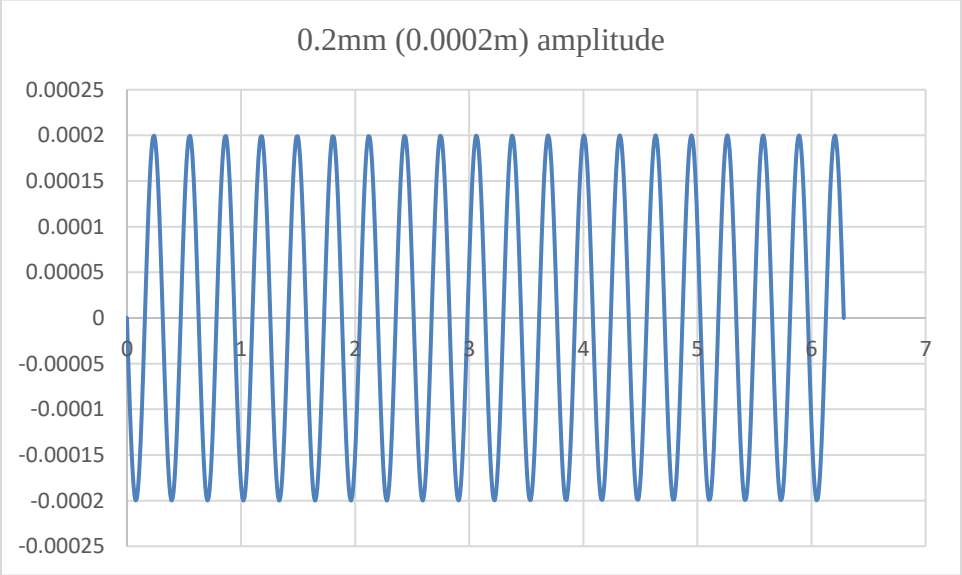

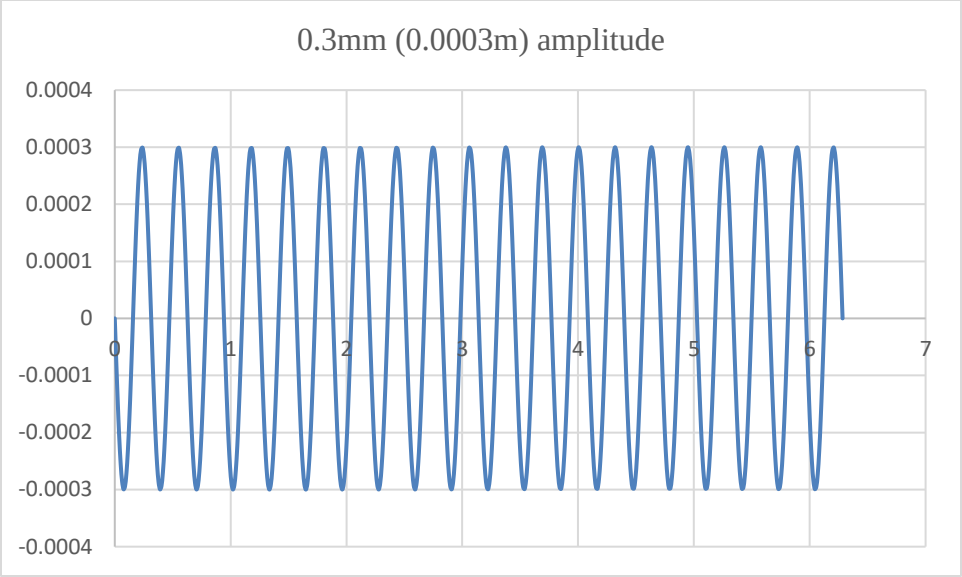

Appendix K: Inserting polygonization number in Simpack

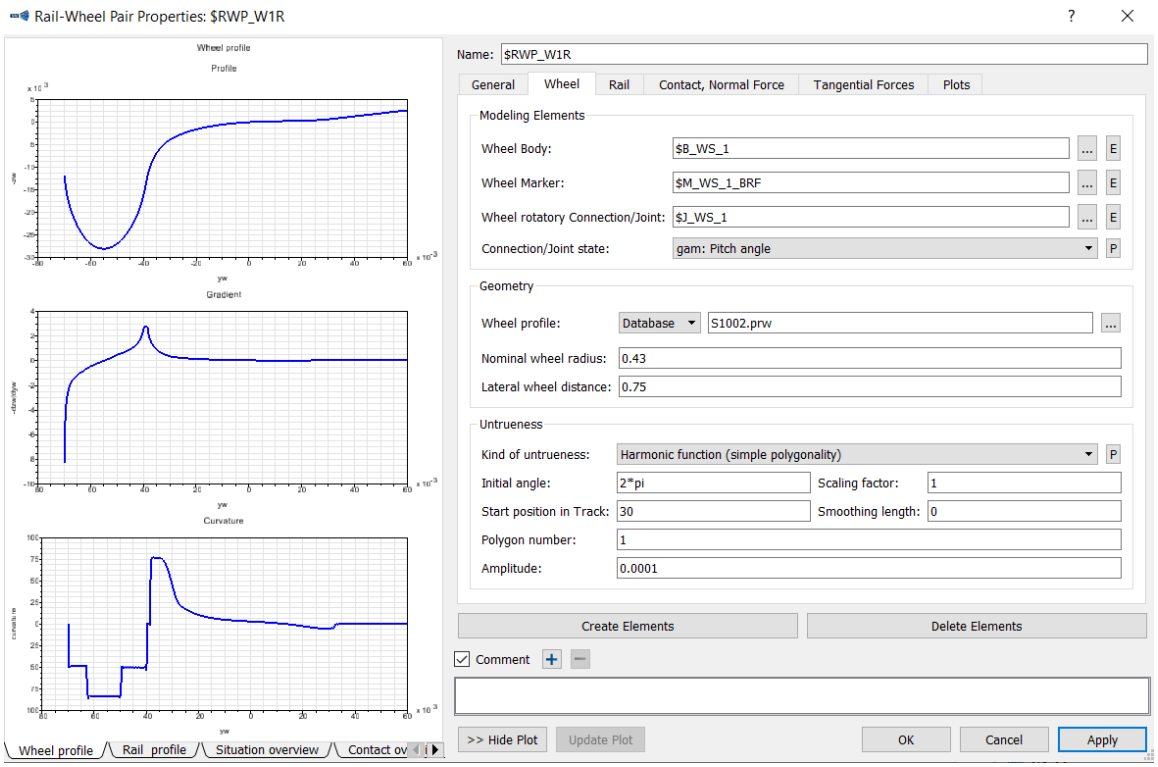

Appendix L: Rail/ wheel vertical impact force due to flexible and rigid wheelsets